Novel insights into the physics of fatigue crack growth

Theoretical and experimental research on the fundamentals of crack growth in isotropic materials
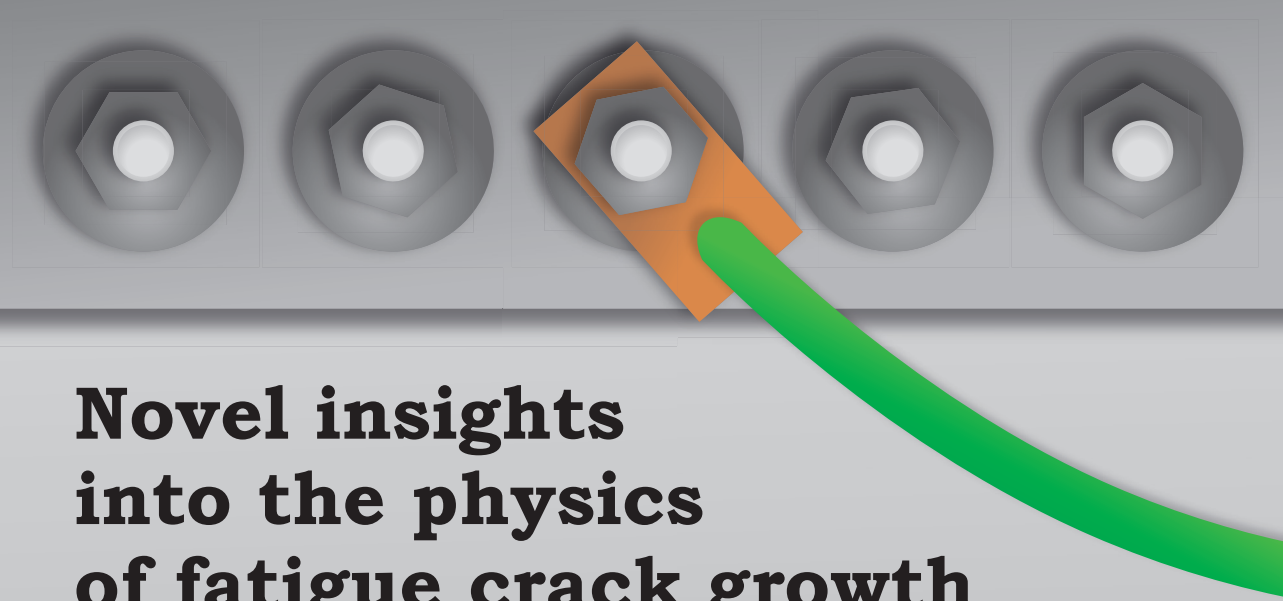
van Kuijk, J.J.A.

Important note
To cite this publication, please use the final published version (if applicable).
Please check the document version above.

Novel insights into the physics of fatigue crack growth

Theoretical and experimental research on the fundamentals of crack growth in isotropic materials

Jesse van Kuijk

Propositions

accompanying the dissertation

Novel insights into the physics of fatigue crack growth

Theoretical and experimental research on the fundamentals of crack growth in isotropic materials

by

Jesse J. A. van Kuijk

1. Fatigue similitude parameters ΔK and ΔK_{eff} have no basis in physics. *This proposition pertains to this dissertation.*

2. Fatigue crack closure corrections based on ΔK_{eff} are at best incomplete, for the required opening stress $S_{\mathrm{op,phen}}$ is not equal to the true physical opening stress $S_{\mathrm{op,phys}}$. *This proposition pertains to this dissertation.*

3. Fatigue load cycles have no place in a continuous and energy based description of fatigue crack growth. *This proposition pertains to this dissertation.*

4. The limited human muscle power output is the least problem with human powered flight.

5. Increasing the fidelity of weather and climate modeling with increased computing power, influences the modeled thermodynamic processes by adding more heat.

6. Equal opportunities do not result in equal outcome, and conversely, forcing equal outcome requires unequal opportunities.

7. The rotor blade geometry development of historic Dutch windmills is proof that iterative or genetic algorithms do not necessarily result in a global optimal solution.

8. The fatigue life of the heart is forgotten when physical activity and sports are promoted for health and longevity reasons.

9. Contemporary wind turbines are of such dimensions that they cause significant mixing of the (nocturnal) atmospheric boundary layer, thereby influencing the local climate.

10. Work meetings in industry are like black holes: a lot of energy goes into them, and what comes out is small and random.

These propositions are regarded as opposable and defendable, and have been approved as such by the promotor prof. dr. ir. R. C. Alderliesten.

Stellingen

behorende bij het proefschrift

Novel insights into the physics of fatigue crack growth
Theoretical and experimental research on the fundamentals of crack growth in isotropic materials

door

Jesse J. A. van Kuijk

1. Vermoeiingsscheurgroei gelijkenisparameters ΔK en ΔK_{eff} hebben geen natuurkundige onderbouwing. *Deze stelling heeft betrekking op dit proefschrift.*

2. Vermoeiingsscheursluitingscorrecties gebaseerd op ΔK_{eff} zijn op zijn minst onvolledig, omdat de gebruikte openingsspanning $S_{\mathrm{op,phen}}$ niet gelijk is aan de fysieke openingsspanning $S_{\mathrm{op,phys}}$. *Deze stelling heeft betrekking op dit proefschrift.*

3. Vermoeiingsbelastingscycli hebben geen plaats in een op energie gebaseerde continue beschrijving van vermoeiingsscheurgroei. *Deze stelling heeft betrekking op dit proefschrift.*

4. Het marginale mechanische vermogen van de menselijke spieren is de minste uitdaging van vliegen op spierkracht.

5. De verbeterde nauwkeurigheid van weer- en klimaatmodellen door middel van toegenomen rekenkracht, beinvloedt de gemodelleerde thermodynamische processen door toevoeging van meer warmte.

6. Gelijke mogelijkheden hoeven niet te resulteren in gelijke resultaten, en omgekeerd, het forceren van gelijke resultaten vereist ongelijke mogelijkheden.

7. De ontwikkeling van wieksystemen van oude Nederlandse windmolens bewijst dat iteratieve of genetische algoritmes niet altijd het absolute optimale resultaat behalen.

8. De vermoeiingslevensduur van het hart wordt vergeten wanneer fysieke activiteiten en sport worden aangeprezen voor een langer en gezonder leven.

9. Hedendaagse windturbines zijn van dergelijke afmetingen dat ze significante menging van de (nachtelijke) atmosferische grenslaag veroorzaken, waardoor het lokale klimaat beïnvloed wordt.

10. Werkvergaderingen in het bedrijfsleven vertonen gelijkenissen met zwarte gaten: er gaat veel energie in zitten, en wat er uit komt is klein en willekeurig.

Deze stellingen worden opponeerbaar en verdedigbaar geacht en zijn als zodanig goedgekeurd door de promotor prof. dr. ir. R. C. Alderliesten.

Novel insights into the physics of fatigue crack growth

Theoretical and experimental research on the fundamentals of crack growth in isotropic materials

Novel insights into the physics of fatigue crack growth

Theoretical and experimental research on the fundamentals of crack growth in isotropic materials

Dissertation

by

Jesse Johan Adriaan VAN KUIJK

Master of Science in Aerospace Engineering,
Delft University of Technology, the Netherlands
born in Budel, the Netherlands

This dissertation has been approved by the promotors.

Composition of the doctoral committee:

Rector Magnificus	chairperson
Dr. ir. R. C. Alderliesten	Delft University of Technology, promotor
Prof. dr. ir. R. Benedictus	Delft University of Technology, promotor

Independent members:

Prof. dr. R. Jones	Monash University, Australia
Prof. dr. D. Kujawski	Western Michigan University, United States of America
Prof. dr. M. N. James	Plymouth University, United Kingdom
Prof. dr. ir. E. Schlangen	Delft University of Technology
Prof. C. A. Dransfeld	Delft University of Technology

An electronic version of this dissertation is available at
http://repository.tudelft.nl/.

Contents

Summary

Fatigue crack growth in metals has been studied intensively for more than half a century. This research field has been closely connected to the engineering industry throughout history. It is therefore no surprise that the main focus has mostly been on developing better prediction models rather than on understanding the phenomenon of fatigue crack growth. This dissertation focuses on improving our understanding of the underlying physics, and presents several novel insights primarily relating to crack closure modeling and crack growth rate modeling.

Crack closure corrections play an important role in many fatigue crack growth models. They are linked to the similitude parameter ΔK_{eff}, which removes the effect of the stress ratio R in fatigue crack growth curves. A literature survey showed that it is nearly impossible to measure crack opening and closure at the exact crack tip. Consequently, many closure measurements are imprecise. A theoretical physical model of a fatigue specimen was developed using multiple springs and an equal energy area analogy, to calculate the closure stress. The important conceptual leap here is that the phenomenological closure stress from measurements and literature can be different from the true physical closure stress. Finite element analysis was used to obtain the physical closure stresses, as they cannot be measured at the exact crack tip. Using the physical closure model in reverse, it was shown that the resulting phenomenological closure stresses fell well within the values reported in literature with similar trends. This was shown for different maximum stresses S_{max} and a range of stress ratios R. This newly developed physical model of crack closure shows that the phenomenological closure stress used in ΔK_{eff} approaches is not equal to the true or physical closure stress, but that they can be linked. It also shows that the ΔK_{eff} similitude parameter, although widely used, is only partially describing the crack closure phenomenon because it neither correctly nor completely includes the closure phenomenon.

In order to measure the fatigue crack length development with high accuracy during fatigue tests, a direct current potential drop setup was developed. Multiple constant amplitude fatigue tests were performed. Environmental effects were minimized by comparing with an identical, uncracked reference specimen placed next to the test specimen. The novelty was the use of an FPGA (field-programmable gate array) allowing kHz rate measurements, which made it possible to measure the potential development several thousand times through each fatigue cycle. These results could be linked to a combination of the Poisson effect and piezoresistivity. A distinct plateau behavior around maximum loading was observed, which was shown to be related to crack tip plasticity, for it is absent during elastic loading of an uncracked specimen. The start and end timing instances of the plateau with respect to the cycle were correlated to the timing instances of the opening and closure stress in the loading cycle.

The link between the potential drop through the cycle measurements and crack tip plasticity was further correlated using specimen surface deformation measurements. A high frequency (6400 Hz), two-dimensional digital image correlation system was used to measure and calculate the in-plane strain during fatigue tests. A load cycle near the end of the fatigue life showed that the crack tip plastic zone translated during part of the load cycle, corresponding well with the observed plateau in the potential drop values during the loading phase. During the unloading phase, this translation was not reversed, suggesting that it is possible to indirectly observe crack growth during a single cycle using this combined technique.

A novel fatigue crack growth model is presented, with a physical basis. It consists of two parts: an energy balance and a model based on the analogy of a sliding box. The energy balance connects the global applied energy to local dissipation terms related to crack growth. This balance models the growth of applied work and dissipation through the fatigue life, but cannot provide the step size in cycles. This is an important outcome of the physical energy balance equation: fatigue cycles are not present in it, because cycles are dimensionless. The sliding box analogy provides a theoretical model which describes the fatigue crack growth per cycle. A coupling with a discrete version of the energy balance provides a qualitatively correct analogy for constant amplitude fatigue crack growth. This is shown by correlation with fatigue test data of aluminum and steel specimens. It is one of the first times that a general fatigue crack growth model uses a proper physical basis.

This PhD research project started by looking into the meaning of common similitude parameters ΔK and ΔK_{eff}, which are functions of the crack length. The realization was made that different starter crack geometries, such as corner cracks, surface cracks, and through cracks, all grow at different rates until they become full through cracks. Using the (projected) crack surface area instead of the crack length as base parameter for the similitude parameter provides a better comparison for fatigue crack growth data from different starter crack geometries. This was studied using a modified Newman-Raju crack growth model, and by developing a cellular automaton. This cellular automaton models the crack front development for single as well as multiple starter cracks, without a direct connection with fatigue. The similar results hint strongly at an underlying and common physical basis for the cellular automaton and the development of fatigue cracks.

The results of the above areas of research have been published in several journal papers, an international conference paper, a data set publication, and this dissertation.

Samenvatting

Vermoeiingsscheurgroei in metalen wordt al meer dan een halve eeuw intensief bestudeerd. Dit onderzoeksgebied is historisch gezien nauw verbonden met de werktuigbouw en de luchtvaart- en ruimtevaartindustrie. Het is daarom geen verrassing dat de nadruk overwegend lag op het verbeteren van voorspellingsmethodieken, in plaats van het natuurkundig doorgronden van het vermoeiingsfenomeen. Deze dissertatie richt zich op het verbeteren van ons begrip van de onderliggende fysica, en presenteert verschillende nieuwe inzichten die voornamelijk betrekking hebben op het fysisch modelleren van scheursluiting en scheurgroeisnelheid.

Scheursluitingscorrecties spelen een belangrijke rol in veel vermoeiingsscheurgroeimodellen. Ze zijn gekoppeld aan de gelijkenisparameter ΔK_{eff}, die het effect van de belastingsverhouding R in scheurgroeisnelheidskrommen normaliseert. Uit literatuuronderzoek bleek dat het bijna onmogelijk is om scheuropening en scheursluiting aan de werkelijke scheurtip te meten. Hieruit volgt dat deze metingen vaak enigzins onnauwkeurig zijn. Een theoretisch natuurkundig model werd opgesteld dat een vermoeiingsproefstuk modelleert als meerdere mechanische veren, en een equivalente energie-oppervlakte analogie, waaruit de werkelijke scheursluitingsbelasting bepaald kan worden. Het belangrijke vernieuwende inzicht hier is dat de fenomenologische scheursluitingsbelasting uit metingen een andere kan zijn dan de werkelijk aanwezige scheursluitingsbelasting. Een eindige-elementenanalyse werd gebruikt om deze werkelijke scheursluitingsbelasting te verkrijgen, omdat metingen aan de werkelijke scheurtip niet mogelijk zijn. Door vervolgens het opgestelde natuurkundige model in omgekeerde richting te gebruiken, werd aangetoond dat de verkregen fenomenologische scheursluitingsbelastingen qua trend en waarden goed overeen kwamen met data uit de literatuur. Dit werd aangetoond voor een reeks belastingsverhoudingen R bij verschillende maximale belastingen S_{max}. Dit nieuw ontwikkelde fysische model van scheursluiting laat zien dat de fenomenologische scheursluitingsbelasting in ΔK_{eff} methodieken niet gelijk is aan de werkelijke of fysische scheursluitingsbelasting, maar dat ze aan elkaar gerelateerd kunnen worden. Het model laat ook zien dat de gelijkenisparameter ΔK_{eff}, hoewel veelvuldig gebruikt in de literatuur, het scheursluitingsfenomeen slechts gedeeltelijk beschrijft, omdat het scheursluiting niet op correcte noch complete wijze meeneemt.

Om de ontwikkeling van de vermoeiingsscheurlengte met hoge nauwkeurigheid te meten, werd een gelijkstroom potentiaaldalingsmeetsysteem verder ontwikkeld. Meerdere constante amplitude vermoeiingstesten werden hiermee uitgevoerd. Omgevingsinvloeden werden geminimaliseerd door het testproefstuk steeds te vergelijken met een identiek en onvermoeid referentieproefstuk dat direct naast het testproefstuk was geplaatst. De noviteit was de toepassing van een FPGA (fieldprogrammable gate array) die een meetfrequentie in kHz mogelijk maakte, waarmee de potentiaal tot wel enkele duizenden keren per belastingscyclus gemeten

werd. De resultaten konden gecorreleerd worden aan een gecombineerd effect van het Poisson effect en piezoresistiviteit. Duidelijk waarneembaar was een pla- teau rond de maximale belasting, welke aan scheurtipplasticiteit gerelateerd kon worden, omdat deze afwezig is gedurende elastische vervorming van een onge- scheurd proefstuk. De begin en eind tijdstippen van het plateau met betrekking tot de belastingscyclus konden gecorreleerd worden aan de respectievelijke tijdstippen van scheuropeningsbelasting en scheursluitingsbelasting.

Het verband tussen de potentiaaldalingsmetingen en de scheurtipplasticiteit werd verder onderzocht door oppervlaktedeformatiemetingen van proefstukken ge- durende vermoeiingstesten. Een hoogfrequent ($6400\,\text{Hz}$), tweedimensionaal digi- taal beeldcorrelatiesysteem werd gebruikt om de vervormingen van het proefstuk- oppervlak te meten, en de gerelateerde rek te berekenen. Een belastingscyclus aan het eind van het vermoeiingsleven toonde aan dat het gebied met scheurtipplastici- teit zich verplaatste gedurende het een gedeelte van de eerste helft van deze cyclus, wat goed overeenkomt met het geobserveerde plateau in de potentiaaldalingsme- tingen. Gedurende de tweede helft van de cyclus bleek de verplaatsing permanent, wat suggereert dat het mogelijk is om met deze combineerde technieken indirect de scheurgroei te observeren, gedurende een enkele belastingscyclus.

Een nieuw vermoeiingsscheurgroeimodel wordt hier gepresenteerd, met een na- tuurkundige basis. Het bestaat uit twee delen: een energiebalans, en een model dat gebaseerd is op een natuurkundige analogie van een schuivende doos. De ener- giebalans verbindt de globaal aangebrachte energie met de lokaal gedissipeerde energietermen die gerelateerd zijn aan scheurgroei. Deze balans modelleert de groei van aangebrachte energie en dissipatie gedurende het hele vermoeiingsle- ven, maar kan de stapgrootte in vermoeiingsbelastingscycli niet weergeven. Dit is een belangrijke uitkomst van de energiebalansvergelijking: vermoeiingsbelastings- cycli zijn afwezig, omdat ze dimensieloos zijn. De schuivende doos analogie geeft wel een theoretisch model voor de scheurgroei per vermoeiingsbelastingscyclus. Een koppeling met een discrete versie van de energiebalansvergelijking geeft een kwalitatief correcte analogie voor een constante amplitude vermoeiingsbelastings- spectrum. Dit is aangetoond door correlatie met experimentele vermoeiingsdata. Het is een van de eerste keren dat een algemeen vermoeiingsscheurgroeimodel een werkelijk fysische basis gebruikt.

Dit promotieonderzoek begon met het onderzoeken van de betekenis van ge- lijkenisparameters ΔK en ΔK_{eff}, die beiden functies zijn van de scheurlengte. Een realisatie was dat verschillende scheurfrontgeometrieen zoals hoekscheuren, op- pervlaktescheuren, en volledige-breedte-scheuren, elk met verschillende snelheden groeien totdat ze allemaal volledige-breedte-scheuren geworden zijn. Door in de gelijkenisparameter de (geprojecteerde) scheuroppervlakte te gebruiken in plaats van de scheurlengte, kan scheurgroeidata van verschillende scheurfrontgeometri- een beter vergeleken worden. Dit is onderzocht aan de hand van een aangepast Newman-Raju model voor scheurgroei, en door middel van een cellulaire automaat. Deze cellulaire automaat modelleert de scheurfrontontwikkeling voor zowel enkele als meervoudige startscheuren, en zonder een directe fysische link met het ver- moeiingsfenomeen. De resultaten zijn vergelijkbaar met het theoretische model,

en duiden sterk op een onderliggende algemene fysische basis is voor de cellulaire automaat en de ontwikkeling van vermoeiingsscheuren.

De resultaten van bovengenoemde onderzoeken zijn gepubliceerd in wetenschappelijke tijdschriften, op een internationaal congres, als een datasetpublicatie, en in deze dissertatie.

Nomenclature

Chapter 1

a	crack length	[mm]
da/dN	crack growth rate	[mm cycle^{-1}]
C	constant in the Paris equation (not dimensionless)	[MPa^{-m} m$^{1-m/2}$]
CA	constant amplitude	[-]
CCT	center crack tension specimen type	[-]
J	applied work	[J]
$\dot{J}$	change in applied work	[-]
m	exponent in the Paris equation	[-]
S_{max}	maximum stress	[MPa]
S_{op}	opening stress	[MPa]
U_{a}	energy related to crack extension	[J]
$\dot{U}_{\text{a}}$	derivative of energy related to crack extension	[-]
U_{e}	elastically stored energy	[J]
$\dot{U}_{\text{e}}$	derivative of elastically stored energy	[-]
U_{ep}	change in elastic energy due to plastic deformation	[J]
$\dot{U}_{\text{ep}}$	derivative of change in elastic energy due to plastic deformation	[-]
U_{p}	energy related to plastic deformation	[J]
$\dot{U}_{\text{p}}$	derivative of energy related to plastic deformation	[-]
β	finite width correction factor	[-]
ΔK	similitude parameter	[MPa m$^{0.5}$]
ΔK_{eff}	similitude parameter	[MPa m$^{0.5}$]

Chapter 2

A_{n}	constants for Newman closure correction	[-]
a	crack length	[mm]
C	constant in the Paris equation (not dimensionless)	[MPa^{-m} m$^{1-m/2}$]
CA	constant amplitude	[-]
COD	crack tip opening displacement	[mm]
CV	coefficient of variation: σ/μ	[-]
da/dN	crack growth rate	[mm

		cycle^{-1}]
E	stiffness	[GPa]
E_Δ	linear elastic stiffness, difference	[GPa]
E_0	linear elastic stiffness, crack closed	[GPa]
E_1	linear elastic stiffness, crack open	[GPa]
GLARE	GLAss REinforced aluminum	[-]
K_I	stress intensity factor (mode I)	[MPa m$^{0.5}$]
K_L	Correia et al. limiting K_max	[MPa m$^{0.5}$]
K_max	similitude parameter, maximum	[MPa m$^{0.5}$]
K_0	similitude parameter, at yield or flow stress	[MPa m$^{0.5}$]
LEFM	linear elastic fracture mechanics	[-]
m	exponent in the Paris equation	[-]
N	number of cycles	[-]
R	stress ratio: $S_\mathrm{min}/S_\mathrm{max}$	[-]
S_cl	closure stress	[MPa]
S_max	maximum stress	[MPa]
S_mean	mean stress: $(S_\mathrm{max} + S_\mathrm{min})/2$	[MPa]
S_min	minimum stress	[MPa]
S_op	opening stress	[MPa]
$S_\mathrm{op,phys}$	true opening stress	[MPa]
$S_\mathrm{op,phen}$	opening stress used in ΔK_eff equation	[MPa]
S_yield	yield stress	[MPa]
t	time	[s]
U	energy	[J]
U_SIF	effective stress intensity factor ratio	[-]
VA	variable amplitude	[-]
W	specimen width	[m]
α_{DK}	De Koning closure correction parameter	[-]
α_N	Newman closure correction factor	[-]
β	finite width correction factor	[-]
ΔK	similitude parameter	[MPa m$^{0.5}$]
ΔK_0	SIF (mode I) at crack tip	[MPa m$^{0.5}$]
ΔK_eff	similitude parameter	[MPa m$^{0.5}$]
ΔK_max	SIF (mode I) at S_max	[MPa m$^{0.5}$]
ΔS	stress range: $S_\mathrm{max} - S_\mathrm{min}$	[MPa]
ΔS_eff	effective stress range: $S_\mathrm{max} - S_\mathrm{op}$	[MPa]
ΔU	change in energy (during loading)	[J]
ΔU_comp	change in compressive energy (during loading)	[J]
ΔU_inf	change in energy (during loading), infinite plate	[J]
$\Delta K_\mathrm{th,0}$	Correia et al. crack propagation threshold at $R = 0$	[MPa m$^{0.5}$]
ΔU_tens	change in tensile energy (during loading)	[J]
γ	Correia et al. material parameter	[-]
ε_max	maximum strain	[-]
ε_min	minimum strain	[-]

ε_{op}	opening strain	[-]
μ	mean	[-]
σ	standard deviation	[-]
σ_0	Flow stress for Newman closure correction: $\left(\sigma_y + \sigma_{uts}\right)/2$	[MPa]
σ_{uts}	ultimate tensile strength	[MPa]
σ_y	yield strength	[MPa]

Chapter 3

A	area, specimen cross-section	[m^2]
A^*	unit area	[m^2]
a	crack length	[mm]
CCT	center crack tension specimen type	[-]
C(T)	compact tension specimen type	[-]
DIC	digital image correlation	[-]
da/dN	crack growth rate	[mm cycle^{-1}]
E	stiffness	[MPa]
EMF	(thermal) electromotive force	[V]
ESE(T)	eccentrically-loaded single edge specimen type	[-]
FPGA	field-programmable gate array	[-]
h	temperature	[°Celsius]
I	electrical current	[A]
L	length	[mm]
L^*	unit length	[m]
LEFM	linear elastic fracture mechanics	[-]
LT	long transverse, material grain direction	[-]
M(T)	middle tension specimen type	[-]
OL	overload	[MPa], [-]
PD	potential drop	[-]
PD TTC	potential drop through the cycle	[-]
R	stress ratio: S_{min}/S_{max}	[-]
S	mechanical stress	[MPa]
S_{cl}	closure stress	[MPa]
$S_{cl,phen}$	closure stress used in ΔK_{eff} equation	[MPa]
$S_{cl,phys}$	true closure stress	[MPa]
S_{max}	maximum stress	[MPa]
S_{min}	minimum stress	[MPa]
S_{op}	opening stress	[MPa]
$S_{op,phen}$	opening stress used in ΔK_{eff} equation	[MPa]
$S_{op,phys}$	true opening stress	[MPa]
S_{yield}	yield stress	[MPa]
TTC	through the cycle	[-]
t	time, fractional time through cycle	[s], [-]

$t_{S,\mathrm{cl}}$	fractional time instant of crack tip closure	[s]
$t_{S,\mathrm{op}}$	fractional time instant of crack tip opening	[s]
V	specimen volume	[mm^3]
V^*	unit volume	[m^3]
W	specimen width	[mm]
β	finite width correction factor	[-]
ΔK	similitude parameter	[MPa m$^{0.5}$]
ΔK_{eff}	similitude parameter	[MPa m$^{0.5}$]
ε	strain	[-]
ν	Poisson's ratio	[-]
ρ	electrical resistivity	[Ohm m]
σ	standard deviation	[-]
ϕ	electrical potential	[V]
Ω	electrical resistance	[Ohm]

Chapter 4

CA	constant amplitude	[-]
DIC	digital image correlation	[-]
da/dN	crack growth rate	[mm cycle^{-1}]
PD TTC	potential drop through the cycle	[-]
R	stress ratio: $S_{\mathrm{min}}/S_{\mathrm{max}}$	[-]
S_{max}	maximum stress	[MPa]
t	time, fractional time through cycle	[s], [-]
$\varepsilon_{\mathrm{yy}}$	strain in loading direction	[-]

Chapter 5

a	crack length	[mm]
a_0	starter crack length	[mm]
b	constant in the Paris equation	[-]
C	constant in the Paris equation (not dimensionless)	[MPa^{-m} m$^{1-m/2}$]
C_{stic}	stiction coefficient	[-]
C_{fric}	friction coefficient	[-]
CA	constant amplitude	[-]
da/dN	crack growth rate	[mm cycle^{-1}]
dU/dN	change in energy or applied work per cycle	[J cycle^{-1}]
dU_{a}/dA	applied work per crack surface creation	[J m^{-2}]
dU_{a}/dN	dissipated crack surface creation energy per cycle	[J cycle^{-1}]
dU_{e}/dN	dissipated elastic energy per cycle	[J cycle^{-1}]

dU_p/dN	dissipated plastic energy per cycle	[J cycle^{-1}]
dU_p/dV_p	dissipated plastic energy per change in plastic volume	[J m^{-3}]
dV_p/da	change in plastic zone volume per crack length extension	[m^2]
E	stiffness	[MPa]
E^*	effective stiffness	[MPa]
$F(t)$	applied force on sliding box	[N]
FEA	finite element analysis	[-]
F_fric	crack growth energy or applied crack growth work	[N]
F_max	maximum applied force	[N]
$F_\text{net}(t)$	net applied force on sliding box	[N]
F_stic	crack growth energy or applied crack growth work	[N]
i	numerical increment counter	[-]
J	applied work	[J]
j	change in applied work	[-]
K	similitude parameter	[MPa m$^{0.5}$]
L	length	[mm]
M	sliding box mass	[kg]
m	exponent in the Paris equation	[-]
N	number of cycles	[-]
Q	generic curve used in the fatigue crack growth energy equation	[-]
R	stress ratio: $S_\text{min}/S_\text{max}$	[-]
r_p	plastic zone radius	[m]
S_max	maximum stress	[MPa]
S_min	minimum stress	[MPa]
S_op	opening stress	[MPa]
$S_\text{op,phen}$	opening stress used in ΔK_eff equation	[MPa]
$S_\text{op,phys}$	true opening stress	[MPa]
S_yield	yield stress	[MPa]
T	specimen thickness	[mm]
t	time, fractional time through cycle	[s], [-]
U	energy or applied work	[J]
U_a	energy related to crack extension	[J]
$\dot{U}_\text{a}$	derivative of energy related to crack extension	[-]
U_e	elastically stored energy	[J]
$\dot{U}_\text{e}$	derivative of elastically stored energy	[-]
U_ep	change in elastic energy due to plastic deformation	[J]
$\dot{U}_\text{ep}$	derivative of change in elastic energy due to plastic deformation	[-]
U_p	energy related to plastic deformation	[J]
$\dot{U}_\text{p}$	derivative of energy related to plastic deformation	[-]
U_max	maximum energy or applied work	[J]
U_spring	energy, applied work	[J]

V_p	plastic zone volume	$[\mathrm{m^3}]$
VA	variable amplitude	$[\text{-}]$
$v(t)$	sliding box velocity	$[\mathrm{m\ s^{-1}}]$
W	specimen width	$[\mathrm{mm}]$
$x(t)$	sliding box displacement	$[\mathrm{m}]$
$z(t)$	sliding box acceleration	$[\mathrm{m^2\ s^{-1}}]$
β	finite width correction factor	$[\text{-}]$
Δa	change in crack length	$[\mathrm{m}]$
$\Delta a/\Delta N$	change in crack length per change in cycles	$[\mathrm{m\ cycle^{-1}}]$
ΔK	similitude parameter	$[\mathrm{MPa\ m^{0.5}}]$
ΔK_eff	similitude parameter	$[\mathrm{MPa\ m^{0.5}}]$
ΔN	change in cycles	$[\mathrm{cycle}]$
ΔU	change in energy or applied work	$[\mathrm{J}]$
$\Delta U/\Delta N$	change in energy or applied work per change in cycles	$[\mathrm{J\ cycle^{-1}}]$
γ	crack surface roughness scale parameter	$[\text{-}]$
ε	strain	$[\text{-}]$
λ	shear lip area increase scale parameter	$[\text{-}]$
ϕ	golden ratio: $(1+\sqrt{5})/2$	$[\text{-}]$

Chapter 6

A	crack surface area	$[\mathrm{mm^2}]$
a	crack length	$[\mathrm{mm}]$
b	crack length through thickness	$[\mathrm{mm}]$
dA	change in crack surface	$[\mathrm{mm^2}]$
dA/dN	crack surface growth rate	$[\mathrm{mm^2\ cycle^{-1}}]$
da	change in crack length	$[\mathrm{mm}]$
da/dN	crack length growth rate	$[\mathrm{mm\ cycle^{-1}}]$
f	crack front length	$[\mathrm{mm}]$
N	number of cycles	$[\text{-}]$
R	stress ratio: $S_\mathrm{min}/S_\mathrm{max}$	$[\text{-}]$
S_max	maximum stress	$[\mathrm{MPa}]$
S_min	minimum stress	$[\mathrm{MPa}]$
S_ol	overload maximum stress	$[\mathrm{MPa}]$
T	specimen thickness	$[\mathrm{mm}]$
W	specimen width	$[\mathrm{mm}]$
β	elliptical crack aspect ratio modifier factor	$[\text{-}]$
ΔK_a	similitude parameter	$[\mathrm{MPa\ m^{0.5}}]$
ΔK_th	similitude parameter	$[\mathrm{MPa\ m^{0.5}}]$
ΔK_A	similitude parameter	$[\mathrm{MPa\ m}]$

γ	elliptical crack aspect ratio: b/a	[-]
ε_{yy}	strain in loading direction	[-]

Chapter 7

A	crack surface area	[mm^2]
a	crack length	[mm]
CA	constant amplitude	[-]
COD	crack tip opening displacement	[mm]
DIC	digital image correlation	[-]
dA	change in crack surface	[mm^2]
dA/dN	crack surface growth rate	[mm^2 cycle^{-1}]
da/dN	crack length growth rate	[mm cycle^{-1}]
$dU_\mathrm{p}/dV_\mathrm{p}$	dissipated plastic energy per change in plastic volume	[J m^{-3}]
FEA	finite element analysis	[-]
N	number of cycles	[-]
PD	potential drop	[-]
PD TTC	potential drop through the cycle	[-]
Q	generic curve used in the fatigue crack growth energy equation	[-]
R	stress ratio: $S_\mathrm{min}/S_\mathrm{max}$	[-]
S	stress	[MPa]
$S_\mathrm{cl_{phen}}$	closure stress used in ΔK_eff equation	[MPa]
S_max	maximum stress	[MPa]
S_min	minimum stress	[MPa]
S_op	opening stress	[MPa]
$S_\mathrm{op,phen}$	opening stress used in ΔK_eff equation	[MPa]
$S_\mathrm{op,phys}$	true opening stress	[MPa]
S_yield	yield stress	[MPa]
$t_{S,\mathrm{cl}}$	fractional time instant of crack tip closure	[s]
$t_{S,\mathrm{op}}$	fractional time instant of crack tip opening	[s]
VA	variable amplitude	[-]
W	specimen width	[mm]
Δa	change in crack length	[m]
$\Delta a/\Delta N$	change in crack length per change in cycles	[m cycle^{-1}]
ΔK_A	similitude parameter	[MPa m]
ΔK_a	similitude parameter	[MPa m$^{0.5}$]
ΔK_eff	similitude parameter	[MPa m$^{0.5}$]
σ	standard deviation	[-]
ϕ	electrical potential	[V]

1

Introduction

This introduction discusses the need for a better understanding of fatigue crack growth physics, with a concise literature review. It positions this PhD research project and its topics within the general fatigue crack growth research field. The aim and scope of the project are given, and the dissertation outline is explained.

1.1. The need for a better understanding of fatigue crack growth

For more than half a century, fatigue crack growth has been a significant area of materials and structures research. Numerous prediction models were developed, based on an abundance of measurement data. These models provide valuable tools for the engineering industry to design structures against fatigue failure, thereby actively preventing enormous financial damages to the economy.

Most of these fatigue crack growth models are based on measurements from fatigue tests: they are phenomenological. The measurements allow verification of the model results. However, it is challenging to measure inside the specimen and at the very crack front, and therefore there exists an inherent uncertainty in these measurements. Furthermore, many models are partially or completely developed using curve fitting of these measurements, often with several fitting constants and corrections. This results in realistic models, but does not necessarily explain the underlying physical principles governing the crack growth.

1.2. From phenomenological literature to a physics based equation

In 1839, the word 'fatigue' was used for the first time in writing by Poncelet [1], describing how cast iron axles used in mill wheels became 'tired' after a certain period of usage. The 1842 Versailles rail accident, Ref. [2], at the time the largest in the world, was caused by metal fatigue. Its accident investigation is widely regarded as the start of the fatigue research field, which later expanded to explicitly include the study of the crack growth phenomenon. In the 1950s several important investigations were carried out regarding the stress field and the plastic zone shape, including notably the work of Irwin [3, 4]. This work, combined with the insights from Paris and Erdogan [5] in the 1960s, gave the research field a large impulse: many fatigue crack growth data could now be expressed as a simple power law:

$$\frac{da}{dN} = C\Delta K^m \tag{1.1}$$

Which is illustrated in Figure 1.1, for constant amplitude (CA) fatigue data. ΔK is the stress intensity factor, a similitude parameter based on the crack tip stress state or intensity, and the geometry:

$$\Delta K = S_{\max}\beta\sqrt{\pi a} \tag{1.2}$$

Fatigue crack growth curves at different stress ratios $R = S_{\min}/S_{\max}$, for a given alloy, could be normalized onto a single curve by replacing ΔK by the similitude parameter ΔK_{eff}:

$$\Delta K_{\mathrm{eff}} = \left(S_{\max} - S_{\mathrm{op}}\right)\beta\sqrt{\pi a} \tag{1.3}$$
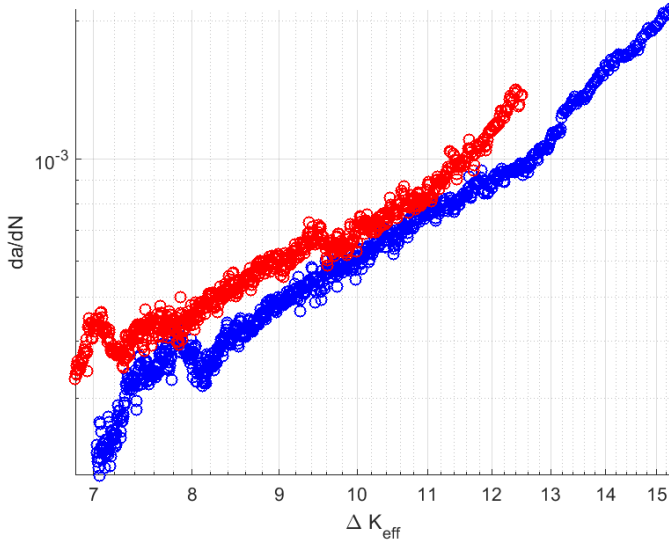
Figure 1.1: Crack growth rate da/dN versus ΔK_{eff} of two CA fatigue tests on Al 2024-T3 CCT specimens. Plotted on double logarithmic axes, each data set resembles a straight line, and can be fitted with a power law.

Which is based on ΔK and includes the opening stress S_{op}. The resulting form of the fatigue power law is widely known, and is the basis of many fatigue crack growth models:

$$\frac{da}{dN} = C\Delta K_{\text{eff}}{}^{m} \tag{1.4}$$

Many descriptive and predictive fatigue models currently used in industry are descendants of this original power law model using ΔK_{eff}, notably FASTRAN [6], NASGRO [7], PREFFAS [8], ONERA [9], CORPUS [10, 11]. There are also several related models based on Dugdale's strip yield model [12] which provides S_{op} values, such as [13–16].

The above mentioned models have become near accurate, yet none of them are physically correct. For example: the ubiquitous 'Paris law' for fatigue crack growth, Equation (1.1), and its modified version Equation (1.4), are dimensionally incorrect. This uncomfortable truth is often neglected, given the abundance of power law models. The constant C in Equation (1.1) is a function of the exponent m too, with the unit being: MPa^{m}m$^{(1-m/2)}$. The real question here is: Does the choice of similitude parameter cause this dimension issue? Furthermore, there is no apparent physical reason why the crack growth rate would follow a power law, as Paris himself noted [17]. It appears that the choice of similitude parameter together with a power law remained a convenient engineering approximation method, for it shows up as a straight line on a double logarithmic plot.

There is another issue, regarding the choice of similitude parameter. The widely used ΔK_{eff} uses an opening stress S_{op}. This opening stress is notoriously difficult to measure accurately, as mentioned in Refs. [18–20]. Finite element analysis can provide insight here, notwithstanding the inherent numerical and modeling limitations. The FEA results differ from the measurements. The hypothesis followed here is that the FEA or physical opening stress $S_{\text{op,phys}}$ is different, but relatable, to the phenomenological opening stress $S_{\text{op,phen}}$ used in the ΔK_{eff} approach. The explanation and discussion show that the understanding of crack closure is incomplete, and that the physical understanding of the phenomenon is not yet correct.

Starting with the power law model in the 1960s, did the research field stay largely empirical and phenomenological. Various improved models were developed from an engineering perspective to more accurately predict constant amplitude (CA) and variable amplitude (VA) fatigue for industry. Only recently does the fatigue research community start to look into fatigue crack growth from a pure physics perspective. Notable examples are, amongst others, the works of Alderliesten [21–24], Jones [25], Ranganathan [26], and Bhangale [27]. Equating dissipation to applied work is a method to describe fatigue crack growth based on physical parameters. The equation is a balance of energy terms, and is therefore called the energy balance (of fatigue crack growth).

The basic form of the energy balance states that the change in applied work equals the dissipation of energy due to crack growth and plastic deformation, plus the elastic energy lost due to the increased plastic zone:

$$\dot{J} = \dot{U}_{\text{a}} + \dot{U}_{\text{p}} + \dot{U}_{\text{ep}} \tag{1.5}$$

Consider a single load cycle of a load-controlled fatigue specimen. Figure 1.2 shows the development of the energy balance terms schematically. During loading, the applied work is first stored as elastic energy. When plasticity increases and crack growth happens, the specimen compliance increases, which requires extra work. During unloading, the decreased effective stiffness relieves a certain amount of energy as elastic energy, but not all energy. The difference is the sum of energy dissipated by crack extension, plasticity generation, and change in elastic energy due to the plasticity increase. This total dissipation is equal to the effective or net applied work. In other words, the change in work also equals the change in elastic energy:

$$\dot{J} = \dot{U}_{\text{e,out}} - \dot{U}_{\text{e,in}} \tag{1.6}$$

The energy balance also holds for any arbitrary increase in crack length or amount of cycles, where integrating on both sides gives the respective energy quantities. This basic form is a starting point for a physics based approach to fatigue crack growth.

1.3. Research focus

This dissertation is a continuation of the quest for understanding the physics of fatigue crack growth. It focuses on the following topics:
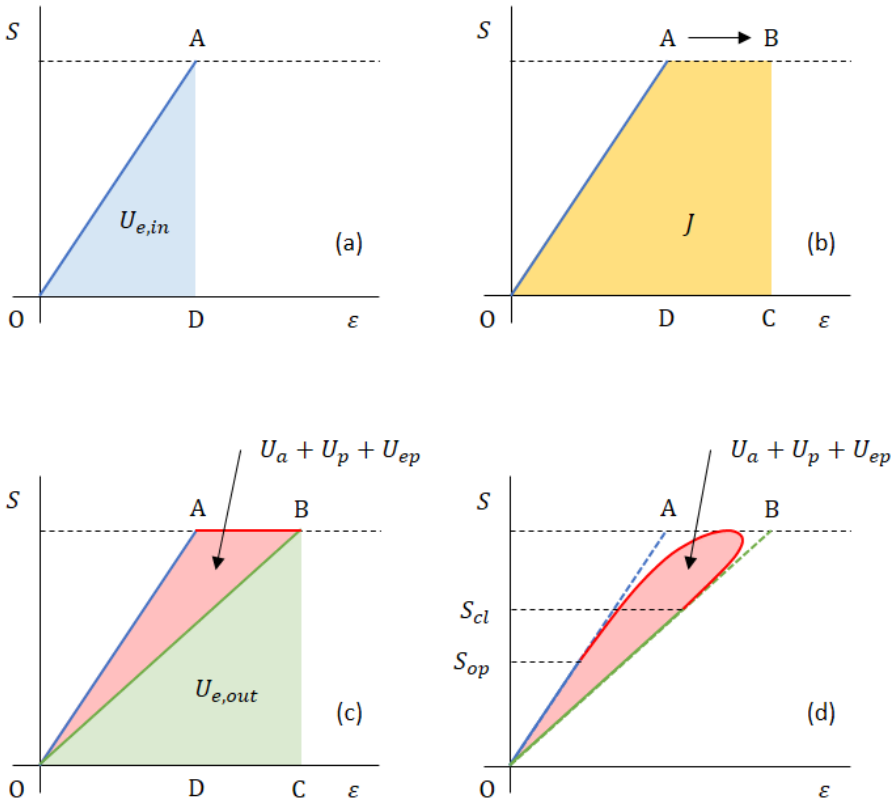
Figure 1.2: Applied work and dissipation in a single cycle of a load-controlled fatigue specimen, schematically explained. (a) During loading, applied work is stored as elastic energy. (b) The total applied work increases when the specimen compliance increases from A to B. (c) During unloading, an increased amount of elastic energy is released. The amount of energy not recovered, equals the energy dissipation related to fatigue crack growth, which caused the compliance increase. (d) A more realistic interpretation of a single fatigue cycle. The dissipated work starts and stops at crack opening and crack closure, respectively.

- The crack opening and closure models: A critical review from a physics point of view.

- The direct current potential drop measurement technique: An extension of this technique provides insight in the crack tip plasticity development.

- A continuous energy balance equation of fatigue crack growth: Presenting an equation which links the applied work on the specimen to fatigue dissipation mechanisms.

- The physical modeling of the crack growth rate throughout the fatigue life: Presenting a physical model with discrete steps over the continuous energy balance equation, thereby modeling fatigue crack growth.

- The choice of crack similitude parameter in fatigue crack growth modeling: A different crack similitude parameter is suggested to remove differences and data scatter originating from different starter crack geometries in fatigue data of small cracks.

1.4. Aim and scope of this dissertation

The aim of this current research is to obtain a better understanding of the physics underlying fatigue crack growth.

The scope of this research project is to investigate fatigue crack growth using both theoretical modeling, finite element analysis, and experimental verification. The main focus is on physics based theoretical modeling with numerical implementation, supplemented by FEA and fatigue tests. Most tests were done by the author, and a small number of other data sets were used to strengthen ideas and conclusions where necessary.

1.5. Dissertation outline

In Chapter 2, a novel insight into the ubiquitous closure corrections found in literature, and used in industry, is explained. It shows how the opening and closure stresses used in ΔK_{eff} approaches are not the physical opening and closure stresses, but that they are, however, related to each other. This allows a conversion from the physical stress to the stress related to the ΔK_{eff} approach. The challenges of measuring the opening and closure stresses at the exact crack tip, and along the crack front within the material, are discussed. To circumvent these challenges, finite element analysis is applied to model the physical opening and closure stresses for a range of stress ratios R. Then, the conversion from these physical stresses to the phenomenological ΔK_{eff} approach stresses is applied. It is shown that the resulting calculated phenomenological closure correction falls well within the known range of closure corrections.

In order to get a more complete picture of what happens during fatigue crack growth, a direct current potential drop measurement system was created, which

could take multiple measurements throughout each fatigue cycle. Chapter 3 explains this ambitious project and the unusual and interesting results gained from it: linking crack tip plasticity to the potential drop signal.

An additional confirmation of the link between plasticity and potential drop measurements was obtained by using digital image correlation to measure and monitor the plastic zone development throughout the load cycle. This confirmation is explained in Chapter 4.

Chapter 5 presents an energy balance equation for fatigue crack growth, in detail. This balance holds for constant amplitude fatigue but insights are given for extension to variable amplitude fatigue. Furthermore, a complementary physical model based on a sliding box analogy is presented which models the discrete steps along the energy balance equation. Together, they make modeling of the fatigue crack growth rate da/dN possible.

Alternative, improved choices for the similitude parameters ΔK and ΔK_{eff} are explained in Chapter 6. Most parameters are a function of the crack length, but the crack itself forms a surface. In order to compare fatigue tests with different starter crack geometries, the use of the crack area as a similitude parameter, rather than the crack length, could remove a significant portion of the data spread in the small crack range.

Finally, the main conclusions and recommendations of these research projects are given in Chapter 7.

References

[1] J. V. Poncelet, *Mécanique Industrielle, exposant les principes de statique et de dynamique, les organes mécaniques et les moteurs* (Meline, Cans et Co., Bruxelles, 1839).

[2] C. F. Adams, *Notes on railroad accidents* (G.P. Putnam's Sons, New York, 1879).

[3] G. R. Irwin, *Analysis of stresses and strains near the end of a crack transversing a plate,* Transactions ASME, Series E, Journal of Applied Mechanics **24**, 361 (1957).

[4] G. R. Irwin, *Linear fracture mechanics, fracture transition, and fracture control,* Engineering Fracture Mechanics **1**, 241 (1968).

[5] P. Paris and F. Erdogan, *A Critical Analysis of Crack Propagation Laws,* Journal of Basic Engineering **85**, 528 (1963).

[6] J. C. Newman Jr., *FASTRAN. A fatigue crack growth life-prediction code based on the crack-closure concept. User guide version 5.4,* Tech. Rep. (Fatigue & Fracture Associates, LLC, 2013).

[7] R. C. McClung, *NASGRO Fracture Mechanics & Fatigue Crack Growth Analysis Software,* Tech. Rep. (Southwest Research Institute, 2002).

1

[8] D. Aliaga, A. Davy, and H. Schaff, *A simple crack closure model for predicting fatigue crack growth under flight simulation loading,* ASTM STP 982 (1988), pp. 491–504.

[9] G. Baudin and M. Robert, *Crack growth model for flight type loading,* in *Proceeding of the 11th ICAF Symposium in the Netherlands* (1981).

[10] A. U. De Koning, *A simple crack closure model for prediction of fatigue crack growth rates under variable-amplitude loading,* ASTM STP 1122 (1981), pp. 63–85.

[11] A. U. De Koning and H. H. Van der Linden, *Prediction of fatigue crack growth rates under variable loading using a simple crack closure model,* Tech. Rep. NLR MP 81023 U (Nederlands Lucht- en Ruimtevaartcentrum, 1981).

[12] D. Dugdale, *Yielding of steel sheets containing slits,* Journal of the Mechanics and Physics of Solids **8**, 100 (1960).

[13] H. Führing and T. Seeger, *Dugdale crack closure analysis of fatigue cracks under constant amplitude loading,* Engineering Fracture Mechanics **11**, 99 (1979).

[14] H. D. Dill and C. R. Saff, *Spectrum crack growth prediction method based on crack surface displacement and contact analyses,* ASTM STP 595 (1976), pp. 306–319.

[15] D. J. Dougherty, A. U. De Koning, and B. M. Hillberry, *Modeling high crack growth rates under variable amplitude loading,* ASTM STP 1122 (1992).

[16] G. Wang and A. Blom, *A strip model for fatigue crack growth predictions under general load conditions,* Engineering Fracture Mechanics **40**, 507 (1991).

[17] P. C. Paris, *Fracture mechanics and fatigue: A historical perspective,* Fatigue & Fracture of Engineering Materials & Structures (Print) **21**, 535 (1998).

[18] J. Schijve, *Fatigue of Structures and Materials*, 2nd ed. (Springer Science+Business Media B.V., 2009).

[19] W. Elber, *The significance of fatigue crack closure,* ASTM STP 486 (1971), pp. 230–242.

[20] M. N. James and J. F. Knott, *Critical aspects of the characterization of crack tip closure by compliance techniques,* Materials Science and Engineering **72**, L1 (1985).

[21] R. C. Alderliesten, *The explanation of stress ratio effect and crack opening corrections for fatigue crack growth in metallic materials,* in *11th International Fatigue Congress*, Advanced Materials Research, Vol. 891 (Trans Tech Publications Ltd, 2014) pp. 289–294.

[22] R. C. Alderliesten, *How proper similitude principles could have improved our understanding about fatigue damage growth,* in *34th ICAF Conference and 28th ICAF Symposium (ICAF 2015)*, Vol. 1, edited by A. Siljander, 28th International Committee on Aeronautical Fatigue and Structural Integrity (ICAF) Symposium (VTT Technical Research Centre of Finland, 2015) pp. 47–57.

[23] R. Alderliesten, *How proper similitude can improve our understanding of crack closure and plasticity in fatigue,* International Journal of Fatigue **82**, 263 (2016), 10th Fatigue Damage of Structural Materials Conference.

[24] R. C. Alderliesten, *Fatigue and Fracture of Fibre Metal Laminates*, 2nd ed., Solid Mechanics and Its Applications, Vol. 236 (Springer International Publishing AG, 2017).

[25] R. Jones and S. Pitt, *An experimental evaluation of crack face energy dissipation,* International Journal of Fatigue **28**, 1716 (2006).

[26] N. Ranganathan, *The energy based approach to fatigue,* Advanced Materials Research **891-892**, 821 (2014).

[27] J. A. Bhangale, *Fatigue analysis of wind turbine blade materials using a continuum damage mechanics framework*, PhD dissertation, Delft University of Technology (2021).

1

2

Unraveling the myth of closure corrections: Sharpening the definition of opening and closure stresses with an energy approach

The substantiation of fatigue crack closure corrections is disputed, based on the closure stress definition. The ΔK_{eff} equation lacks a physical explanation. An inconsistency is observed between the opening stress $S_{\text{op,phen}}$ as used by this equation and the physical opening stress $S_{\text{op,phys}}$. This $S_{\text{op,phys}}$ is related to $S_{\text{op,phen}}$ through an energy equivalent area approach. Furthermore, an elastic spring model is used as a physical approach to crack closure effects. An FEA approach generates $S_{\text{op,phys}}$ values, which are reworked into $S_{\text{op,phen}}$. This physical model agrees well with existing closure corrections, and is able to provide a physical explanation for their necessity.

2.1. Introduction

F atigue crack growth in metals can be described using linear elastic fracture me-
chanics (LEFM). One of the key concepts of LEFM is the range of stress intensity
factors ΔK indicating the severity of the stress distribution around the crack tip, as
function of the applied far field stress range ΔS and half crack length a.

In 1961 Paris et al. [2] observed that the crack growth rate da/dN is a function
of both ΔK and the stress ratio R. The R dependency can be accounted for by
replacing ΔS with an effective stress range $\Delta S_{\mathrm{eff}} = S_{\mathrm{max}} - S_{\mathrm{op}}$, which results in the
effective stress intensity factor:

$$\Delta K_{\mathrm{eff}} = \Delta S_{\mathrm{eff}} \beta \sqrt{\pi a} \tag{2.1}$$

The stress level S_{op} is considered the stress level corresponding to the first
moment in the loading cycle where the crack tip is fully opened. The existence of
such a stress value is widely reported, among others in refs. [3–9].

The use of the effective stress range results in crack growth curves collapsing
onto each other. Elber [10] was one of the first to relate this reduced stress range to
the observed phenomenon of crack closure. The current state of the art models [11–
13] use the stress intensity factor ΔK_{eff} as similitude parameter, because different
fatigue cases can then be compared using the unique relationship between ΔK_{eff}
and da/dN, independent of R. The similitude parameter ΔK_{eff} is often linked to the
crack growth rate using a power law, such as the Paris equation, ref. [14], which is
a purely empirical correlation, for which the physical explanation is unknown, ref.
[15].

$$\frac{da}{dN} = C \Delta K_{\mathrm{eff}}{}^{m} \tag{2.2}$$

In ref. [10] it is reported that during the loading phase of a fatigue cycle an initial
nonlinear relationship is observed between the crack opening displacement and the
applied stress. This initial nonlinearity is ascribed to crack closure effects, imposed
by plasticity. During unloading the plastically deformed area around the crack tip
can close before S_{min} is reached, and similarly during loading the crack tip starts to
open at a stress level above S_{min}. This crack tip plasticity plays an important role
in crack closure, yet it does not correspond well with the LEFM theory on which the
ΔK_{eff} parameter is based. A main LEFM assumption is that plasticity is concentrated
in an infinitesimally small area at the crack tip. The plasticity related contradiction
between LEFM and the ΔK_{eff} parameter therefore suggests that ΔK_{eff} and related
closure corrections are not complete. Moreover, ΔK_{eff} is often assumed to be the
driving force for crack growth, while this statement has little physical basis: it is not
a force, but it rather is a representation of stress effects at the crack tip.

There is no reason why the ΔK approach using ΔS would give a correct result,
as the method is not physically correct. The improved approach of ΔK_{eff} using ΔS_{eff}
with S_{op} still suffers from the same oversight, it tries to correct a method that was
not physically correct to begin with. In this paper a discrepancy in opening stress
values and closure corrections is explained, and a physical method is presented to

transform true opening stresses to S_{op} values used in the ΔK_{eff} closure correction approach. As a first step, the incompleteness of closure corrections based on this ΔK_{eff} approach are further elaborated on below.

Equation (2.1) is a function of S_{op} to account for closure effects. Closure corrections such as Elber [10], Schijve [16], De Koning [17], and Newman [18], describe closure effects using the nondimensional parameter S_{op}/S_{max}. The latter three predict crack closure for all stress ratios R, even though there is a range of R values where the crack tip never closes during the full load cycle, as suggested by refs. [19–22]. Three other closure corrections, refs. [23–25] report similar closure behavior but for steel instead of aluminum, suggesting that the existence of non-closure near $R = 1$ is not material dependent. Furthermore, all seven mentioned closure corrections start to differ significantly for negative R values, showing that there is no true consensus on the crack closure behavior at compressive S_{min}.

Multiple sources suggest that crack closure is not the main driver for the spread seen in the closure corrections, but that the environment is significant. Kirby et al. [29] note from fatigue tests on aluminum 7075-T7351 that the environment itself plays a significant role; in vacuum the effect of stress ratio R was observed to be nearly absent. Suresh et al. [30], reach the same conclusion, again using aluminum 7075. They state that ΔK_{th} and da/dN are practically independent of the stress ratio R in the range $0.1 < R < 0.8$, both for wavy and planar slip alloys. Recently, Vasudevan et al. [31], after more experimental work using aluminum, suggest that the major influence of the stress ratio R on da/dN in air (or non-vacuum) may be the result of processes at the crack tip, rather than crack closure effects in the crack wake. Furthermore, environmental effects on the crack surface roughness are not a significant cause of the spread in closure corrections, as shown by refs. [8, 26–28] for different metals and different environments.

A large literature base, refs. [32–40], suggests that known closure corrections are not sufficient to collapse da/dN versus ΔK curves for various R onto a single da/dN versus ΔK_{eff} curve. Refs. [33, 41] discuss a theoretical model to account for asperity effects behind the crack tip, showing that closure is only significant when the crack is fully closed, and that the measured asperity effects are small. Vasudevan et al. [33] note that despite several decades of literature, there seems to be no accurate method of observing crack closure.

According to refs. [18, 42] S_{op}/S_{max} varies with $\Delta K_{max}/K_o$, and ref. [43] observed the same with a strip-yield model. This suggests $S_{op}/S_{max} = f(R, S_{max}, S_{yield})$, implying that, according to refs. [10, 16–18], all crack closure corrections as $f(R, S_{max})$ cannot accurately or uniquely describe closure for every R and metal (or isotropic material), and that S_{yield} or σ_0 needs to be taken into account.

If $S_{op}/S_{max} = f(R, S_{max}, S_{yield})$, it appears logical that there is also a finite width effect. The finite width raises the net-section stress in the crack plane, increasing the stress around the crack tip even more as the crack grows. Therefore it could be that $S_{op}/S_{max} = f(R, S_{max}, S_{yield}, a/W)$.

The incompleteness of common closure corrections to describe closure for all R and for different materials raises a question about the definition of opening stress S_{op} in the ΔK_{eff} equation: is it actually S_{op}? This line of thought is further developed

2

below.

In this paper a distinction is made between the phenomenologically observed stress $S_{op,phen}$, assumed to be the opening stress mentioned in literature and used in crack closure corrections through Equation (2.1), and the true physical opening stress $S_{op,phys}$. The choice of the opening stress value $S_{op,phen}$ in the ΔS stress range is addressed, and is linked to the true opening stress $S_{op,phys}$ using a theoretical model based on multiple linear elastic springs. A FEA simulation is used to generate realistic $S_{op,phys}$ values, and together with an energy based model the corresponding $S_{op,phen}$ for the ΔS range is obtained. The resulting $S_{op,phys}$ derived closure correction resembles existing closure corrections, but is based on a physics approach. It is shown that this new crack closure correction is a function of R, S_{max}, S_{yield}, and a/W.

2.2. How experiments support closure corrections

The crack closure corrections, proposed in [10, 16–18] are of similar trend but of increasing complexity: see Table 2.1 and Figure 2.1. All these corrections are indirectly related to measurements: either indirect phenomenological observations of the crack (tip) opening displacement (COD), or by scaling da/dN data (Paris crack growth curves) over ΔK_{eff} for various R values.

The De Koning [17] and Newman [18] equations need nondimensional fitting parameters, to incorporate plane strain or plane stress conditions, or to include a dependency on the flow stress σ_0. And all these closure corrections are based on curve fitting of a limited amount of measurements. This has several implications for the accuracy of the corrections, relating to applicable R range, measurement techniques, and curve fitting.

The measurements on which closure corrections are based are inevitably made over a limited R range. The corrections are then easily extrapolated beyond their original R range, a danger that Schijve [16] warns of. Elber's equation (Table 2.1) is a clear example, since the original R range is known. Extrapolating this equation for negative R ratios gives unrealistic results, and it is generally assumed that it holds correct only for $R \geq -0.1$.

The empirical nature and subsequent curve fitting practice of some closure corrections is illustrated by Overbeeke et al. [25]: a discontinuity is present at $R = -0.5$ while there is no physical reason for such a discontinuity to exist.

Furthermore, measuring S_{op} is not straightforward since no measurement device can measure directly at the crack tip. For example, Elber [10] placed a clip gauge system 2 mm behind the crack tip. Such strain gauge measurements or COD measurements give an indication of crack opening, but do not distinguish which part of the crack has opened. Figure 2.2 explains this schematically, where a COD measurement indicates an open crack, while the protrusion from an earlier (over)load prevents the crack tip from opening at this particular load. The measured S_{op} is therefore not necessarily the physical opening. Duan et al., ref. [45], propose a crack opening ratio parameter with an elaborate experimental setup to assess fatigue crack closure. Notwithstanding the validity of the method, it remains an

Table 2.1: Several well-known closure corrections are reproduced here, with their respective R validity range and material type.

| Author	Equation	Validity range	Material	Reference
Elber	$\dfrac{S_{op}}{S_{max}}\bigg\vert_{Elber} = 0.5 + 0.1R + 0.4R^2$	$-0.1 < R < 0.7$	Al 2024-T3	[10]
Schijve	$\dfrac{S_{op}}{S_{max}}\bigg\vert_{Schijve} = 0.45 + 0.22R + 0.21R^2 + 0.12R^3$	$-1.0 < R < 1.0$	Al 2024-T3	[16]
De Koning	$\dfrac{S_{op}}{S_{max}}\bigg\vert_{De\,Koning} = 0.45 + (0.1 + \alpha_{DK})R + (0.45 - 2\alpha_{DK})R^2 + \alpha_{DK}R^3$	$-1 < R < 1$	Al 7075-T6	[17]
Newman	$\dfrac{S_{op}}{S_{max}}\bigg\vert_{Newman} = A_0 + A_1 R + A_2 R^2 + A_3 R^3$ $A_0 = (0.825 - 0.34\alpha_N + 0.05\alpha_N^2)\left[\cos\left(\pi S_{max}/(2\sigma_0)\right)\right]^{1/\alpha_N}$ $A_1 = (0.415 - 0.071\alpha_N)\,S_{max}/\sigma_0$ $A_2 = 1 - A_0 - A_1 - A_3$ $A_3 = 2A_0 + A_1 - 1$ $\dfrac{S_{op}}{S_{max}}\bigg\vert_{Newman} = A_0 + A_1 R$ $A_0 = (0.825 - 0.34\alpha_N + 0.05\alpha_N^2)\left[\cos\left(\pi S_{max}/(2\sigma_0)\right)\right]^{1/\alpha_N}$ $A_1 = (0.415 - 0.071\alpha_N)\,S_{max}/\sigma_0$	$R \geq 1$ $-1 < R < 0$	Unspecified	[18]
Iwasaki	$\dfrac{S_{op}}{S_{max}}\bigg\vert_{Iwasaki} = 1 + 0.316R^3 + 0.259R^2 + 0.137R - 0.712$	$-1.0 < R \leq 0.4$ $0.4 < R < 1.0$	S355	[23]
Kurihara et al.	$\dfrac{S_{op}}{S_{max}}\bigg\vert_{Kurihara\,et\,al.} = \dfrac{1}{2R - 3}$	$-1.0 < R \leq 0.5$ $0.5 < R < 1.0$	S355	[24]
Overbeeke et al.	$\dfrac{S_{op}}{S_{max}}\bigg\vert_{Overbeeke\,et\,al.} = 1 - \left(0.707\,(1-R)^{0.19}\right)$ $1 - \left(0.716\,(1-R)^{0.31}\right)$	$-1.0 < R \leq 0.5$ $-0.5 < R \leq 0.38$ $0.38 < R < 1.0$	S460	[25]
Correia et al.	$\dfrac{S_{op}}{S_{max}}\bigg\vert_{Correia\,et\,al.} = 1 - \left(1 - \left(\dfrac{\Delta K_{th,0}}{K_{max}}\right)\right)(1-R)^{\gamma}$ (an R based correction factor is needed)	$K_{max} \leq K_L$ $K_{max} \geq K_L$	P355NL1	[44]

2
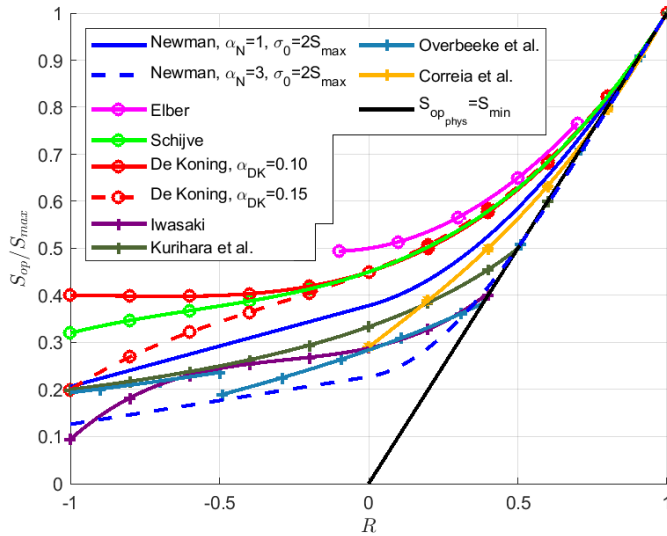
Figure 2.1: Closure corrections from literature. Curves with 'o' relate to aluminum, curves with '+' relate to steel, and other curves relate to metals in general. Note the limited Elber validity range, and the empirical fitting parameters on some corrections.

indirect, phenomenologically derived measurement of crack opening or closure.
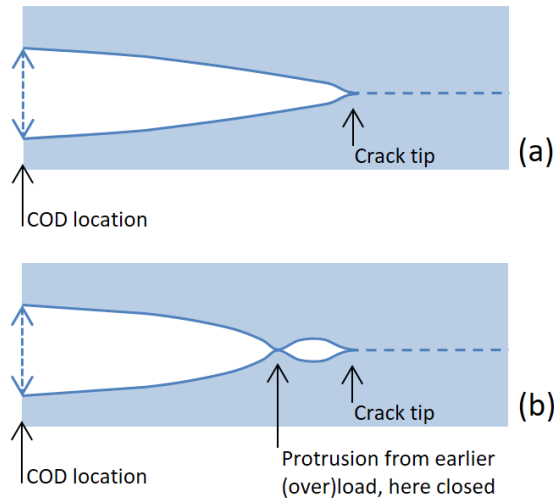

Figure 2.2: Two schematic crack tip cases. (a) Text book crack tip. (b) A protrusion from an earlier (over)load is still closed, preventing crack tip opening and crack development. COD can incorrectly suggest crack opening here.

The closure corrections shown in table:cceq do not provide scatter bands or error bars on the original measurements. One possible reason is the indirect construction of $S_{\mathrm{op}}/S_{\mathrm{max}}$ values: these values can be constructed from da/dN versus ΔK_{eff} crack growth curves by having them coincide through introducing a shift in ΔK_{eff}. This shift indicates the ΔS_{eff} needed and hence defines the opening stress S_{op}, or more precise: $S_{\mathrm{op,phen}}$.

To give a demonstration of this ambiguity; Schijve [4] used the same data, ref. [5], as De Koning [17], yet arrived at a slightly different crack closure correction. Using the same data set while arriving at two different equations suggests that there is no consensus on the method how to extract the curve from the data. For this particular data set Schijve gives values of the coefficient of variation CV. The ΔK_{eff} shift as described above is used to generate $S_{\mathrm{op}}/S_{\mathrm{max}}$ values for six different R values $-1 \leq R \leq 0.54$, which result in CV values ranging from 4.5% to 8.6%. When data point $R = -1$ is omitted, the CV range improves towards 4.2% to 6.5%. This illustrates the significant differences at low R values of closure corrections, as shown in Figure 2.1. The associated curve fittings are thereby affected too. These variations are partially due to measurement scatter, but are also partially caused by the inadequacy of the closure correction to match the observed ΔK_{eff} shift.

The issues mentioned above affect closure correction measurements, relating to ΔS_{eff}. ΔK_{eff}, using ΔS_{eff}, is an improvement over ΔK. This improvement is not complete either, as the overall validity of the ΔK_{eff} equation is questioned in literature. Kujawski [46] observes that ΔK tends to underpredict and ΔK_{eff} tends to overpredict crack closure effects. Scaling parameters need to be applied to both ΔK and ΔK_{eff} to match observations more closely. Castro et al. [47] mention experimental results which cannot be fully explained by using either ΔK or ΔK_{eff} as similitude parameter. Furthermore, while the incompleteness to describe crack closure of ΔK is noticed, it is not explained why ΔK_{eff} is incomplete too.

The closure correction measurement issues presented here suggest that ΔK_{eff} does not fully or not correctly account for crack closure. There appears to be an inconsistency in the definition of S_{op}: the phenomenologically derived opening stress is likely not the physical opening stress. $S_{\mathrm{op,phen}}$ can be understood as a virtual stress representing the applied work used for crack growth, in accordance with the ΔK_{eff} approach. It is hypothesized that $S_{\mathrm{op,phen}}$ is not necessarily equal to $S_{\mathrm{op,phys}}$, and this line of thought is further tested as explained in the next sections.

2.3. Why S_{op} is phenomenological

Consider Equation (2.1); it is often implicitly assumed to hold for all R. Note that for R close to unity, the crack might not close at all, because during the load cycle, the stress never drops below the physical crack opening stress; in other words $S_{\mathrm{min}} > S_{\mathrm{op,phys}}$. In such a case, in principle there should not be any closure correction. Literature confirms that closure is not measured at high R values; $R = 0.7$ is the maximum value for which closure has been reported [18, 32].

Furthermore, plane strain conditions (mid-thickness) see significantly less plasticity induced closure compared to plane stress conditions (near or at the surface).

Observing crack closure at a specimen surface therefore tends to overestimate the amount and influence of closure on the crack growth rate. The combination of geometry and $S_{\max}$ results in differences in the transition from plane strain to plane stress conditions during crack growth, which affects the observation of closure in different tests. It follows that $S_{\text{op,phys}}/S_{\max} = f(R, S_{\max})$: even though closure corrections are normalized by $S_{\max}$, there is still an $S_{\max}$ dependency related to the internal stress conditions. This finding is in line with the aforementioned doubts that Kujawski [46] states about the accuracy of ΔK_{eff}.

The choice of $S_{\max}$ (for example as ratio of flow stress σ_0) at a given R also affects $S_{\text{op,phen}}/S_{\max}$, as the amount of crack tip plasticity changes. This effect is mentioned since the 1980s by Newman [32, 48] and McClung et al. [49, 50], but a physical explanation is not given in literature. Figure 2.3 is reproduced from ref. [32], and shows the dependency of $S_{\text{op,phen}}$ on $S_{\max}$. It clearly demonstrates the significant changes of $S_{\text{op,phen}}/S_{\max}$ versus R for plane stress.
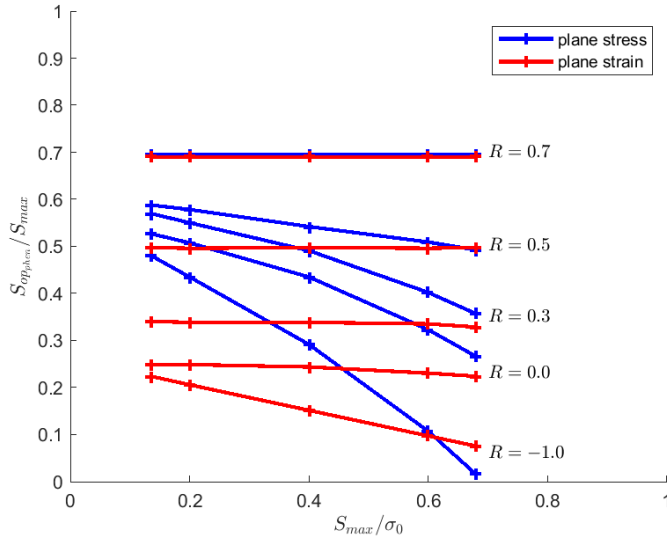

Figure 2.3: Opening stress $S_{\text{op,phen}}/S_{\max}$ versus the ratio of $S_{\max}$ over the flow stress σ_0 for a range of R values, for both plane stress and plane strain.; reproduced from [32].

Furthermore, McClung [42] notes that the correlation of ratio of $S_{\max}$ over the flow stress σ_0 and $S_{\text{op,phen}}/S_{\max}$ works for CCT specimens only, as the correlation of this ratio and $S_{\text{op,phen}}/S_{\max}$ for other geometries and/or loading conditions is not successful. A new correlation is obtained by introducing a normalized stress intensity parameter $\Delta K_{max}/K_0$, which appears to work well for small-scale yielding. This example serves to illustrate that improvements or corrections to Equation (2.1) are sought using other parameters, rather than looking at the discrepancy between $S_{\text{op,phys}}$ and $S_{\text{op,phen}}$. This results in corrections to the phenomenological description of ΔK, and does not necessarily constitute a physically correct approach.

It is shown that closure corrections, even with fitting parameters or alterations to the ΔK_{eff} method, are not complete in describing crack closure. This paper suggests therefore another approach: an explanation and a solution for the incompleteness can be found in the opening stress itself: $S_{\text{op,phen}} \neq S_{\text{op,phys}}$. They are related, but not equal. The true background of $S_{\text{op,phen}}$ is explained in more detail further on.

2

2.4. An energy equivalent area approach to $S_{\text{op,phen}}$

Alderliesten [51] provides a first step to an energy related explanation of crack closure corrections. An energy equivalent area analogy is presented, showing that $\Delta S_{\text{eff}} = S_{\text{max}} - S_{\text{op,phen}}$ is correlated to the actual cyclic energy applied between S_{min} and S_{max}, through an equivalent area in the stress-strain curve. It is best explained graphically, using the bilinear force-displacement curves in Figure 2.4. For a given S_{max}, S_{min}, and an elastic material, the area under the curve between ε_{min} and ε_{max} relates to the cyclic energy ΔU. A rectangular area is spanned by a strain range $0 \leq \varepsilon \leq \varepsilon_{\text{max}}$ and a stress range $S_{\text{op,phen}} \leq S \leq S_{\text{max}}$ such that the area is equal to ΔU, and is called the equivalent area.
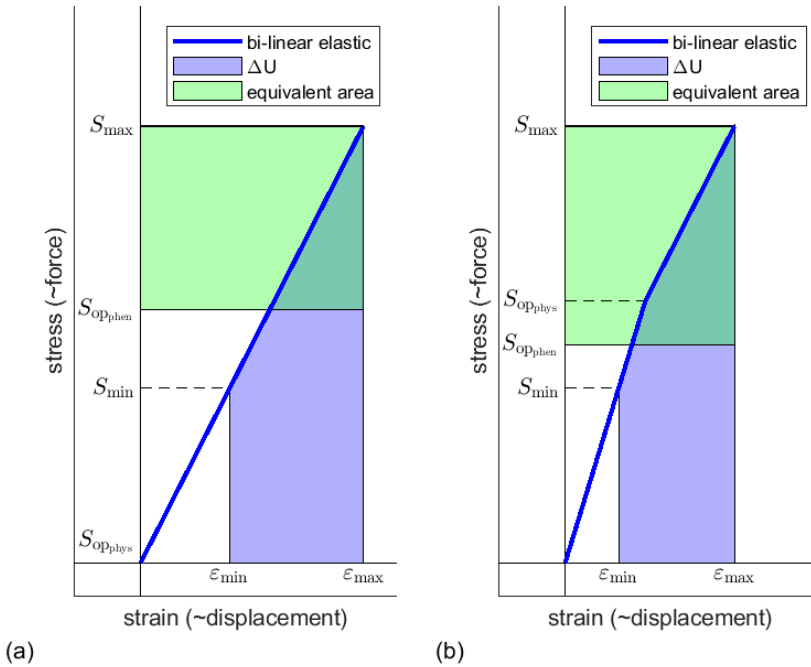

Figure 2.4: Schematic bilinear stress-strain curves, explaining the energy equivalent area analogy of Alderliesten [51] and the difference between $S_{\text{op,phys}}$ and $S_{\text{op,phen}}$. (a): $S_{\text{op,phys}} = 0$. (b): $S_{\text{op,phys}} > 0$.

Alderliesten assumed for this example that the crack opens or closes at $S = 0$,

seen as a change of slope at this stress level. In reality the crack opening happens at a positive stress value $S_{op,phys}$, ref. [10], and the change of slope is actually a gradual nonlinear change over a certain small stress range. Crack tip plasticity effects will smooth the transition between a closed and an open crack.

For modeling purposes, the stress-strain loading curve is simplified as a bilinear elastic curve with an instant change of slope at a positive nonzero $S_{op,phys}$ value. Both simplifications; the bilinear approximation, and only considering the loading curve, do not alter the applicability or trend of the energy equivalent area analogy. Both cases in Figure 2.4 are rather similar, but show how the true crack opening stress alters the stress-strain slope and subsequent decrease of ε_{max}.

The difference in absolute U values in Figure 2.4 is irrelevant since these are two different cases. The equivalent area approach holds for each individual case separately, and links the ΔU area to the rectangular equivalent area within that particular case. The increase of $S_{op,phys}$ thus results in a larger ΔU and equivalent area, which is only possible with a smaller $S_{op,phen}$.

This improved analogy obtains $S_{op,phen}/S_{max}$ values which closely follow known closure corrections, although the equivalent area has no direct physical meaning. It explains how $S_{op,phen}$ can be derived from the actual cyclic energy ΔU, but shows that this value is not equal to $S_{op,phys}$.

The analogy holds for all R. For sufficiently large R close to 1, where $S_{min} > S_{op,phys}$, the energy equivalent area approach shows correctly that the crack stays open during the full cycle: $S_{min} > S_{op,phen}$. The closure corrections however still predict $S_{op,phen} > S_{min}$.

Closure corrections can be described as corrections for closure effects with respect to the ideal bilinear elastic case where closure happens at $S_{op,phys} = 0$, shown in Figure 2.5. The stress-strain curve for the ideal bilinear elastic case is similar to case (a) in Figure 2.4. Alderliesten [51] demonstrated that the ideal bilinear elastic case can be derived using the energy equivalent area approach. The area under the curve (such as shown in Figure 2.4) is a function of R^2 (relates to the stress values), and a function of $S_{op,phys}$ (which influences the corresponding strain). Existing closure corrections are effectively correcting this ideal bilinear elastic case, $S_{op,phys} = 0$, for cases where $S_{op,phys} \neq 0$, however not by using $S_{op,phys}$ but using the virtual $S_{op,phen}$ value. The corrections become more pronounced for decreasing R as plasticity and reverse plasticity effects increase.

Figure 2.4 is a function of R^2 (relates to the stress values), and a function of $S_{op,phys}$ (which influences the corresponding strain). For $S < 0$, a compressive energy is present, but this does not affect crack growth as the crack is closed during this phase of the load cycle. The ideal bilinear elastic case therefore remains constant for $R < 0$, while the actual total cyclic energy increases as the sum of the tensile and compressive energy. The ideal curve can be described analytically:

$$
\begin{aligned}
\left.\frac{S_{op,phen}}{S_{max}}\right|_{elastic} &= \frac{1}{2} + \frac{1}{2}R^2 \quad && \text{for } R \geq 0 \\
\left.\frac{S_{op,phen}}{S_{max}}\right|_{elastic} &= \frac{1}{2} && \text{for } R < 0
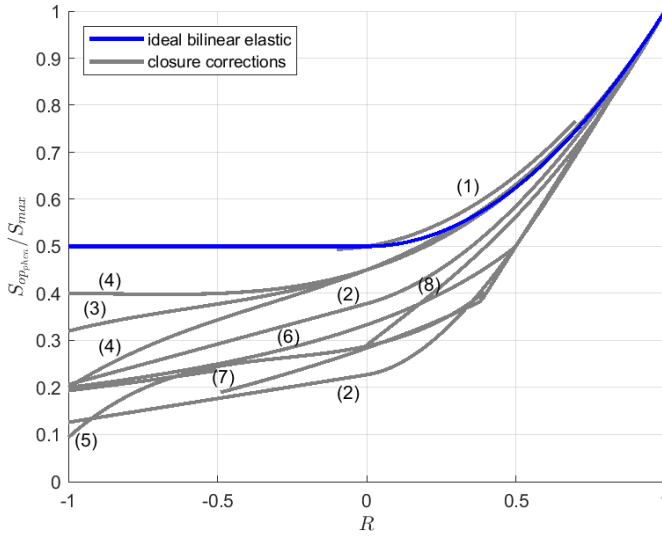\end{aligned}
\tag{2.3}
$$

Figure 2.5: Closure corrections; as $S_{op,phen}/S_{max}$ versus R. Shown are: Elber[1], Newman[2], Schijve[3], De Koning[4], Iwasaki[5], Kurihara et al.[6], Overbeeke et al.[7], Correia et al.[8], and the ideal bilinear elastic case as described by Alderliesten with closure at $S_{op,phys} = 0$.

Correcting the ideal bilinear case for $S_{op,phys} \neq 0$ results in $S_{op,phen}$ values similar to existing closure corrections. The approach of Alderliesten [51] therefore also holds for $S_{op,phys} \neq 0$, providing a link between $S_{op,phys}$ and $S_{op,phen}$.

2.5. A spring analogy to crack closure using $S_{op,phys}$

The physics based energy approach put forward by Alderliesten is extended below with a model of the crack closure effect. Figure 2.6 shows the storable energy in a plate with a crack for two different R values: $R < 0$ and $R > 0$ with in both cases $S_{op,phys} > S_{min}$. It is a similar schematic stress-strain curve as Figure 2.4, but compressive energy is taken into account for negative R. It is assumed that the crack is either fully open or fully closed: there is a distinct region with linear elastic stiffness E_0 (crack closed), and a region with linear elastic stiffness E_1 (crack open), with $E_1 < E_0$.

Consider a uniaxially loaded fatigue plate specimen. It is either loaded in tension or compression, or unloaded. With a crack present, it is convenient to model the plate as two springs of different stiffness working in parallel, with an equal displacement constraint. Figure 2.7 provides a schematic view of this model. If the plate has developed a crack, the spring system is no longer linear elastic for all S. Below the opening stress $S_{op,phys}$, the total stiffness still equals E_0. At the opening stress $S_{op,phys}$ the stiffness changes to just E_1 (note that the line with slope E_1 does not start at the origin). The change in stiffness is expressed as $E_\Delta = E_0 - E_1$.
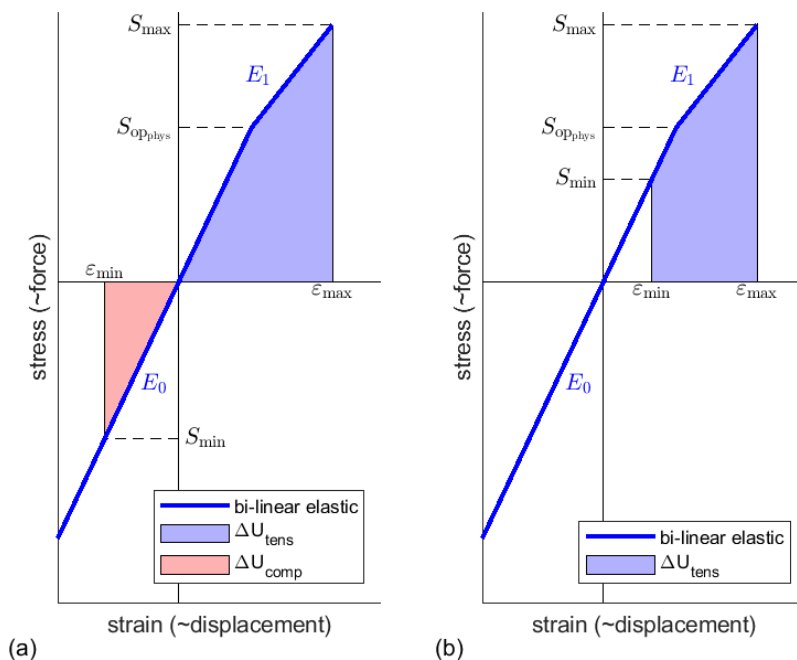
2

Figure 2.6: Two schematic force-displacement curves for a CCT fatigue specimen: (a) for $R < 0$, and (b) for $R > 0$. Tensile energy area depicted in blue, compressive energy area depicted in red.
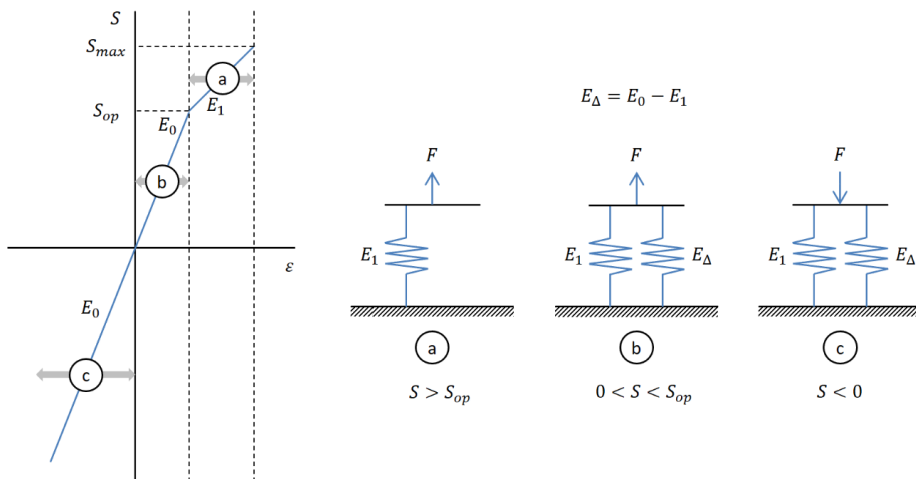

Figure 2.7: Schematic view of two-spring system analogy of a linear elastic cracked plate. Two parallel springs of different stiffness represent the plate stiffness. Case (a) shows an open crack: decreased stiffness and one spring is absent from model.

The cyclic energy, the change in energy during loading, is equal to the area under the force-displacement curve $f(\varepsilon)$ of the plate, and indicated with ΔU:

$$\Delta U = \Delta U_{\text{tens}} \text{ for } R \geq 0$$
$$= \int_{\varepsilon_{\text{min}}}^{\varepsilon_{\text{max}}} f(\varepsilon)\, d\varepsilon$$
$$\Delta U = \Delta U_{\text{comp}} + \Delta U_{\text{tens}} \text{ for } R < 0 \tag{2.4}$$
$$= -\int_{\varepsilon_{\text{min}}}^{0} f(\varepsilon)\, d\varepsilon + \int_{0}^{\varepsilon_{\text{max}}} f(\varepsilon)\, d\varepsilon$$

More specifically, the cyclic energy ΔU is the sum of the three regions or a part thereof, depending on the value of S_{min} and $S_{\text{op,phys}}$:

$$\Delta U = \Delta U_a \text{ for } S_{\text{op,phys}} < S_{\text{min}} \leq S_{\text{max}}$$
$$= \int_{\varepsilon_{\text{min}}}^{\varepsilon_{\text{max}}} f(\varepsilon)\, d\varepsilon$$
$$\Delta U = \Delta U_b + \Delta U_a \text{ for } 0 < S_{\text{min}} \leq S_{\text{op,phys}}$$
$$= \int_{\varepsilon_{\text{min}}}^{\varepsilon_{S_{\text{op,phys}}}} f(\varepsilon)\, d\varepsilon + \int_{\varepsilon_{S_{\text{op,phys}}}}^{\varepsilon_{\text{max}}} f(\varepsilon)\, d\varepsilon \tag{2.5}$$
$$\Delta U = \Delta U_c + \Delta U_b + \Delta U_a \text{ for } S_{\text{min}} \leq 0$$
$$= -\int_{\varepsilon_{\text{min}}}^{0} f(\varepsilon)\, d\varepsilon + \int_{0}^{\varepsilon_{S_{\text{op,phys}}}} f(\varepsilon)\, d\varepsilon + \int_{\varepsilon_{S_{\text{op,phys}}}}^{\varepsilon_{\text{max}}} f(\varepsilon)\, d\varepsilon$$

ΔU is the total cyclic energy stored in the plate. The change in stiffness during loading results in increased cyclic energy. The energy equivalent area approach then obtains a lower $S_{\text{op,phen}}$ compared to the linear elastic case. Contrary to the ideal bilinear elastic curve outlined earlier, it is assumed that the compressive component of the cyclic energy is also involved even though the crack is closed during this part of the cycle: elastic stresses and reverse plasticity occur around the crack tip, influencing crack opening in the next loading phase.

Furthermore, this physics based approach does not need fitting parameters as used in several closure corrections such as Newman [18] and [17]. The use of FEA to obtain $S_{\text{op,phys}}$ values already includes S_{yield} and a/W effects. This also reduces the need for fatigue tests to gather phenomenological fitting data.

2.6. Finite element analysis to obtain $S_{\text{op,phys}}$

In order to find true opening stress $S_{\text{op,phys}}$, and given the difficulties of determining it experimentally, a finite element simulation approach was chosen. Literature contains many finite element analysis studies investigating crack closure effects. The majority of these are 2D simulations, refs. [42, 50, 52–59], using either plane stress or plane strain conditions. Newman [60] notes that since the

mid-1980s relatively few 3D FEA studies have been undertaken, refs. [61–64]. Kotousov et al., ref. [65], note that progress in 3D FEA is still well behind that of 2D FEA. In nearly all FEA studies, the crack is instantaneously extended at maximum load, which corresponds well with measurement data. FEA of small crack growth, ref. [66], might raise questions regarding the mesh size in comparison to the plastic zone size, but apart from that, literature shows that closure can be modeled well with FEA. The FEA analysis discussed below uses instantaneous crack extension at maximum load, and simulates a developed crack and plastic zone, in accordance with FEA studies in literature.

A finite element analysis was performed with SIMULIA Abaqus software on a CCT plane stress plate under constant amplitude (CA) loading. Symmetry conditions apply, therefore only one quarter of the plate was simulated. An infinitely stiff beam was used to model contact along the crack path. Figure 2.8 shows the quarter plate and a detail of the mesh around the crack tip. A 2D mesh of quadrilateral element type CPS4R was generated, with enhanced hourglassing control for error reduction. An FEA mesh study showed that a two times finer mesh resulted in similar convergence rates, and similar $S_{\mathrm{op,phys}}$ values ($< 3\%$). The material was an elastic-plastic model of Al 2024-T3, ref. [67], of which the stress versus engineering strain curve is given in Figure 2.9. This is a monotonic elastic-plastic curve. A cyclic curve may be used as well without changing the validity of the method. Crack opening was defined as contact removal between the node pair directly behind the crack tip. The starter crack length equals $a = 10\,\mathrm{mm}$, on a total plate width of $160\,\mathrm{mm}$.
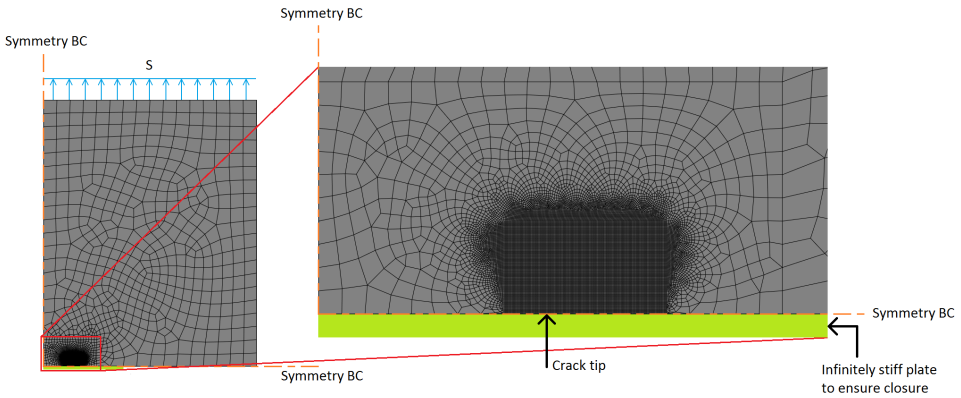

Figure 2.8: FEA model of CCT specimen, with detail of mesh. Due to symmetry conditions, only one quarter of the plate is modeled; center of plate at the left lower corner. Stress S is distributed as a pressure over the plate edge.

FEA simulations were made at different S_{max} values over the range $-1 \leq R \leq 1$ in steps of 0.05. For each R, the model was run for 24 full cycles, with each half cycle divided in 200 equidistant partial loading steps. At maximum load of each cycle, a node on the crack center line was released to simulate crack propagation of one
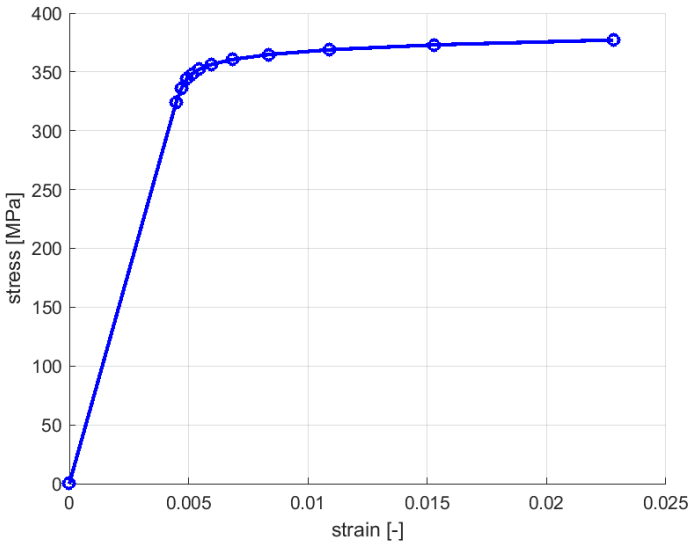
Figure 2.9: Stress versus engineering strain curve of Al 2024-T3 material used for the opening stress FEA. Curve based on data from [67]. Dots indicate the points used in the Abaqus material model, which linearly interpolates in between them.

element distance; 0.05 mm. Note that the simulation does not try to mimic a realistic increase of the crack growth rate over a significant part of the crack life, but rather, it tries to obtain the opening stress at a crack length which is (nearly) constant. This strengthens the assumption of constant da/dN (equal to one element length), and constant a/W. The initial crack length is 10.00 mm, the end crack length is 11.20 mm, giving a final crack length over width ratio of $a/W = 0.07$. Figure 2.10 shows details of the loading sequence and the node release.

The instant during the cycle where crack opening occurs is cross-referenced with the applied loading curve, to obtain the corresponding opening stress value $S_{\text{op,phys}}$. The FEA results showed that for every R value, within a few cycles the $S_{\text{op,phys}}$ value had already converged to a steady state value, and the $S_{\text{op,phys}}$ value of the last cycle was taken as the steady state value for that particular R value. Figure 2.11 shows such convergence of the opening stress for $R = 0.5$: within a few cycles, the crack tip plastic zone is well developed and reaches a steady state. This plastic zone development is the result of starting the FEA at a crack length without any plasticity history from prior cycles.

Katcher [68], Zhang [69], and Newman [52] mention that releasing a node at maximum load is a realistic approach to crack growth simulation, and together with Schijve [16] they also suggest that steady state opening and closing stresses are generally observed to be quite similar which vindicates this approach to find the opening stress to assess closure effects.

The results of the FEA analysis is shown in Figure 2.12, for different values of
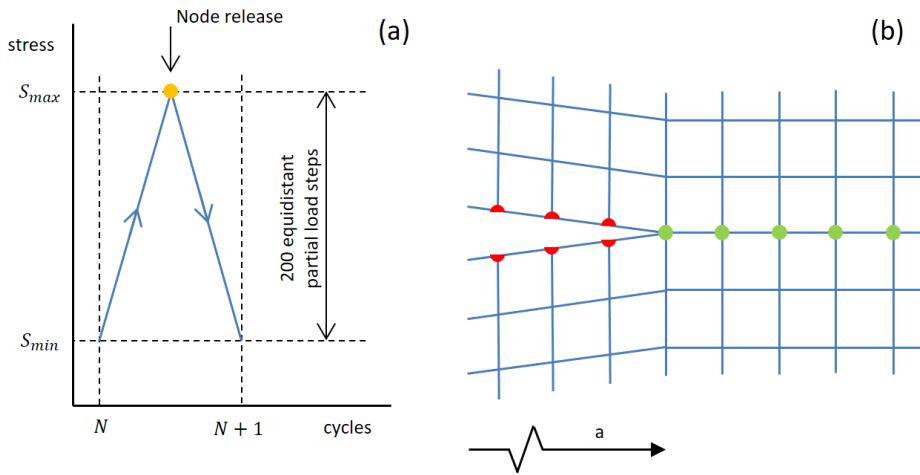
2

Figure 2.10: (a): Schematic view of one cycle in the CA spectrum, indicating the 200 loading steps per half cycle and when mesh nodes are released to simulate crack growth. (b): Schematic mesh around crack tip, with the horizontal crack plane shown in red (cracked) and green (uncracked) nodes.
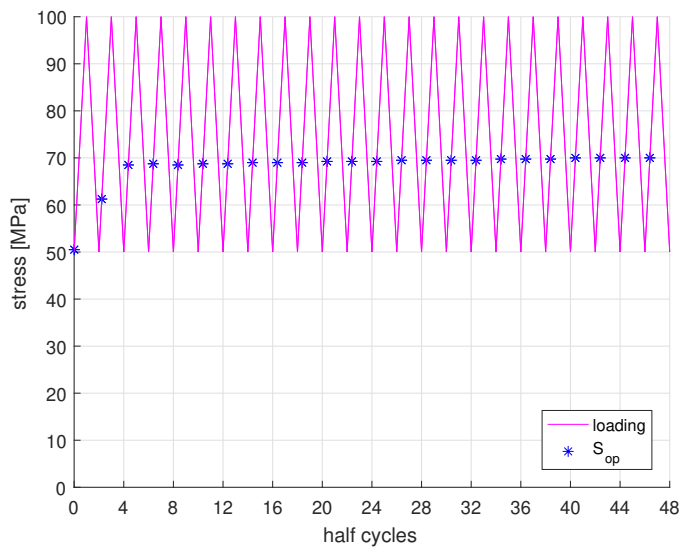

Figure 2.11: FEA convergence of opening stress of Al 2024-T3 plate at $S_{\max} = 100$ MPa and $R = 0.5$ over 24 cycles, $a/W = 0.07$. Within a few cycles the opening stress is already close to the stabilized end level. The $S_{\mathrm{op,phys}}$ value of the last cycle is used for analysis.

S_{max}. Note that these are $S_{\mathrm{op,phys}}/S_{\mathrm{max}}$ values. Four distinct R regions are observed in each data set. In region 1 and 2 the values of $S_{\mathrm{op,phys}}/S_{\mathrm{max}}$ are linear functions of R, but the slopes are different. It is hypothesized that the more shallow slope of region 1 is a consequence of the force-displacement curve of the plate being influenced more by the closure effect at negative R. The compressive energy increases the reverse plasticity volume, thereby slightly raising the $S_{\mathrm{op,phys}}$ value for the subsequent cycles. compared to the trend of region 2. Region 3 shows a transition to a crack that never fully closes. The FEA simulation shows that crack opening happens increasingly early with increasing R, until $S_{\mathrm{op,phys}} = S_{\mathrm{min}}$. This upper limit matches the apparent maximum R limit where closure can be experimentally observed (such as $R = 0.7$ in Newman's data, ref. [18]). In region 4 ($R \gtrsim 0.7$) the crack stays open during the full cycle, and as a result the simulation assumes $S_{\mathrm{op,phys}} = S_{\mathrm{min}}$, meaning that the crack opens immediately at the beginning of the cycle.
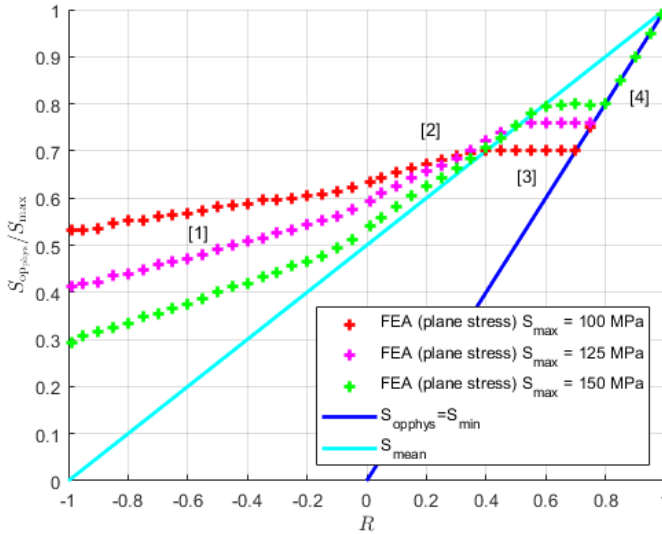

Figure 2.12: FEA results: $S_{\mathrm{op,phys}}/S_{\mathrm{max}}$ versus R, plane stress, $a/W = 0.07$. The four bracketed numbers indicate four distinct discernible R regions of each curve.

Three FEA data sets are shown in Figure 2.12. Even though $S_{\mathrm{op}}/S_{\mathrm{max}}$ values are normalized with respect to S_{max}, there is still an obvious S_{max} dependency. In regions 1 and 2 it holds that for a given R, an increase in S_{max} results in a decrease of $S_{\mathrm{op,phys}}/S_{\mathrm{max}}$. This trend becomes stronger for smaller R, and is the equivalent of closure corrections moving away (down) from the ideal bilinear elastic curve. The increased S_{min} values for a given R result in more compressive stress, which needs to be overcome before the crack opens. This provides a physical explanation for the observations of Newman [32], as shown in Figure 2.3, but now explained using FEA. Furthermore, the boundary between region 1 and 2 is observed to stay

2

around $R = 0$ for all cases as compressive stress only becomes significant for $R < 0$. The slope of region 1 slightly increases at larger $S_{\max}$, lowering the aforementioned $S_{\mathrm{op,phys}}/S_{\max}$ values. Increasing $S_{\max}$ also increases the R value at which the crack stays permanently open (boundary between region 3 and 4).

It should not be attempted to directly compare the FEA opening stress results with other closure corrections from literature, as $S_{\mathrm{op,phys}} \neq S_{\mathrm{op,phen}}$. Assuming that the FEA results are representative of real fatigue tests, ΔU values for each point can be obtained by determining the area under the actual force-displacement graph for each corresponding $S_{\max}$ and R value. As explained earlier, the force displacement curve is modeled as bilinear, with a change of slope at $S = S_{\mathrm{op,phys}}$. The energy equivalent area analogy then reworks the $S_{\mathrm{op,phys}}$ based ΔU values into $S_{\mathrm{op,phen}}/S_{\max}$ values, which are shown in Figure 2.13. Note how these reworked FEA results closely follow the known closure correction trends, and the obtained values are mainly within the spread of various published closure corrections. This implies that the $S_{\mathrm{op,phen}}$ values found by the known crack closure corrections are a good measure of the equivalent area, but do not constitute the physical opening stress $S_{\mathrm{op,phys}}$.
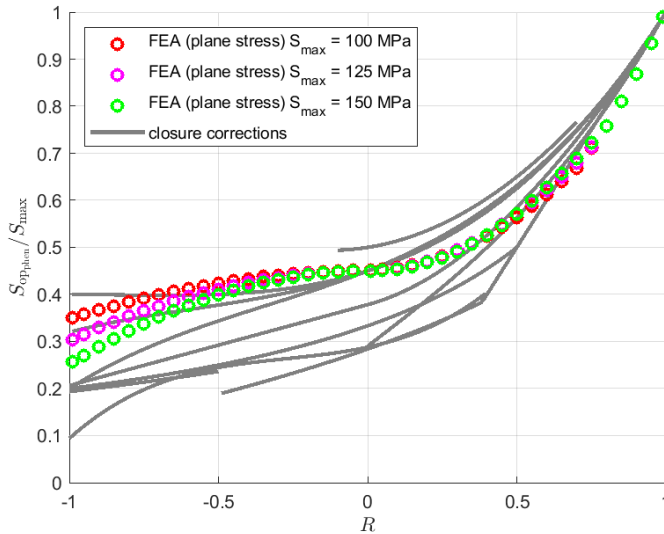

Figure 2.13: Energy equivalent approach results from FEA output. The $S_{\mathrm{op,phys}}/S_{\max}$ data from Figure 2.12 is reworked to $S_{\mathrm{op,phen}}/S_{\max}$ versus R. Three $S_{\max}$ cases at $a/W = 0.07$ are shown. While $S_{\mathrm{op,phen}}/S_{\max}$ is assumed to correct for an $S_{\max}$ dependency, there is still a clear $S_{\max}$ dependency, most pronounced at negative R.

Another observation from the FEA is also seen in literature for different metals and alloys: the R dependency of the effective stress intensity factor ratio. This ratio is defined as:

$$U_{\mathrm{SIF}} = \frac{\Delta K_{\mathrm{eff}}}{\Delta K} \tag{2.6}$$

Maljaars et al. [70] have compiled several equations of U_{SIF} for steel and aluminum from literature, refs. [3, 23–25, 71–73], including the respective valid R ranges. Figure 2.14 shows (a), a comparison of the effective SIF ratio U_{SIF} for steel reproduced from ref. [70], and (b), the calculated effective SIF ratio for Al 2024-T3 from the FEA data. The trend for the curves is similar, even though the absolute values differ, likely due to the different material parameters considered, such as S_{yield} and E. The flat section of $U_{\mathrm{SIF}} = 1$ near $R = 1$ is correctly predicted by FEA, showing R values for which the crack is permanently open ($S_{\mathrm{min}} > S_{\mathrm{op,phys}}$).
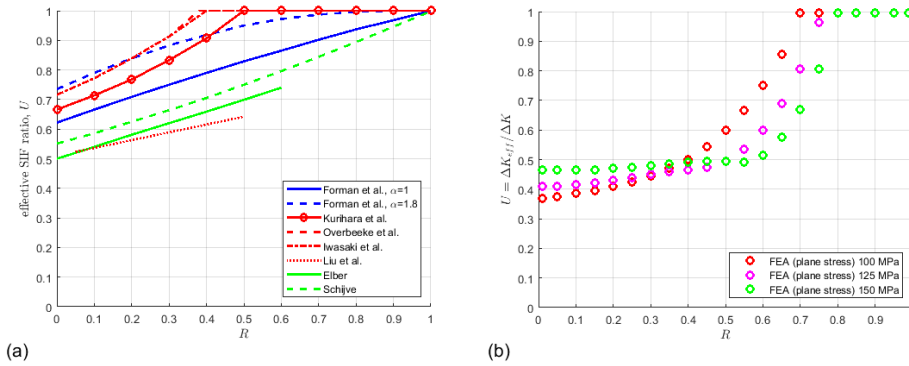

Figure 2.14: Comparison of effective SIF ratios for plane stress. (a) Reproduced from [70], showing data for steel (red) and aluminum (green) from [3, 23–25, 71–73]. (b) Reworked FEA results for the same R range for Al 2024-T3. Both show a flat section near $R = 1$, meaning that the crack is permanently open.

2.7. Closure corrections and the finite width correction

Fatigue specimens have a finite width, contrary to most theoretical models, including crack closure models. The finite width causes the crack growth to increase faster compared to the theoretical ideal infinite plate case. As the crack grows in a finite width plate, the remaining cross-section decreases, causing the net-section stress over the crack plane to increase. This effect is usually accounted for in ΔK_{eff}, Equation (2.1), by a finite width correction β. For completeness it must be stated that β generally can include other effects as well, such as a crack front shape correction. Given the thin plate with a through crack used here, it is assumed that β includes only the finite width effect.

There are various analytical expressions for β, often as a function of a and W; the Feddersen equation, ref. [74], is well known. Similar to the closure corrections it holds that these equations can be excellent approximations (of experimental data)

2

but they do not describe the underlying physics. The finite width correction β follows from the change in specimen compliance due to reduced stiffness resulting from the decreasing cross-section. Zhao et al. [75, 76] and Alderliesten [77] describe this effect from a physics standpoint in the non-isotropic composite material GLARE, but it holds for isotropic materials as well since it is a consequence of the geometry, not the material.

Crack closure is a local phenomenon around the crack tip, and is related to the local stress state and amount of crack tip plasticity. In a finite width specimen, this local stress increases related to the global specimen compliance, for reasons explained above. For a given R and $S_{\max}$, crack closure is thus affected by the ratio a/W. During crack growth a/W and β increase, leading to increased stress around the crack tip, which results in the value of $S_{\mathrm{op,phen}}/S_{\max}$ decreasing. This movement of the closure correction is schematically shown in Figure 2.15. It appears that closure corrections from literature implicitly assume $S_{\mathrm{op,phen}} \neq \mathrm{f}(a)$, likely because the effect is small for positive R values. The R range of the original closure correction by Elber [10] (Figure 2.1) contains mostly positive R values, and presumably the crack length dependency therefore went unnoticed.

The spread in closure corrections from literature mentioned earlier can be partly explained by different a/W ratios in the measurements. Since these a/W ratios are not reported, it is difficult to assess the extent of the finite width effect on known closure corrections from literature. To properly observe crack closure by experimental methods such as COD, it is beneficial to have a sufficiently large crack length a and a corresponding large change in specimen compliance upon loading (large da/dN). Because the finite width effect acts on local phenomena such as crack closure, it is therefore not the cause of the difference between $S_{\mathrm{op,phen}}/S_{\max}$ and $S_{\mathrm{op,phys}}/S_{\max}$ which are based on global parameters. It does mean that both $S_{\mathrm{op,phen}}/S_{\max}$ and $S_{\mathrm{op,phys}}/S_{\max}$ are $f(R, S_{\max}, S_{\mathrm{yield}}, a/W)$. The FEA approach of finding $S_{\mathrm{op,phys}}$ already contains the a/W dependency, removing the need for phenomenological fitting and correction parameters in the proposed model.

2.8. Variable amplitude crack growth prediction with energy based closure correction for ΔK_{eff}

Many models for variable amplitude (VA) fatigue prediction make use of the ΔK_{eff} Equation (2.1): crack closure models and strip yield models such as ONERA [78], CORPUS [79, 80], PREFFAS [81], NASGRO [12], and refs. [82–85], based on Dugdale's original work regarding strip yield models, ref. [86]. In this section it is shown that the energy based closure correction may be used to obtain more accurate values for $S_{\mathrm{op,phen}}$ from $S_{\mathrm{op,phys}}$, on a cycle-to-cycle basis, compared to strip yield models.

A typical VA model would predict the $S_{\mathrm{op,phen}}$ value for each load cycle, taking into account a certain amount of the spectrum history. Schijve [16] states that strip yield models are superior to other types of (global stress based) crack closure models, since the crack geometry around the crack tip is directly modeled. This statement corresponds with the idea that a strip yield model should be based on
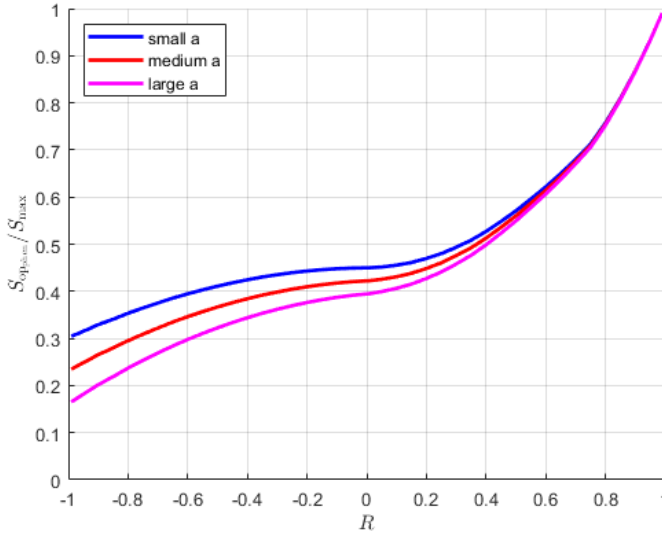
Figure 2.15: Illustration of the effect of finite width on crack closure. The finite width of a specimen increases the crack growth rate due to increased net-section stress on the remaining crack plane cross-section. As a result, crack tip plasticity increases too, lowering $S_{op,phen}/S_{max}$. For a given S_{max}, the crack closure correction moves down as the crack progresses.

$S_{op,phys}$, Figure 2.12, rather than on $S_{op,phen}$, Figure 2.13. However, Matias et al. [87] evaluated the strip yield model of NASGRO [12] for various aircraft loading spectra (VA), and reported that it correlates reasonably only for negative R ratios. Note that for a given S_{max}, positive R values affect the tensile energy terms ΔU_a and ΔU_b of Equation (2.5) which are dependent on $S_{op,phys}$, while negative R values affect only the compressive energy term ΔU_c where the crack is closed. The energy approach outlined earlier can therefore be a more suitable candidate for fatigue modeling at any R: it works over the full R range unlike several closure corrections and strip yield methods, and it does not need scaling or fitting parameters as the energy based physics approach is used to obtain $S_{op,phys}$ and $S_{op,phen}$. It is thereby also applicable for VA spectrum modeling. We will now discuss the qualitative example of an overload in a CA spectrum introducing crack growth retardation.

Consider a cracked plate loaded with a CA fatigue spectrum at a small positive R with a single overload. A schematic view of the force-displacement curves of the plate at various cycles during the spectrum is given in Figure 2.16. The cyclic energy ΔU during the few CA cycles just before the overload can be considered essentially constant. When the single overload cycle occurs, the increase in S_{max} increases ΔU. It also raises the amount of plasticity and therefore $S_{op,phys} = f(S_{min}, S_{max})$ significantly. While for subsequent cycles the S_{max} value has returned to the CA spectrum level, the crack needs to grow through the enlarged plastic zone generated by the overload, which slowly lowers $S_{op,phys}$ from the elevated level back

to its original level. Our method correctly predicts this behavior from the physical $S_{\mathrm{op,phys}}$ instead of the phenomenological $S_{\mathrm{op,phen}}$.
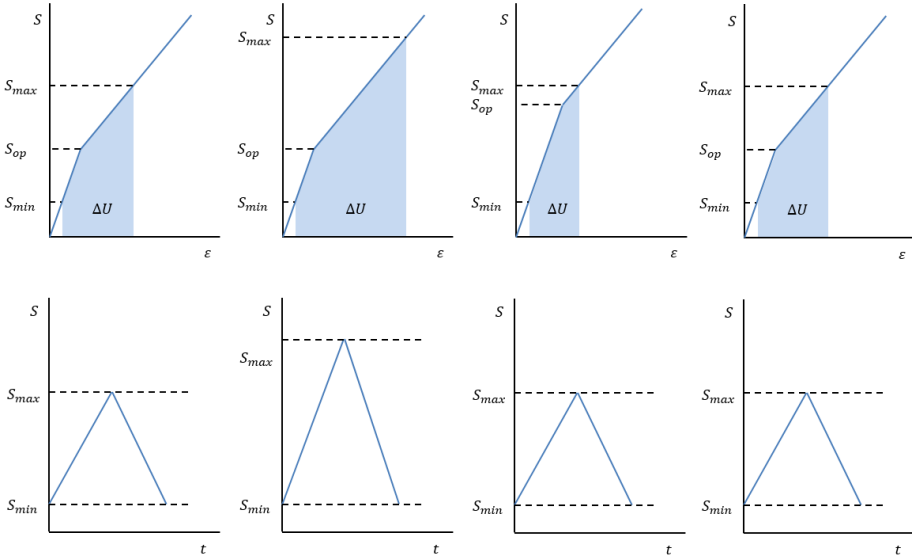

Figure 2.16: Schematic view of ΔU (top) during a CA spectrum (bottom) with a single overload. Four specific cycles in the spectrum are shown, from left to right: a CA spectrum before an overload, a single overload, the first CA cycle after overload, a CA cycle many cycles after the overload.

Refs. [16, 88] report that the opening stress $S_{\mathrm{op,phen}}$ indeed changes after an overload. Figure 2.17 is reproduced from ref. [88]. From the energy equivalent area approach it follows that $S_{\mathrm{op,phys}}$ will have a similar behavior. It proves that our theoretical model of the effect of an overload on a CA spectrum is in agreement with what is reported in literature, such as results from COD measurements.

In a truly random VA spectrum, every half cycle sees a new (S_{min}, S_{max}) pair. $S_{\mathrm{op,phys}}$ and ΔU change virtually every half cycle, but a steady state is never reached during each half cycle. This means that the $S_{\mathrm{op,phys}}$ and ΔU are continuously chasing a non-existing CA equilibrium which changes each half cycle. The history of many consecutive cycles (ideally all previous cycles), needs to be taken into account to properly model the behavior of $S_{\mathrm{op,phys}}$, ΔU, plasticity, and da/dN, in order to understand and predict VA fatigue crack growth. Amsterdam [89] describes a method that uses a maximum reference stress different from S_{max} to account for VA spectra and pivot points. Pivot points connect multiple power law exponents at different crack length ranges of a Paris type crack growth curve. The altering of the maximum stress results in better power law curve fitting of the crack growth rate, but implicitly leaves $S_{\mathrm{op,phys}}$ unaffected. Applying the method proposed here, i.e. calculating $S_{\mathrm{op,phys}}$ for each half cycle, would give a similar outcome to the Amsterdam approach, as it would affect the ΔS_{eff} used in the ΔK_{eff} equation. Our method therefore gives a physical explanation for the ΔK_{eff} value used in the Amsterdam
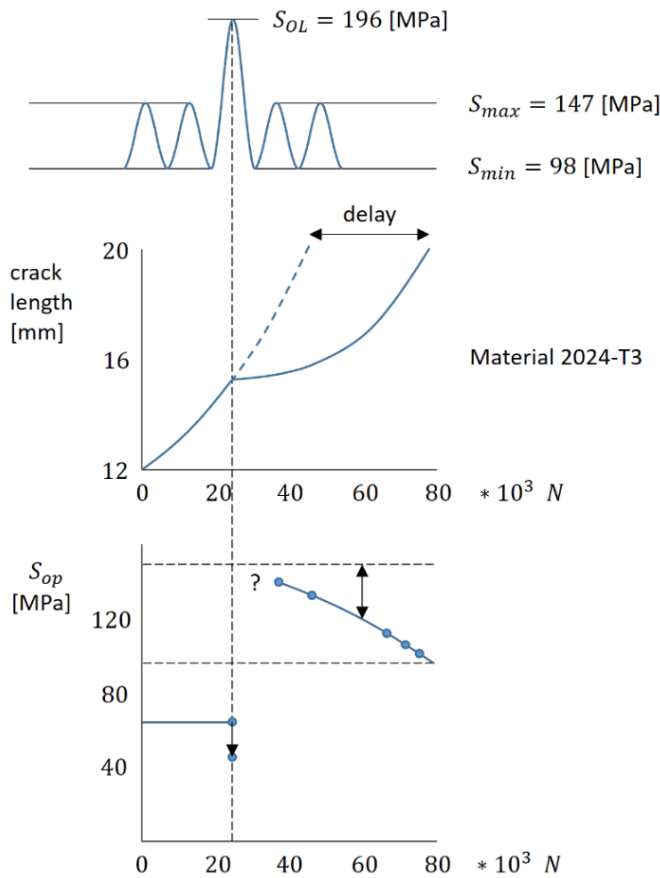
2

Figure 2.17: CA spectrum with a single overload, associated crack growth retardation, and associated $S_{op,phen}$ measured with a COD technique. Figure reproduced from Schijve [88].

approach.

The shortcomings of the closure corrections and the inconsistency between plasticity effects and the LEFM ΔK_{eff} approach suggest that an energy based approach ($S_{\mathrm{op,phys}}$, the elastic spring model, and the energy equivalent area approach) is an improvement over existing methods to properly include closure and plasticity effects. It results in more accurate descriptions of $S_{\max}$, $S_{\mathrm{op,phys}}$, and a/W effects on the crack growth behavior, which can improve modeling accuracy for CA and VA fatigue. VA fatigue modeling will likely still require a cycle-by-cycle prediction method to include the (full) loading history effects on $S_{\mathrm{op,phys}}$.

This new physics based approach is more realistic than existing closure models, as it is based on the true opening stress. It may be the way forward to increase prediction and modeling accuracy for both CA and VA fatigue crack growth cases.

2.9. Conclusions

Ample fatigue crack growth closure corrections exist which result in opening stress S_{op} values used in the ΔK_{eff} approach. Literature shows that these corrections still do not fully account for closure effects, and that they have a large spread. This led to the hypothesis that there are two distinct S_{op} values: $S_{\mathrm{op,phen}}$ used in the ΔK_{eff} approach, and $S_{\mathrm{op,phys}}$ which is the true crack opening stress. The subsequent investigation has shown that this is true, and resulted in the following conclusions:

1. Many known closure corrections, refs. [10, 16–18] result in different corrections for the same phenomenon, for unknown reasons. Our research suggests that existing closure corrections do not properly take into account the physical opening stress $S_{\mathrm{op,phys}}$.

2. The same known closure corrections, refs. [10, 16–18], contain empirically determined correction factors, and different corrections result in different $S_{\mathrm{op}}/S_{\max}$ values based on $S_{\mathrm{op,phen}}$ for the same load cycle. Our results suggest that these observations may be explained by a failure to correctly account for the effect of $S_{\max}$ and a/W on the physical opening stress $S_{\mathrm{op,phys}}$. Thus the corresponding $S_{\mathrm{op,phen}}$ needs to be corrected to make up for this.

   By applying the equivalent energy approach, ref. [51], a value of $S_{\mathrm{op,phen}}$ can be determined based on the correct $S_{\mathrm{op,phys}}$, as found via FEA. The $S_{\mathrm{op,phen}}$ values found in this way matches the $S_{\mathrm{op,phen}}$ found via previously known correction methods, but without relying on empirical correction factors. Thus our new method is more physically realistic, and potentially requires less experimental calibration than existing methods.

3. FEA shows that $S_{\mathrm{op,phys}}$ follows four distinct regions over the full R range. From low to high R, these are: tensile-compressive loading with closure, tensile-tensile loading with closure, transition to an always open crack, and an always open crack. In the last case, it can be assumed that $S_{\mathrm{op,phys}} = S_{\min}$. Using the energy equivalent area analogy to obtain $S_{\mathrm{op,phen}}$ values for the full

R range, the FEA results show close agreement with known correction curves, especially for $R \geq 0$. This confirms that $S_{\mathrm{op,phen}}$ in $S_{\mathrm{op,phen}}/S_{\max}$ is not the true opening stress.

4. FEA confirmed that it at least holds that $S_{\mathrm{op,phys}} = f(R, S_{\max})$ and that the derived $S_{\mathrm{op,phen}}/S_{\max} = f(R, S_{\max})$ too.

During crack growth, the local net-section stress in the crack plane increases due to the finite width effect. This does not affect $S_{\max}$, but it does affect the local phenomenon which is crack closure. During crack growth at constant R and $S_{\max}$, the $S_{\mathrm{op,phen}}/S_{\max}$ or $S_{\mathrm{op,phys}}/S_{\max}$ values slowly decrease because of the decreasing cross-section area. This dependency on a/W is not mentioned in literature, but may partly explain the spread of closure corrections.

Furthermore, several closure corrections include a fitting parameter to match measurement data, which tends to be dependent on R. In literature it is noted that $S_{\mathrm{op,phen}}$ also depends on the ratio between $S_{\max}$ and σ_0, where σ_0 is related to S_{yield}.

These observations combined suggest that $S_{\mathrm{op,phen}} = f(R, S_{\max}, S_{\mathrm{yield}}, a/W)$ and $S_{\mathrm{op,phys}} = f(R, S_{\max}, S_{\mathrm{yield}}, a/W)$.

Inclusion of the energy approach into the ΔK_{eff} equation may improve the accuracy over known models. $S_{\mathrm{op,phys}}$ might be found through FEA or strip yield models. For VA fatigue a cycle-by-cycle integration of the loading history might still be necessary to keep track of changes in $S_{\mathrm{op,phys}}$ and subsequent $S_{\mathrm{op,phen}}$.

Acknowledgments

References

[1] J. J. A. van Kuijk, R. C. Alderliesten, and R. Benedictus, *Unraveling the myth of closure corrections: Sharpening the definition of opening and closure stresses with an energy approach,* International Journal of Fatigue **143**, 106016 (2021).

[2] P. C. Paris, M. P. Gomez, and W. E. Anderson, *A rational analytic theory of fatigue,* The Trend in Engineering **13**, 9 (1961).

[3] W. Elber, *Fatigue crack closure under cyclic tension,* Engineering Fracture Mechanics **2**, 37 (1970).

[4] J. Schijve, *Some formulas for the crack opening stress level,* Engineering Fracture Mechanics **14**, 461 (1981).

[5] H. H. Van der Linden, *NLR test results as a database to be used in a check of crack propagation prediction models: A Garteur activity*, Tech. Rep. NLR TR 79121 (Nederlands Lucht- en Ruimtevaartcentrum, 1979).

[6] H. L. Ewalds and R. T. Furnée, *Crack closure measurement along the fatigue crack front of center cracked specimens,* International Journal of Fracture **14**, R53 (1978).

[7] R. Sunder and P. K. Dash, *Measurement of fatigue crack closure through electron microscopy,* International Journal of Fatigue **4**, 97 (1982).

[8] M. N. James and J. F. Knott, *Critical aspects of the characterization of crack tip closure by compliance techniques,* Materials Science and Engineering **72**, L1 (1985).

[9] K. Minakawa, J. C. Newman Jr., and A. J. McEvily, *A critical study of the crack closure effect on near-threshold fatigue crack growth,* Fatigue & Fracture of Engineering Materials & Structures **6**, 359 (1983).

[10] W. Elber, *The significance of fatigue crack closure,* ASTM STP 486 (1971), pp. 230–242.

[11] J. A. Harter, *AFGROW users guide and technical manual*, Tech. Rep. AFRL-VA-WP-TR-1999-3016 (Wright-Patterson Air Force Base, 1999).

[12] R. C. McClung, *NASGRO Fracture Mechanics & Fatigue Crack Growth Analysis Software*, Tech. Rep. (Southwest Research Institute, 2002).

[13] J. C. Newman Jr., *FASTRAN. A fatigue crack growth life-prediction code based on the crack-closure concept. User guide version 5.4*, Tech. Rep. (Fatigue & Fracture Associates, LLC, 2013).

[14] P. Paris and F. Erdogan, *A Critical Analysis of Crack Propagation Laws,* Journal of Basic Engineering **85**, 528 (1963).

[15] P. C. Paris, *Fracture mechanics and fatigue: A historical perspective,* Fatigue & Fracture of Engineering Materials & Structures (Print) **21**, 535 (1998).

[16] J. Schijve, *Fatigue of Structures and Materials*, 2nd ed. (Springer Science+Business Media B.V., 2009).

[17] A. U. De Koning, *Crack growth prediction methods, Part 1: A survey*, Tech. Rep. NLR TR 84121 L Part I (Nederlands Lucht- en Ruimtevaartcentrum, 1984).

[18] J. C. Newman Jr., *A crack opening stress equation for fatigue crack growth,* International Journal of Fatigue **24**, 131 (1984).

[19] R. Jones and D. Tamboli, *Implications of the lead crack philosophy and the role of short cracks in combat aircraft,* Engineering Failure Analysis **29**, 149 (2013).

[20] P. C. Paris, D. Lados, and H. Tada, *Reflections on identifying the real ΔKeff in the threshold region and beyond,* Engineering Fracture Mechanics **75**, 299 (2008), International Conference of Crack Paths.

[21] P. C. Paris, H. Tada, and J. Keith Donald, *Service load fatigue damage — a historical perspective,* International Journal of Fatigue **21**, S35 (1999).

[22] R. Jones and S. Pitt, *An experimental evaluation of crack face energy dissipation,* International Journal of Fatigue **28**, 1716 (2006).

[23] T. Iwasaki, A. Katoh, and M. Kawahara, *Fatigue crack growth under random loading,* International Journal of Naval Architecture and Ocean Engineering **20**, 194 (1982).

[24] M. Kurihara, A. Katoh, and M. Kawahara, *Effects of stress ratio and step loading on fatigue crack propagation ratio,* in *Current research on fatigue cracks (Current Japanese Materials Research)* (Elsevier Applied Science, London, 1987).

[25] J. L. Overbeeke and J. de Back, *The influence of stress relieving and R-ratio on the fatigue of welding joints,* in *Fatigue of welded constructions: international conference, Brighton, England, 7-9 April 1987*, edited by S. Maddox (Welding Institute, United Kingdom, 1988) pp. 11–22.

[26] A. Clerivet and C. Bathias, *Study of crack tip opening under cyclic loading taking into account the environment and r ratio,* Engineering Fracture Mechanics **12**, 599 (1979).

[27] T. T. Shih and R. P. Wei, *A study of crack closure in fatigue,* Engineering Fracture Mechanics **6**, 19 (1974).

[28] H. L. Ewalds, *The effect of environment on fatigue crack closure in aluminium alloys,* Engineering Fracture Mechanics **13**, 1001 (1980).

[29] B. R. Kirby and C. J. Beevers, *Slow fatigue crack growth and threshold behaviour in air and vacuum of commercial aluminium alloys,* Fatigue & Fracture of Engineering Materials & Structures **1**, 203 (1979).

[30] S. Suresh, A. K. Vasudevan, and P. E. Bretz, *Mechanisms of slow fatigue crack growth in high strength aluminum alloys: Role of microstructure and environment,* Metallurgical Transactions A **15**, 369 (1984).

[31] A. K. Vasudevan and D. Kujawski, *Implications of ΔK-R ratio in vacuum,* Fatigue & Fracture of Engineering Materials & Structures **45**, 1739 (2022).

[32] J. C. Newman Jr., *A crack-closure model for predicting fatigue crack-growth under aircraft spectrum loads*, Tech. Rep. NASA TM 81941 (National Aeronautics and Space Administration, 1981).

[33] A. K. Vasudevan, K. Sadananda, and N. Louat, *A review of crack closure, fatigue crack threshold and related phenomena,* Materials Science and Engineering **A188**, 1 (1994).

[34] R. S. Vecchio, J. S. Crompton, and R. W. Hertzberg, *Anomalous aspects of crack closure,* International Journal of Fracture **31**, R29 (1986).

[35] R. E. Garz and M. N. James, *Observations on evaluating fatigue crack closure from compliance traces,* International Journal of Fatigue **11**, 437 (1989).

[36] R. I. Murakami, Y. H. Kim, and W. G. Ferguson, *The effects of microstructure and fracture surface roughness on near threshold fatigue crack propagation characteristics of a two-phase cast stainless steel,* Fatigue & Fracture of Engineering Materials & Structures **14**, 741 (1991).

[37] M. Okazaki, A. J. McEvily, and T. Tanaka, *The wedge mechanism of fatigue crack growth in silicon nitride,* Materials Science and Engineering: A **143**, 135 (1991), structural Materials: Properties, Microstructure and Processing.

[38] B. K. Parida and T. Nicholas, *Effect of stress ratio on fatigue crack growth in a titanium aluminide alloy,* International Journal of Fracture **52**, R51 (1991).

[39] S. A. Seetharam and P. K. Dash, *Load-CMOD data analysis for crack closure,* International Journal of Fracture **53**, R53 (1992).

[40] M. P. Gómez, H. Ernst, and J. Vázquez, *On the validity of Elber's results on fatigue crack closure for 2024-T3 aluminum,* International Journal of Fracture **12**, 178 (1976).

[41] N. Louat, K. Sadananda, M. Duesbery, and A. K. Vasudevan, *A theoretical evaluation of crack closure,* Metallurgical Transactions A **24**, 2225 (1993).

[42] R. C. McClung, *Finite element analysis of specimen geometry effects on fatigue crack closure,* Fatigue Fracture Engineering Materials Structures **17**, 864 (1994).

[43] J. Kim and S. Lee, *Fatigue crack opening stress based on the strip-yield model,* Theoretical and Applied Fracture Mechanics **34**, 73 (2000).

[44] J. A. F. O. Correia, A. M. P. De Jesus, P. M. G. P. Moreira, and P. J. S. Tavares, *Crack closure effects on fatigue crack propagation rates: Application of a proposed theoretical model,* Advances in Materials Science and Engineering **2016**, 3026745 (2016).

[45] Q. Duan, J. Li, Y. Li, Y. Yin, H. Xie, and W. He, *A novel parameter to evaluate fatigue crack closure: Crack opening ratio,* International Journal of Fatigue **141**, 105859 (2020).

[46] D. Kujawski, *ΔKeff parameter under re-examination,* International Journal of Fatigue **25**, 793 (2003), international Conference on Fatigue Damage of Structural Materials IV.

[47] J. T. P. Castro, M. A. Meggiolaro, and J. A. O. González, *Can Delta Keff be assumed as the driving force for fatigue crack growth?* Frattura ed Integrità Strutturale **9**, 97 (2015).

[48] J. Newman and J. Ruschau, *The stress-level effect on fatigue-crack growth under constant-amplitude loading,* International Journal of Fatigue **29**, 1608 (2007), fatigue Damage of Structural Materials VI.

[49] R. McClung and H. Sehitoglu, *On the finite element analysis of fatigue crack closure — 1. Basic modeling issues,* Engineering Fracture Mechanics **33**, 237 (1989).

[50] R. McClung and H. Sehitoglu, *On the finite element analysis of fatigue crack closure — 2. Numerical results,* Engineering Fracture Mechanics **33**, 253 (1989).

[51] R. C. Alderliesten, *The explanation of stress ratio effect and crack opening corrections for fatigue crack growth in metallic materials,* in *11th International Fatigue Congress*, Advanced Materials Research, Vol. 891 (Trans Tech Publications Ltd, 2014) pp. 289–294.

[52] J. C. Newman Jr., *A finite-element analysis of fatigue crack closure,* ASTM STP 590 (1976), pp. 281–301.

[53] K. Ohji, K. Ogura, and Y. Ohkubo, *Cyclic analysis of a propagating crack and its correlation with fatigue crack growth,* Engineering Fracture Mechanics **7**, 457 (1975).

[54] M. Nakagaki and S. N. Atluri, *Elastic-plastic analysis of fatigue crack closure in modes I and II,* AIAA Journal **18**, 1110 (1980).

[55] A. F. Blom and D. K. Holm, *An experimental and numerical study of crack closure,* Engineering Fracture Mechanics **22**, 997 (1985).

[56] N. Fleck, *Finite element analysis of plasticity-induced crack closure under plane strain conditions,* Engineering Fracture Mechanics **25**, 441 (1986).

[57] E. J. Bednarz, *A numerical study of plasticity induced closure in short cracks by the finite element method*, PhD dissertation, Air Force Institute of Technology, Wright-Patterson Air Force Base (1990).

[58] T. Nicholas, A. Palazotto, and E. Bednarz, *An analytical investigation of plasticity induced closure involving short cracks,* ASTM STP 982 (1988), pp. 361–379.

[59] H. Sehitoglu, K. Gall, and A. M. Garcia, *Recent advances in fatigue crack growth modeling,* International Journal of Fatigue **80**, 165 (1996).

[60] J. C. Newman Jr., *The merging of fatigue and fracture mechanics concepts: a historical perspective,* Progress in Aerospace Sciences **34**, 347 (1998).

[61] R. G. Chermahini, K. N. Shivakumar, and J. C. Newman Jr., *Three-dimensional finite-element simulation of fatigue crack growth and closure,* ASTM STP 98 (1988), pp. 398–413.

2

[62] R. G. Chermahini and A. F. Blom, *Variation of crack-opening stresses in three-dimensions: finite thickness plate,* Theoretical and Applied Fracture Mechanics **15**, 267 (1991).

[63] D. S. Dawicke, A. F. Grandt Jr., and J. C. Newman Jr., *An inverse method for the calculation of through-thickness fatigue crack closure behavior,* ASTM STP 1131 (1992), pp. 46–57.

[64] J. Newman, C. Bigelow, and K. Shivakumar, *Three-dimensional elastic-plastic finite-element analyses of constraint variations in cracked bodies,* Engineering Fracture Mechanics **46**, 1 (1993).

[65] A. Kotousov, A. Khanna, R. Branco, A. M. De Jesus, and J. A. Correia, *Review of current progress in 3d linear elastic fracture mechanics,* in *Mechanical Fatigue of Metals*, edited by J. A. Correia, A. M. De Jesus, A. A. Fernandes, and R. Calçada (Springer International Publishing, Cham, 2019) pp. 125–131.

[66] J. LLorca, *Roughness-induced fatigue crack closure: a numerical study,* Fatigue Fracture Engineering Materials Structures **15**, 655 (1992).

[67] FAA US, *Metallic materials properties development and standardization (MM-PDS),* Federal Aviation Administration, Washington, DC, Paper No. MMPDS-05 (2010).

[68] M. Katcher, *Crack growth retardation under aircraft spectrum loads,* Engineering Fracture Mechanics **5**, 793 (1973).

[69] J. Zhang and P. Bowen, *On the finite element simulation of three-dimensional semi-circular fatigue crack growth and closure,* Engineering Fracture Mechanics **60**, 341 (1998).

[70] J. Maljaars, R. Pijpers, and H. Slot, *Load sequence effects in fatigue crack growth of thick-walled welded C–Mn steel members,* International Journal of Fatigue **79**, 10 (2015).

[71] G. S. Booth and S. J. Maddox, *Correlation of fatigue crack growth data obtained at different stress ratios,* ASTM STP 982 (1988), pp. 516–527.

[72] Y.-P. Liu, C.-Y. Chen, and G.-Q. Li, *Fatigue crack growth and control of 14MnNbq welding plates used for bridges,* Journal of Engineering Mechanics **138**, 30 (2012).

[73] J. Schijve, *Fatigue crack closure, observations and technical significance*, Tech. Rep. LR-485 (Delft University of Technology, Department of Aerospace Engineering, 1986).

[74] C. E. Feddersen, *Discussion,* ASTM STP 410 (1966), pp. 77–79.

[75] Y. Zhao, R. C. Alderliesten, Z. Zhou, G. Fang, J. Zhang, and R. Benedictus, *On the physics of applying finite width and geometry correction factors in fatigue crack growth predictions of GLARE,* International Journal of Fatigue **117**, 189 (2018).

[76] Y. Zhao, R. C. Alderliesten, Z. Wu, Z. Zhou, G. Fang, J. Zhang, and R. Benedictus, *Determining finite-width-correction factors for fatigue crack growth prediction in GLARE using the equivalent compliance method,* International Journal of Fatigue **127**, 74 (2019).

[77] R. C. Alderliesten, *Fatigue and Fracture of Fibre Metal Laminates*, 2nd ed., Solid Mechanics and Its Applications, Vol. 236 (Springer International Publishing AG, 2017).

[78] G. Baudin and M. Robert, *Crack growth model for flight type loading,* in *Proceeding of the 11th ICAF Symposium in the Netherlands* (1981).

[79] A. U. De Koning, *A simple crack closure model for prediction of fatigue crack growth rates under variable-amplitude loading,* ASTM STP 743 (1981), pp. 63–85.

[80] A. U. De Koning and H. H. Van der Linden, *Prediction of fatigue crack growth rates under variable loading using a simple crack closure model*, Tech. Rep. NLR MP 81023 U (Nederlands Lucht- en Ruimtevaartcentrum, 1981).

[81] D. Aliaga, A. Davy, and H. Schaff, *A simple crack closure model for predicting fatigue crack growth under flight simulation loading,* ASTM STP 982 (1988), pp. 491–504.

[82] H. Führing and T. Seeger, *Dugdale crack closure analysis of fatigue cracks under constant amplitude loading,* Engineering Fracture Mechanics **11**, 99 (1979).

[83] H. D. Dill and C. R. Saff, *Spectrum crack growth prediction method based on crack surface displacement and contact analyses,* ASTM STP 595 (1976), pp. 306–319.

[84] D. J. Dougherty, A. U. De Koning, and B. M. Hillberry, *Modeling high crack growth rates under variable amplitude loading,* ASTM STP 1122 (1992), pp. 214–233.

[85] G. Wang and A. Blom, *A strip model for fatigue crack growth predictions under general load conditions,* Engineering Fracture Mechanics **40**, 507 (1991).

[86] D. Dugdale, *Yielding of steel sheets containing slits,* Journal of the Mechanics and Physics of Solids **8**, 100 (1960).

[87] C. Matias and E. Katsav, *Evaluation of the strip-yield retardation model for predictions of fatigue crack growth under typical aircraft loading spectra,* in *Proceedings of the 27th Symposium of the International Committee on Aeronautical Fatigue and Structural Integrity, Jerusalem, Israel* (2013).

[88] J. Schijve, *Observations on the prediction of fatigue crack growth propagation under variable-amplitude loading,* ASTM STP 595 (1976), pp. 3–23.

[89] E. Amsterdam, *Effect of crack length and reference stress on variable amplitude fatigue crack growth rate,* in *ICAF 2019 – Structural Integrity in the Age of Additive Manufacturing*, edited by A. Niepokolczycki and J. Komorowski (Springer International Publishing, Cham, 2020) pp. 539–550.

2

3

Potential drop through the cycle

To improve resolution of in-situ measurement of crack closure and opening in fatigue, potential drop (PD) measurement technique has been further developed to measure thousands of times through each load cycle with high precision. The results are interpreted with physical phenomena like strain, Poisson's effect, piezo-resistivity, plasticity, and crack growth. Application of the technique to fatigue crack growth tests on Al 2024-T3 CCT specimens at different maximum stresses and stress ratios, demonstrate that indeed variations in PD can be associated to development of plasticity and crack opening and closure. Hence, the technique allows to measure timing and magnitude of crack opening and closure stresses in-situ in fatigue crack growth experiments.

3.1. Introduction

Fatigue crack growth of long cracks in metal alloys can be described using linear elastic fracture mechanics (LEFM). It is often expressed as the crack growth rate da/dN versus a similitude parameter ΔK, function of crack length a and maximum stress $S_{\max}$, or ΔK_{eff}, which is a function of the crack length a, maximum stress $S_{\max}$, and stress ratio R. Measurement of the crack length is generally performed using in situ observations of the specimen surface [2], or using a clip gauge to measure specimen compliance. Crack length measurements can also be performed using the potential drop (PD) technique [3–9], which measures the electrical potential over the remaining cross-section area of the crack plane in metal or other electrical conductive materials, and relates this analytically to the average crack length. Si et al. [10] provide an extensive review of the various PD techniques and their application. While not directly addressing the measurement of crack opening and closure, they do note that PD is reported to be an accurate crack length measurement tool for various crack geometries and loading conditions.

ASTM International provides the E 647 standard [11] on usage of the technique for compact tension C(T), middle tension M(T), and eccentrically-loaded single edge crack tension ESE(T) specimen types since 1978. Compared to (manual) photograph analysis, PD can be measured at each individual cycle which generates larger data sets, to which smoothing and averaging techniques can be applied, resulting in crack length and crack growth rate data of higher resolution and better quality. Furthermore, PD gives a significantly improved estimate of the mean crack progression as it measures the conductive area along the crack plane, rather than only the crack length on the specimen surface.

Most crack growth literature discusses phenomenological approaches and results, based on measurements and simulations. Many theoretical models of plasticity and crack opening and closure share the same limitation: the related (similitude) parameters are expressed per full cycle, implicitly assuming that changes per cycle are instantaneous or averaged over the cycle; d/dN. In reality, crack growth and plasticity development do not occur instantaneously and are dependent on the applied load throughout the cycle. This dependency can be expressed as function $f(d/dt)$, where t is either the real time, or a fictitious, nondimensional time where a cycle runs from $t = 0$ to $t = 1$. The latter option has the advantage of decoupling the observed signal changes from the applied test frequency, and is the time definition used in this paper. Fatigue phenomena are generally not time dependent [2], except for secondary effects like creep or corrosion which tend to be orders of magnitude smaller. Integrating the aforementioned function over one full cycle results in a value belonging to that specific cycle:

$$\int_{t_N}^{t_{N+1}} f\left(\frac{d}{dt}\right) dt = \left[\frac{d}{dN}\right]_N \tag{3.1}$$

If fatigue phenomena such as crack growth and plasticity are observable with the potential drop technique, their behavior and development can be tracked during

each cycle using multiple potential drop measurements per cycle. Such a measurement system was developed for this study, and is called: 'potential drop through the cycle', or PD TTC. Of interest here is the work of Andersson et al. [12], who used PD measurements and in situ SEM observations during fatigue tests, albeit not continuously. Notable conclusions are that crack opening and closure are the main contributors to the observed PD curve shape, suggesting that PD is capable of measuring these events.

Figure 3.1 illustrates several different stages during a fatigue cycle, the associated plasticity, and electrical path length. It is clear that the measurement path length is affected, and that it traverses plastically deformed regions which vary in size during a cycle. A standard PD setup takes high frequency measurement(s) at $S_{\max}$ only during each cycle (stage (d) in Figure 3.1) to prevent closure effects from interfering with the potential measurement, and is therefore unable to capture these effects. The difference in the signal over a period of one cycle from maximum load to maximum load relates to the crack growth rate da/dN found with standard PD measurements. In Figure 3.1, it would be from stage (d) in cycle N to stage (d) in cycle $N + 1$.

The PD TTC setup can perform several hundred to several thousand measurements during each cycle. This high frequency measurement rate throughout the full S range and improved resolution allow for observing the development of the potential through each cycle, creating the opportunity to study the development of plasticity and crack growth within each cycle. This idea is further developed in this paper.

3.2. Crack opening and closure: the added value of potential drop through the cycle

Elber [13] introduced the concept of crack opening and closure: the crack is open only during part of the cycle, and closed during the other part. Of the different sources reported for this crack tip opening and closure (plasticity, roughness, asperity, etc.) the current work focuses on plasticity induced crack closure and opening, which is generally considered the dominant source.

The related similitude parameter ΔK_{eff} is supposed to incorporate the closure effect and thereby removing the stress ratio effect R, as improvement over the ΔK similitude parameter. Based on this assumption, the closure concept has led to multiple crack closure models such as [2, 13–18] which are phenomenologically derived, and validated for various metals, alloys, and R ranges. This closure-based ΔK_{eff} concept is an improvement but not fully successful, given discussions in literature [19–26]. This is partly due to the actual opening and closure happening over a certain range of loading and time [13, 27], rather than being instantaneous, and there is some uncertainty regarding the definition of opening and closure [2].

Part of this uncertainty is due to measurement techniques. Crack opening and closure is generally measured using the crack opening displacement (COD) technique. The basic concept is a strain gauge applied in loading direction over the center of the crack, or over the very crack tip, to measure how the local strain

(a) Minimum load
(b) Crack tip plasticity starts
(c) Opening stress reached
(d) Maximum load, crack has grown
(e) Just after maximum load
(f)   Closing stress, crack has closed
(g) Reverse plasticity starts
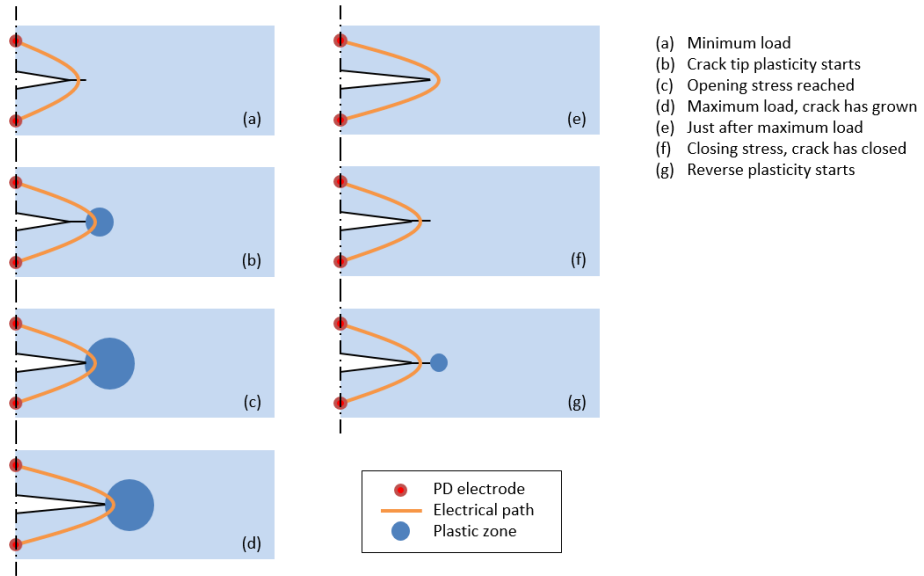
PD electrode
Electrical path
Plastic zone

Figure 3.1: Schematic view of the PD measurement electric path through a fatigue specimen, at several stages during a fatigue cycle. The applied current flows vertically in each stage.

changes with the globally applied loading. A change of the slope in this correlation signals the occurrence of opening or closure, but the method is not precise in observing the exact strain and load where the slope becomes constant [2, 13, 27]. Pippan et al. [28] performed fatigue tests with both PD measurements and strain gauge measurements near the crack tip, and noted that strain gauge measurements may be less accurate than the PD measurements.

One of the reasons is that the physical gauge locations are influenced by plastic deformation, while this effect is neither accounted for nor corrected for in the COD technique. Convention states that crack opening S_{op} occurs when the crack tip first becomes fully open. Similarly, crack closure S_{cl} happens when the crack tip first starts to close. Schijve [29] states that the values of S_{op} and S_{cl} are generally found to be sufficiently close enough, that S_{op} is used for the closure corrections and the ΔK_{eff} parameter.

It is possible to measure the potential change during crack opening and crack closure with a PD technique, because it will observe changes in potential when the crack length changes. Since these events are connected with the growth of the plastic zone at the crack tip, development of this zone might affect the signal too. From Figure 3.1 it can be inferred that the change in potential $d\phi$ within a cycle might not be linearly related to the instantaneous crack extension da. This leads to the hypothesis that measurements from a potential drop through the cycle (PD TTC) technique can be used to relate energy dissipation events such as crack growth and crack tip plasticity development, as well as true crack opening and true

crack closure, to specific time intervals and time instants within a fatigue cycle.

Crack opening and closure can be studied in greater detail using PD TTC. In earlier work [30], the authors pointed out that there is a difference between the physical opening stress $S_{op,phys}$ and the phenomenological opening stress $S_{op,phen}$. $S_{op,phys}$ is the true stress at which the crack tip opens, which is challenging to measure accurately as no measurement devices can measure at the crack tip itself. Only FEA appears to be able to give accurate $S_{op,phys}$ values. The $S_{op,phen}$ values are widely used by closure corrections and the ΔK_{eff} approach, but originate from measurements in the vicinity of the crack tip, not directly at it. $S_{op,phys}$ and $S_{op,phen}$ can be linked through an energy equivalent area approach [30, 31]. PD TTC can indirectly observe the true physical opening stress $S_{op,phys}$, which can be reworked into a $S_{op,phen}$ value for existing closure corrections. The same procedure holds for reworking $S_{cl,phys}$ into $S_{cl,phen}$.

The PD TTC technique in general measures a potential over a crack in a specimen, and the change of potential is the summation of several effects. These effects are only present during parts of a cycle and with varying magnitude, such as extension of the crack and crack tip plasticity growth. The development of these effects can be analyzed from the potential, and are explained in more depth below, to illustrate the applicability and suitability of the PD TTC technique.

3.3. Change of potential through one cycle

The measured potential is the result of the constant direct current applied to the specimen and the electrical resistance between the PD electrodes, through Ohm's law:

$$\phi = \Omega I \qquad (3.2)$$

The resistance Ω changes due to the strain resulting from the applied loading, and crack growth. Assume that at any given point in time the electrical situation is constant. The specimen is a conductor of uniform cross-section with a uniform current, such that the resistance can be calculated using Pouillet's law:

$$\Omega = \rho \frac{L}{A} \qquad (3.3)$$

Where the specimen geometry parameters length L and cross-section area A, and the resistivity coefficient ρ relate to the total electrical resistance.

The value of ϕ in Equation (3.2) will change when Ω changes, as I is constant. It is this potential that is measured with the PD setup.

Two effects have a major influence on the change of Ω: the Poisson effect, which changes with the geometry of the conductor, and piezoresistivity, which changes the resistivity coefficient. Both effects are explained below, and are both present globally when loading is applied to a specimen. There are also two fatigue crack growth specific effects, which are local subsets of the aforementioned effects: crack tip plasticity, and crack extension. Crack tip plasticity changes the local geometry

and increases local strain; it is a combined effect of the Poisson effect and piezore-
sistivity. Crack growth results in a cross-section area reduction and effective over-
all stiffness reduction: it relates to the Poisson effect. Furthermore it results in a
lengthening of the PD electrical conductive path. A schematic view of the electrical
conductive path is presented in Figure 3.2, showing how crack growth and plas-
ticity affect the conductivity. The relations between the four effects are shown in
Figure 3.3, and discussed in more detail further on.
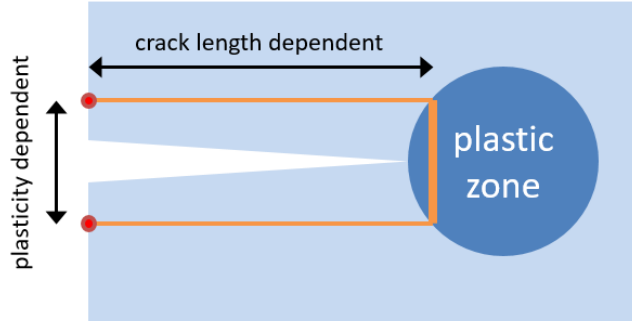
Figure 3.2: Schematic view of a fatigue specimen with a crack (one half of a CCT specimen). Crack
tip plasticity is present. The effective PD TTC measurement electric path around the crack is shown in
orange, connecting the two red electrodes. The current flows vertically through the specimen.
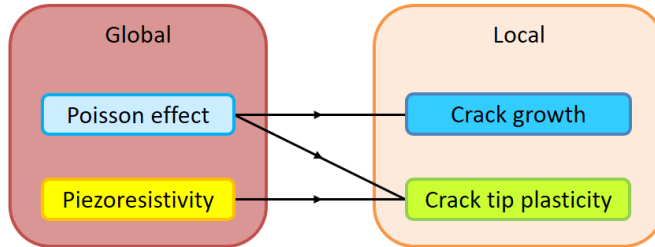

Figure 3.3: A schematic view of how the global and local PD effects are related.

3.3.1. Poisson effect

Consider a unit cell of a homogeneous isotropic material. When a mechanical load
is applied in one direction, then the geometry will elongate in the loading direc-
tion, and contract in the transverse directions. The elongation and contractions are
related through the Poisson's ratio ν:

$$\nu = -\frac{d\varepsilon_{\text{transversal}}}{d\varepsilon_{\text{axial}}} \tag{3.4}$$

For $\nu \neq \frac{1}{2}$ which holds for most materials and metals, a change in strain results in a change in volume. A fatigue specimen acts as a large unit cell, similarly affected by the Poisson effect. When (a part of) the metal specimen is used as an electrical conductor, the geometric changes due to loading will cause a change of electrical resistance over this conductor. A tensile load increases the length between the electrodes, and decreases the cross-section. Both increase the resistance of the conductor.

The change of potential for a given strain can be derived using the following equations. Consider a unit cell of length L^*, cross-section area $A^* = (L^*)^2$, and volume $V^* = (L^*)^3$. Upon an elongation of amount $\Delta L^* = \varepsilon L^*$, resulting in a new length $L^*_\text{new} = L^* + \Delta L^*$, the ratio of the new volume over the initial volume becomes:

$$\frac{\Delta V^*}{V^*} = \left(1 + \frac{\Delta L^*}{L^*}\right)^{(1-2\nu)} - 1 \tag{3.5}$$

The new volume then becomes:

$$V^*_\text{new} = V^* + V^* \frac{\Delta V^*}{V^*} \tag{3.6}$$

And the new cross-section area follows from:

$$A^*_\text{new} = \frac{V^*_\text{new}}{L^*_\text{new}} \tag{3.7}$$

Substituting L^*_new and A^*_new into Equations (3.2) and (3.3), results in the new electric potential. For a typical value of $\nu = 0.33$ for Al 2024-T3 [32], the volume increases when a tensile load is applied. For an electric conductor, not the volume but the length and the cross-section are of importance. In this case, the length increases faster than the volume, and through Equation (3.7) the cross-section is found to decrease. Both the increased length and the reduced cross-section result in a higher electric resistance, and thus an increased potential.

3.3.2. Piezoresistivity

Piezoresistivity is the change in the electrical resistance of a metal when mechanical strain is applied. The resistivity coefficient ρ in Equation (3.3) is affected by temperature [33] and mechanical loading [34–39], which both alter the strain on the material. The mechanical loading dependency is of interest here, as most tests are performed at constant temperature. Hunter and Nabarro [34] mention that electrons tend to flow from compressed to expanded regions, meaning that tensile strained regions attract electrons and thus lower the resistivity. This holds for the whole elastically strained specimen, but also for local plastically strained zones such as the crack tip plastic zone. The change is dependent on the crystal structure, and varies therefore with the type of metal and alloy. For typical metal fatigue specimens the effect is observed to be small, less than 0.1 % of the total resistivity. For aluminum it holds that the resistance decreases with increasing strain.

Morozov et al. [40] show this nonlinear behavior between the strain and the electrical resistance of thin aluminum rectangular strip specimens. Figure 3.4 shows this relationship for Al 2024-T3 strips for various amounts of plastic strain and for longitudinal and transverse grain directions.
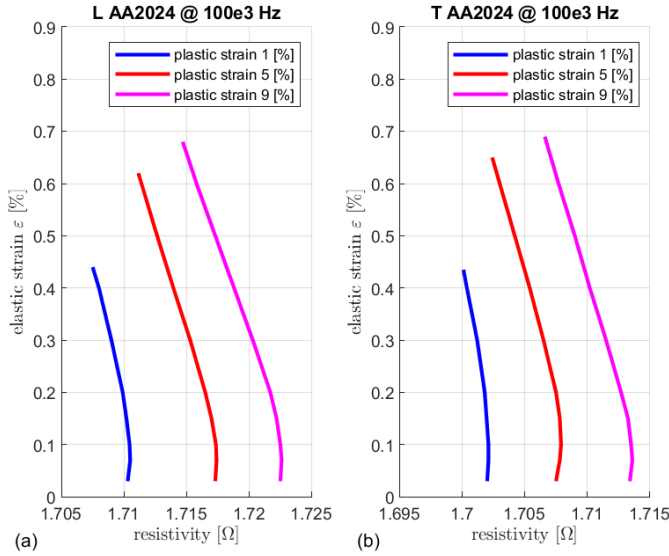

Figure 3.4: Piezoresistivity curves for various amounts of plastic strain for Al 2024-T3: (a) longitudinal grain, (b) transverse grain. Note initial nonlinearity with increasing strain. Redrawn from [40].

3.3.3. Crack tip plastic deformation

Consider a fatigue specimen under increasing strain. At the crack tip, a region with $S > S_{\text{yield}}$ exists where plastic deformation occurs. The local strain increases significantly, affecting the local electrical resistivity through the Poisson effect and piezoresistivity. Because plastic deformation happens around the crack tip, it is a very local phenomenon during the majority of the specimen life. The effect on the general dimensions and resistivity of the total specimen are therefore negligible. However, since the PD electrodes are positioned such that the electrical path between them sees a large part of the plastically deformed crack tip region (see Figure 3.1), the effect is large enough to significantly influence the resistivity of the PD electrical path. Additional changes in plasticity occur around the crack tip during the crack growth phase as the plastic zone moves along with the crack tip.

It was concluded earlier that the PD TTC curve is proportional to the loading due to the Poisson effect and piezoresistivity. For crack tip plastic deformation it is the piezoresistivity that is affected the most here, making the PD TTC curve depart from the initial proportionality with the loading curve. A similar but smaller discrepancy might be observed near the end of each cycle, where compressive stresses generate

reverse plasticity.

3.3.4. Crack growth

The crack growth per cycle is generally small, around nm up to μm for the majority of the crack life as observed in fatigue crack growth tests discussed below. The process of crack opening, extension, and closure during part of the cycle should in theory be observable in the PD TTC signal. The electrical path length increases during crack growth, and the remaining cross-section area of the specimen decreases.

3.4. Potential drop through the cycle measurement setup

The continuous potential drop measurement system developed in the current study is used to measure the electric potential with high resolution, several orders of magnitude better than required for standard PD. A subset of this data containing the potentials at S_{max} is used as input for the ASTM method [11] to calculate the crack length a and crack growth rate da/dN. The crack growth rate is plotted versus ΔK_{eff} to generate typical fatigue crack growth curves. The measurement setup and the specimen geometry are discussed separately.

3.4.1. PD TTC measurement setup

A dedicated PD measurement system was developed in-house at Delft University of Technology. The standard PD procedure is to measure the potential at peak load (S_{max}), either by a single measurement or by averaging multiple (high frequency) measurements at or around S_{max}. PD TTC is capable of continuous high frequency measurements at varying S throughout the full load cycle, which result in more information about the potential with respect to the applied load compared to standard PD. The basic design goals of the new system were:

- Measure the potentials over a test and a reference specimen, and calculate the potential ratio needed for the crack growth equation given in the ASTM E 647 standard [11].

- Measure these two potentials simultaneously to reduce data scatter.

- Perform continuous PD measurements at kHz rate for a test frequency up to several Hz for data smoothing.

- Perform continuous PD TTC measurements at kHz rate for a test frequency of several Hz to observe the change in potential through every cycle of a sine signal.

- Automatically track the minima and maxima of the sine spectrum, to find the standard PD potential at S_{max} for every cycle.

The potential drop measurements and subsequent data operations are handled by an FPGA (field-programmable gate array), here a National Instruments CompactRIO Controller cRIO 9074 [41]. It controls two separate potential measurement circuits, and it can store temperature measurements of ambient air or the specimens using thermocouples. These temperature measurements can be used during post-processing to correct for stiffness changes. PD measurement wires of equal length were used, and were twisted to minimize thermal EMF. The use of the potential ratio between a test and a reference specimen also minimizes thermal EMF by canceling out most temperature effects. A constant current power supply is connected to the specimens to generate the potentials. Most tests use the Delta Elektronika SM100-AR-75, set at 75 A. The electrical resistance of total circuit gives a potential of about 0.5 V. This results in about 37.5 W of power being supplied to the circuit. This power heats up the specimens until a thermal equilibrium up to 5 °C above ambient is reached, verified by thermocouples. The test is not started before this equilibrium is reached. The complete setup is illustrated in Figure 3.5.
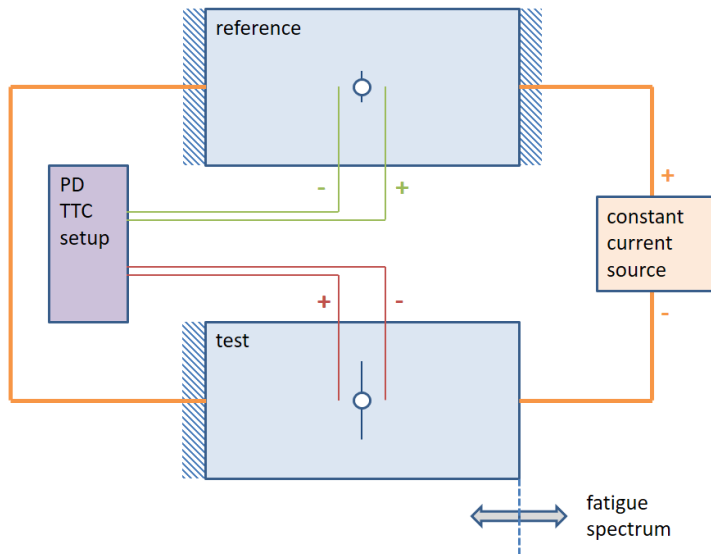

Figure 3.5: Schematic view of the test setup with potential drop measurement device and constant current source. Actual tests were performed with a 250 kN MTS fatigue machine.

The FPGA is programmed using LabVIEW, and the measurement routines are developed in-house at the Delft Aerospace Structures and Materials Laboratory (DASML) of Delft University of Technology. The FPGA is concerned with seven tasks:

- Take simultaneous potential measurements at a frequency of 50 kHz, and apply an averaging function per 10 measurements, resulting in a smoothed signal of 5 kHz.

- Regularly take zero-current potential measurements, for calculating the true potentials.

- Track the test specimen load signal from the fatigue machine as measured by a load cell for sine loading peak-valley detection, to obtain the start and end times of each cycle.

- Calculate the potential ratio used in the ASTM E 647 standard [11].

- Reduce data scatter by using a moving average smoothing over a user-defined number of cycles.

- Measure the temperature of both specimens with thermocouples.

- Write the moving average smoothed measurements of one cycle to a data file every user-defined amount of cycles.

A flow chart of the FPGA software routine is given in Figure 3.6.
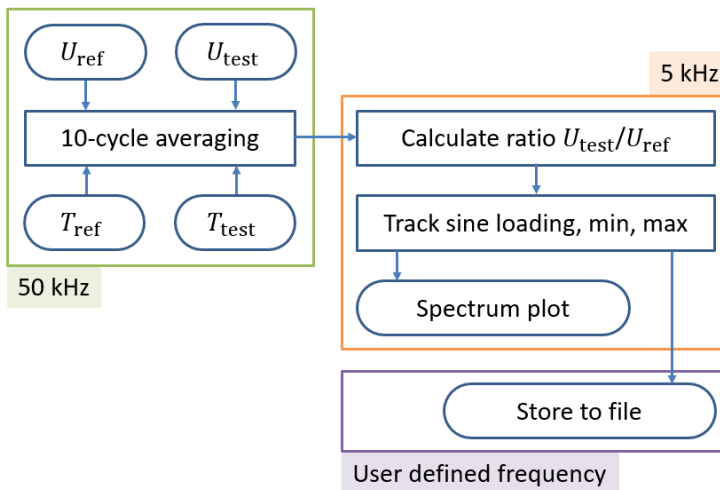
Figure 3.6: Potential drop measurement FPGA flow chart.

3.4.2. Fatigue specimen material and geometry

The test and reference specimens were made as identical copies from the same material batch, of which only the test specimens were fatigued. A typical specimen was CNC milled from Al 2024-T3 plate of 6.1 mm thickness. The test specimens were loaded in L-T direction, and had on each end five attachment holes of 10.5 mm diameter for clamping. Figure 3.7 shows the specimen geometry and location of the PD electrodes. A center hole of 4 mm made it possible to create starter cracks by fretsaw, with $a = 8.0 \pm 0.2$ mm based on visual inspection.

The electrode attachment was similar for all specimens. Two M2 tapped holes were used for attaching M2 brass bolts. Figure 3.8 shows a close-up of an electrode attachment. PD measurement wires with appropriate crimp fittings were bolted onto these brass bolts and were not in direct contact with the specimens.
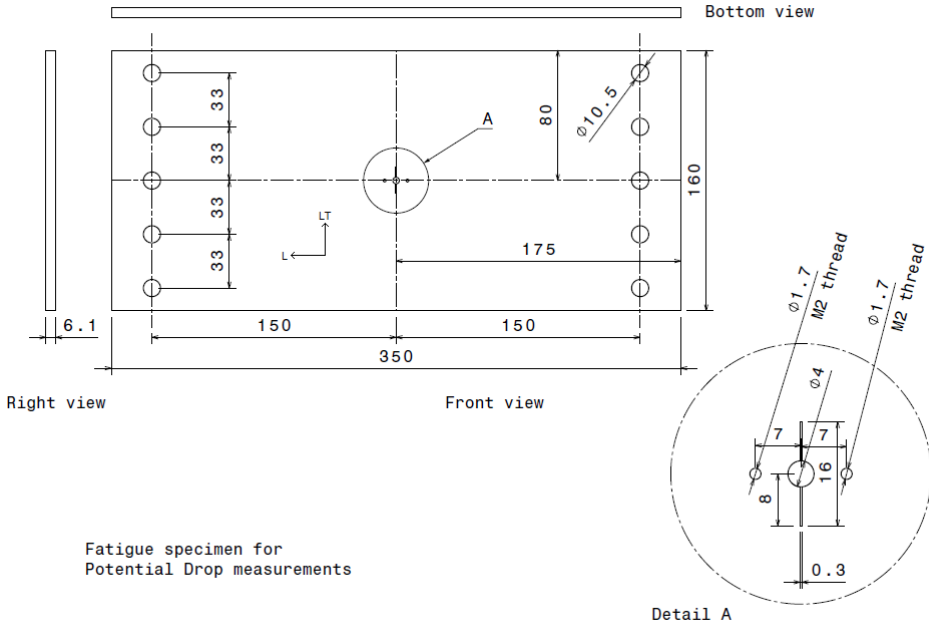

Figure 3.7: Drawing of a typical fatigue test specimen as used with the PD TTC setup. Loading direction horizontal. The constant current was connected through the edge holes on the horizontal centerline.

3.5. PD TTC test results

A number of PD CCT fatigue tests were performed using a constant amplitude spectrum, with and without overloads. The test results are published as data set [42], and Table 3.1 gives an overview of these tests. Test 8 is a sine spectrum on an uncracked specimen to investigate the potential behavior in absence of crack growth and plasticity. For the other tests it holds that the observed PD TTC curves behave similar for various S_{max} and R values. Test 1 is a representative example used below to illustrate the findings of the PD TTC measurements.

3

Figure 3.8: Close-up of a representative PD electrode attachment. The M2 brass bolt connects the PD wire with the specimen.

Table 3.1: PD TTC tests. Al 2024-T3, CCT fatigue specimens, constant amplitude. Tests 6 and 7 had an overload approximately equal to twice S_{max}. Test 8 is not a fatigue test.

Test no.	S_{max}	R	N	OL
[-]	[MPa]	[-]	[cycles]	[-]
1	97.06	0.063	24594	no
2	174.8	0.608	23534	no
3	145.9	0.607	50254	no
4	116.6	0.608	112644	no
5	87.4	0.608	335791	no
6	87.8	0.100	48170	yes
7	87.8	0.101	44998	yes
8	160.0	0.025	-	no

For all tests except test 8, a moving average smoothing of 500 cycles was applied. A PD TTC cycle was stored every 50 or 100 fatigue cycles, resulting in data sets in the order of several hundred PD TTC cycles each. The AFGROW software [43] was used to generate predictions using the NASGRO equation and the material choice of Al 2024-T3 clad, plt & sht, L-T direction.

The differences between both crack growth curves is mostly in the different crack formation lives, as result of the fact that in the tests cracks had to nucleate from the fretsaw cut tip. To compare both crack growth curves, the AFGROW curve is translated to start at nearly the same crack length as the measured curve.

Increasing R and/or lowering S_{max} would result in a longer life at lower da/dN and more PD TTC cycles. However, at lower da/dN the relative precision is less given the measurement resolution, and a larger number of cycles is needed for moving average smoothing. This is discussed in more detail in section Section 3.6, and a rather short fatigue life test was chosen to increase the relative measurement precision.

The measured PD TTC potentials include the potential ratios of the test and reference specimens. The reference specimen potential was observed to be virtually constant, resulting in the potential ratio being effectively proportional to the test specimen potential. The output files of the measurement device contain the test specimen potential and the potential ratio.

3.5.1. Standard PD results from PD TTC data set

Using only values at $t = 0.5$ at S_{max}, the crack growth potential ratio per cycle appears which is commonly used as input for the ASTM PD crack length calculation. The results of test 1 are shown below as a representative example. The measured PD TTC ratio is shown in Figure 3.9. Each curve starts at a higher potential ratio, because each cycle starts at an increased crack length. The change in potential through a single cycle increases during the specimen life too, and deviations become more pronounced as well.

The values at $t = 0.5$ in Figure 3.9 constitute the standard, once per cycle PD measurements. Figure 3.10 shows the ASTM PD crack length calculation results of
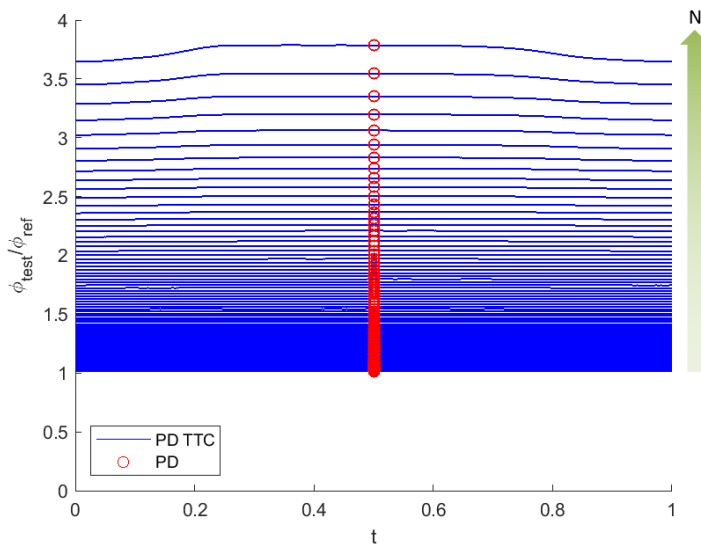
Figure 3.9: Potential ratio curves of test 1, per cycle time t. A subset of each 250th curve is shown for clarity. With increasing crack length, the ratio increases. The values at $t = 0.5$ correspond to standard S_{max} PD values.

this subset, together with the AFGROW prediction. The AFGROW curve has been slightly translated horizontally to match the measurement curve due to a deviation in crack formation life.

The corresponding crack growth rate da/dN versus ΔK_{eff} is shown in Figure 3.11, where a rather linear section (Paris region II) on double logarithmic scales is observed.

This example illustrates that the standard, once per cycle PD data point is only a subset of the full PD TTC signal, and that consequently more information is present in the PD TTC signal.

3.5.2. A closer look at the PD TTC signal

In order to compare the potential curve shapes from Figure 3.9, all the curves are translated in vertical direction to start at zero. Note that they are only translated, not scaled. This translation preserves the relative changes in potential, but not the absolute values. The result is shown in Figure 3.12. Most curves have only a small change in potential throughout the cycle as the largest part of the specimen life at a relatively low da/dN, apparent from Figure 3.11, whereas the most pronounced curves are the ones near the end of the specimen life. Nevertheless, Figure 3.12 shows that a consistent behavior of the potential is observed throughout a wide range of cycles.

One of the PD TTC curves from Figure 3.12 is examined in more detail to explain the behavior of the potential seen in all cycles. In Figure 3.13 this curve is overlaid
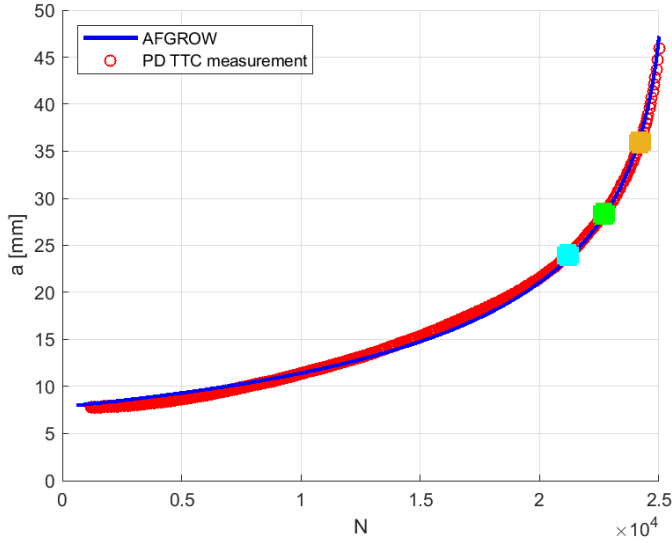
Figure 3.10: Crack length versus cycles for test 1. Red data points are generated using the method given in ASTM E 647 [11], using the potential values at $t = 0.5$ from the curves shown in Figure 3.9. AFGROW curve shown for comparison. The orange, green, and cyan markers correspond with the points in Figure 3.11 and curves in Figure 3.12.
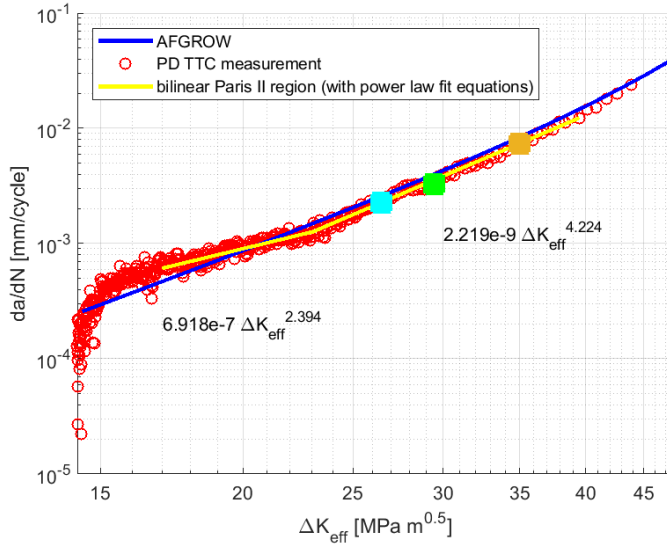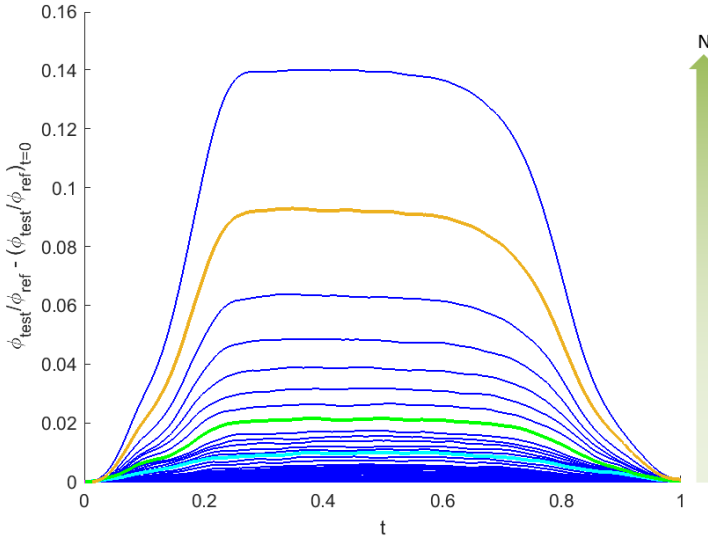

Figure 3.11: Crack growth rate curve of test 1. A bilinear Paris region II is observed in the range $17 < \Delta K_{eff} < 40$. AFGROW curve shown for comparison. The orange, green, and cyan markers correspond with the points in Figure 3.10 and curves in Figure 3.12.

Figure 3.12: Potential TTC curves of test 1, per cycle time t. These are the same curves as in Figure 3.9, now translated vertically to start from zero to facilitate comparison of the PD TTC curve shape. The orange, green, and cyan curves correspond with the similarly colored points in Figures 3.10 and 3.11.

with a sine to show the similarities with the sine loading spectrum. Initially the potential follows this sine behavior very closely. Around one-quarter of the cycle duration does the potential break away into a plateau-like behavior until about three-quarters of the cycle duration. After this plateau, until the end of the cycle, does the potential follow a sine-like behavior again, although not exactly on top of the loading sine.

To give a sense of the plateau significance, the standard deviation of the plateau data range of the green curve from Figure 3.12 was calculated. Figure 3.14 shows this PD TTC data and the 1σ and 3σ standard deviation boundaries, which encompass $68.2\,\%$ and $99.7\,\%$ of the plateau data respectively. It is clear that the virtually all plateau data points fall within a small band of potential ratio values, showing that the plateau is a significant feature of the PD TTC curve.

3.5.3. The origin of the PD TTC plateau

To demonstrate that the observed PD TTC plateau relates to plasticity, a similar but uncracked Al 2024-T3 panel was subjected to a low-stress sine loading cycle; test 8. The choice of $S_{\mathrm{max}} = 160\,\mathrm{MPa}$, well below the material yield stress $S_{\mathrm{yield}} = 324\,\mathrm{MPa}$ [32], ascertained absence of any plasticity. With plasticity and crack growth absent, it was expected that the change in potential would be proportional to the change in loading. The observed PD TTC curve closely follows the sine shape, as is shown in Figure 3.15. The Poisson and piezoresistivity effects both fluctuate in close accordance with the loading, resulting in the ratio between these effects being rather
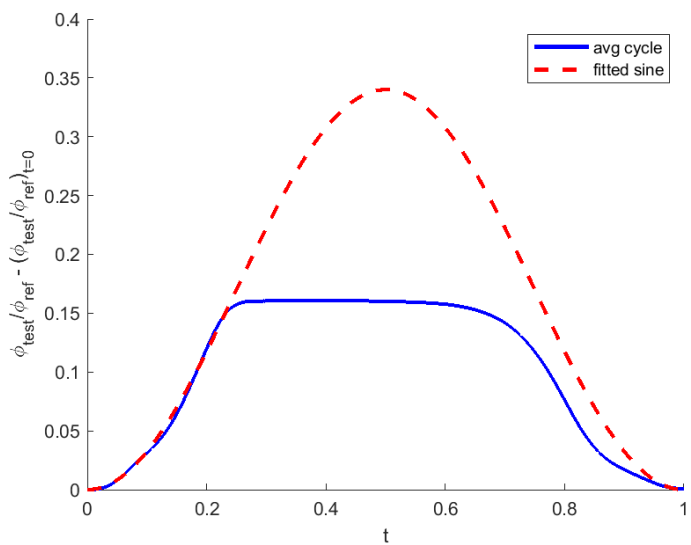
Figure 3.13: A single TTC curve from measurements, with an overlaid sine curve representing the applied loading. A correlation is observed during the first and last quarter of the cycle. A plateau appears in between, at a certain load level.
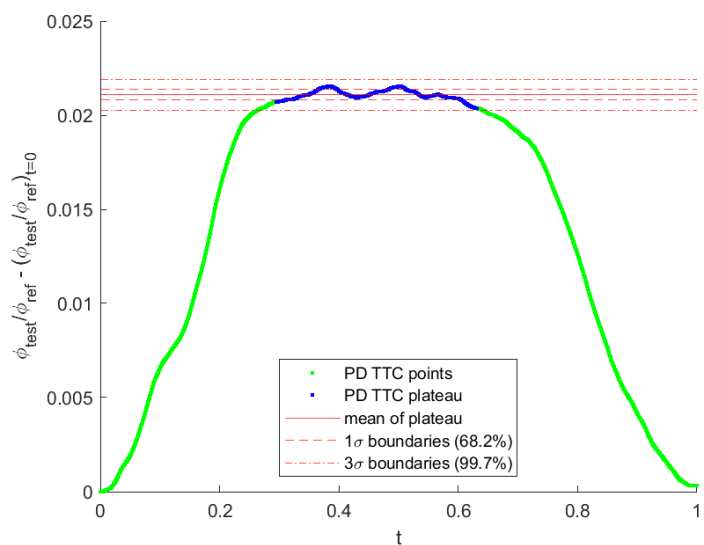

Figure 3.14: Potential TTC curve of test 1, corresponding to the green curve in Figure 3.12. The plateau data is shown in blue, with 1σ and 3σ standard deviation bands.

constant and following the loading signal.

A small flattening of the curve is seen directly around $S_{\min}$, which is a result of the initial nonlinearity of the piezoresistivity near zero strain (see Figure 3.4). Because the plate does not contain a crack, the change in potential due to elastic loading is small compared to the potential signal of a well developed crack. The relative scatter in Figure 3.15 is therefore orders of magnitude larger than the scatter observed in Figure 3.13. It also explains the choice for a large $S_{\max}$ compared to the fatigue tests.
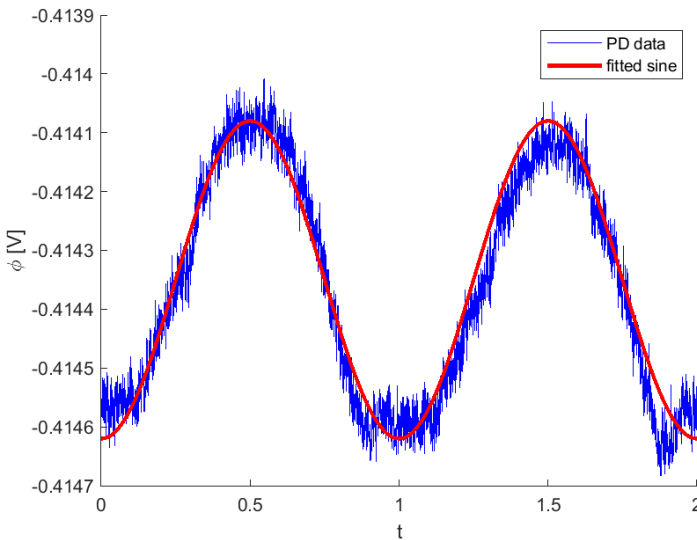

Figure 3.15: Two PD TTC cycles from test 8, with an overlaid sine curve representing the applied loading. A clear correlation is observed throughout the cycles. Compare with Figure 3.12; the plateau only appears when crack tip plasticity is present.

A further strengthening of the concept follows from a better understanding of what PD TTC is measuring. This is explained using Figure 3.2, where the effective electric path through a part of the specimen is shown schematically. During one cycle, the extension of the crack is small compared to the existing crack. The electric path therefore does not significantly extend in direction of the crack growth (horizontal). During that same cycle the crack tip plastic zone does develop and extend as a result of the applied loading, which is captured by the section of the electric path going around the crack tip (vertical). This shows that the PD TTC signal primarily measures crack tip plasticity. In reality there is not one unique conductive path but rather a conductive field, however the strongest signals are observed near the shortest path. Furthermore it is not a purely geometric function, as the signal strength is also strain dependent and thus a function of plasticity too.

Given the shape of the plastic zone and the electric path, it cannot be directly concluded that the measured signal is linearly proportional with the amount of

plasticity. But if the crack tip plasticity is proportional to the total plastic energy dissipation in the plastic zone, then it can be argued that a proportionality exists between the PD TTC signal, the applied load, and the amount of plastic dissipation.

During the plateau phase, there is a difference in potential between the sine loading curve and the plateau level. The sine loading is proportional to the elastic energy present in the global specimen, and the PD TTC signal shows a local effect. Nevertheless, the vertical difference between both in Figure 3.13 is a measure for the local energy being dissipated by plastic deformation. The plateau can be explained using an elastic perfectly plastic stress-strain curve, as shown in Figure 3.16. Once the local stress reaches a certain level, near or at S_{yield}, the stress stays at this level but the strain increases due to plasticity. It is this effect that causes the PD TTC plateau. In reality there is a slight stress increase during plastic deformation, which accounts for the gradual potential increase at the start of the plateau, and the gradual decrease at the end of the plateau, visually appearing as the rounded corners at the start and end of the plateau.
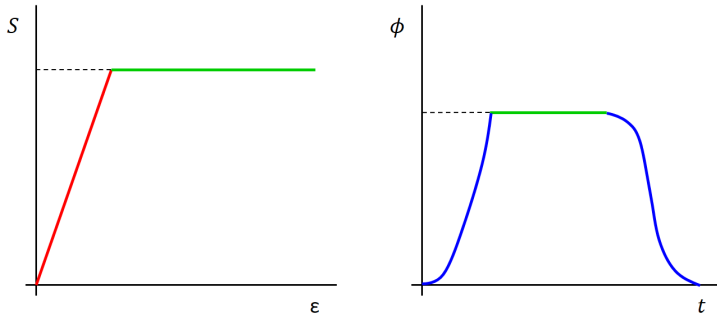

Figure 3.16: Elastic perfectly plastic stress-strain curve and corresponding schematic PD TTC curve. Above a certain stress level near or at S_{yield}, plastic deformation exists, which increases ε at constant stress and constant potential, resulting in a plateau (green).

3.5.4. Observing S_{op} and S_{cl} with PD TTC

Consider that if the PD TTC curve is related to crack tip plasticity, it also indicates crack growth phenomena such as crack opening and crack closure. As stated earlier, the change in potential due to crack growth itself is too small to be observed with the current measurement setup. However, the change in plasticity behavior can indirectly indicate crack growth effects. This is shown in Figure 3.17, based on the curve shown in Figure 3.13. The PD TTC curve shows again a sine-like behavior until about one quarter of the cycle length. Here the signal levels off onto the plateau quite abruptly, Figure 3.17 shows a short time range around $t = 0.23$ where this occurs. This range is believed to be the change in global stiffness E as schematically shown in Figure 3.18, which occurs when the crack opens and crack growth begins.

The first instant that the PD TTC curve moves away from the sine loading curve proportionality, could be seen as the start of plastic flow. This is the start of the

transition phase shown in Figure 3.18. Because of the plastic flow, the crack tip is pulled open during the transition point. Residual compressive stresses might be present around the crack tip, originating from previous cycles and depending on the loading conditions. These compressive stresses need to be alleviated first before the crack tip fully opens an crack growth can develop.

In accordance with [19], crack opening was defined as the moment that the crack tip finally becomes completely open. This occurs at the end of the transition phase in Figure 3.18, and is the start of the plateau in the PD TTC curve in Figure 3.17. Moreover, this point is more easily defined and observed than the start of the transition phase. An analogy can be found in a typical material stress-strain curve. The $0.2\,\%$ offset yield point assumption is often used in engineering practice, because the actual elastic limit point is difficult to define accurately.

Noting that opening occurs over a finite time interval, combined with reported [2, 13, 27] COD measurement scatter of the S_{op} timing, in a similar way the assumption is made that $t_{S,op}$ occurs at the crossing of the tangents at start and end of this opening time interval. This is shown in Figure 3.17, from which it is clear that the tangent crossing is easy to determine. S_{op} then follows from the loading curve at $t_{S,op}$.

In a similar way the closing stress S_{cl} can be calculated from $t_{S,cl}$. However, from Figure 3.17 it is clear that the time interval during crack closing is significantly larger than during crack opening. The exact reason is yet unknown, but a plausible explanation is that the new crack tip shape after crack extension causes a smooth, gradual closure of this newly formed crack extension. The tangent crossing procedure results in a S_{cl} value slightly higher than S_{op}, which is consistent with literature [29]. This strengthens the idea that the PD TTC concept is capable of deriving indirectly, but rather precise, the load levels at which the crack opens and closes, and how these levels may change throughout the life of the fatigue specimen.

3.6. Measurement precision and accuracy, signal sensitivity, and smoothing

A brief discussion is given on the sensitivity of PD TTC compared to standard PD, and the application of PD TTC signal smoothing over several successive cycles.

3.6.1. Measurement precision and accuracy

The measured potentials are in the order of μV, which are amplified by the PD setup to mV. These small signals make the overall electric circuit and measurement setup extremely sensitive to electrical and magnetic interference. The electronic amplifiers must be exceptionally stable to allow for good precision. An improvement in noise reduction is roughly proportional to the improvement of the lower effective da/dN limit. Significant but short-lived potential changes due to local temperature interference have been observed as well, arising from tiny air currents or simply by touching a specimen. The measurement scatter in the amplified mV signal is in the order of mV or smaller, requiring smoothing over multiple cycles.
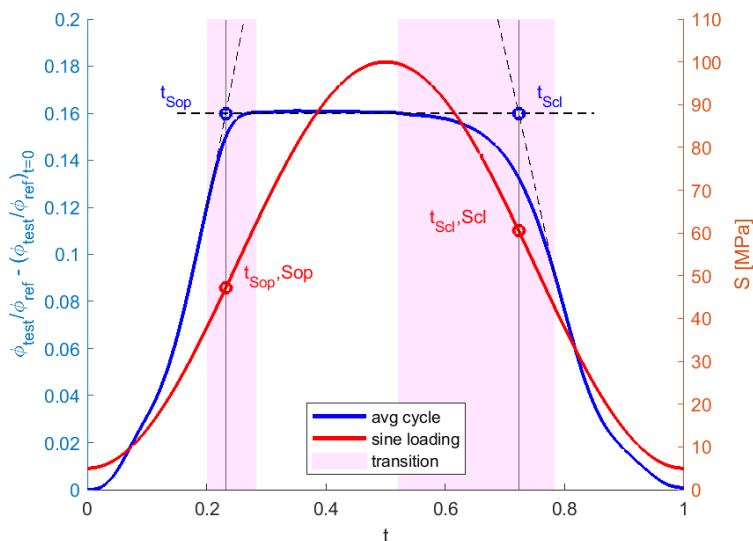
Figure 3.17: The plateau region has a nearly constant potential, showing a balanced act between the Poisson effect and the piezoresistivity. Crack opening and closure transition time intervals shown in magenta.
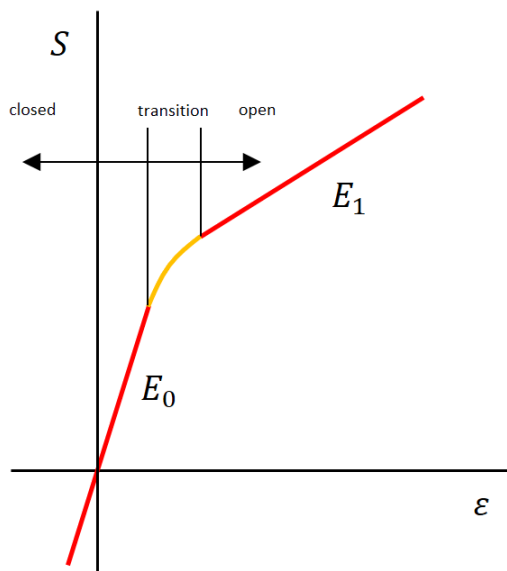

Figure 3.18: A schematic, global stress-strain diagram of the specimen belonging to Figure 3.17. The nonlinear section (orange) relates to the transition from a closed crack (E_0) to an open crack (E_1, PD TTC plateau).

With the changes in potential through the cycle initially being small, a moving average technique is applied over a constant number of successive cycles. This reduces measurement scatter and improves accuracy. Each measurement point of a given PD TTC cycle is thus the average of a predefined number of previous successive measurements taken at the same PD TTC time instant t. This procedure takes place in the measurement setup FPGA in real time during the test.

The use of this data scatter reduction technique is justified on the basis that for sufficiently small da/dN, it can be assumed that a certain number of subsequent cycles have essentially a constant da/dN at equal a. It appears self-contradictory since a nonzero da/dN results in a change of a, but consider that $da/dN \ll a$. Consecutive PD TTC cycles are thus nearly equal. To further improve measurement precision and accuracy over the current PD TTC setup, electronic amplifiers with less noise ($< 2\,\%$ of absolute signal) and an improved electrical insulation from external disturbances of the whole circuit are paramount.

3.6.2. PD TTC signal resolution versus standard PD signals

The observed potential changes through the cycle, as indicated in Figure 3.1. The presence or absence of plasticity and the occurrence of crack growth influence the signal strength and the signal path length. The ratio of test potential over reference potential generally grows from unity to a value about ten times larger. The change in potential during a single cycle is several orders of magnitude smaller, and is through plasticity and crack growth effects linked to da/dN.

The standard PD technique is a well-established method of observing crack growth during the fatigue life, and generally takes (high frequency) measurements at S_{max} only. One of the reasons for doing so is that closure effects do not play a role as $S_{\mathrm{max}} > S_{\mathrm{op}}$. The PD TTC technique takes continuous high frequency measurements at varying S values during each full cycle, on purpose measuring how the potential is affected by plasticity and crack growth effects.

With standard PD, the increase in crack length per cycle da/dN is derived from the increase in potential. Measurements are generally taken at only one time instance per cycle, often at S_{max} at $t = 0.5$. This means that the observed potential increase per cycle is actually the peak to peak value of two successive cycles. A slightly more accurate determination of the potential increase per cycle can be made using the PD TTC data, as the change in potential per cycle can now be properly observed as $d\phi/dN = \phi_{\mathrm{t=1}} - \phi_{\mathrm{t=0}}$, which is directly related to da/dN.

Note that the energy dissipation in plasticity is significantly larger than the energy used to extend the crack. This means for PD TTC that the maximum change in potential through the cycle, equal to $\phi_{\mathrm{t=0.5}} - \phi_{\mathrm{t=0}}$, is orders of magnitude larger than the net change between $\phi_{\mathrm{t=1}}$ and $\phi_{\mathrm{t=0}}$, as is evident from Figures 3.9 and 3.12. Plasticity effects are thus visible using standard PD resolution in this PD TTC setup. In theory, the crack extension within the cycle should be visible too in PD TTC data. However, the current setup has insufficient resolution to do so. Improved resolution (several orders of magnitude) may be required to observe crack extension directly.

3.6.3. Post-processing data set smoothing

The internal moving average smoothing cannot always provide sufficient relative scatter reduction, especially at PD TTC curves below a certain small da/dN value. A second smoothing step can be performed on the full data set after the test. The chosen method here is smoothing over several successive cycles, centered around a particular N value.

This smoothing range cannot be chosen arbitrarily large, due to three reasons, illustrated in Figure 3.19:

1. The relative PD signal scatter is larger at the lower end of the range. The arithmetic mean of the smoothing causes data scatter at the lower end to have a more pronounced effect on the smoothed signal.

2. The monotonous increasing slope of the crack growth rate da/dN makes the higher end of the smoothing range have a stronger effect on the mean or absolute or values of the smoothed PD TTC curve.

3. The growth of a in this range causes the finite width effect to change the increase in plasticity, which affects the PD TTC signal. This effect only becomes significant at large a/W ratios near the end of the specimen life.

While reason 1 and 2 are inherent in data smoothing, and the finite width effect mentioned in reason 3 is always present in fatigue tests, the effect of the latter on plasticity influences the PD TTC curve itself, which is unique to the PD TTC method.
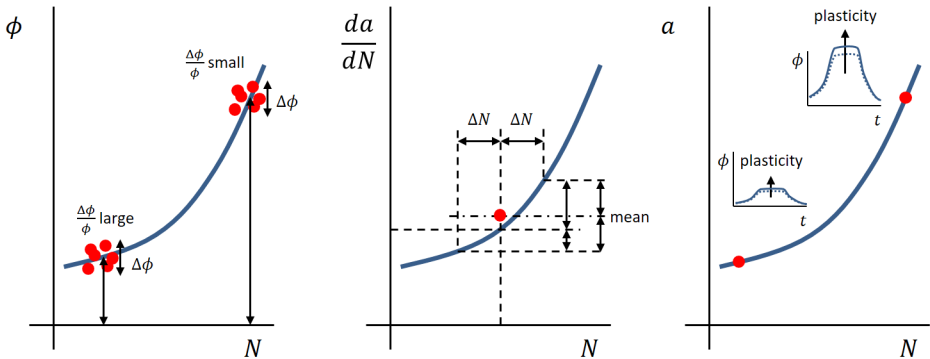

Figure 3.19: The three effects of data smoothing and averaging. One: relative scatter versus signal strength. Two: the larger end dominates the symmetric smoothing range. Three: changes in plasticity due to the finite width effect cause the larger end to dominate too, a case unique for PD TTC over standard PD.

To summarize, the main limitations are that in a given centered smoothing range the lower end increases the overall scatter, while the higher end increases the absolute mean potential.

Based on post-processing of the tests mentioned in Table 3.1, good results can be obtained by smoothing data sets within certain parameter limits. The ideal post-processing PD TTC curve smoothing needs to be performed on a small data range where:

- The change in da/dN values is sufficiently small (viz. a change up to several %).

- The a/W ratio is sufficiently small (viz. $a/W < 0.125$ such that the finite with correction factor $\beta < 1.05 \approx 1$).

- The da/dN values are such that the relative scatter (unsmoothed) is not too large (viz. up to several %).

The first and second requirement are test geometry and loading dependent, the third requirement is only geometry dependent.

3.7. Conclusions and recommendations

The extended potential drop (PD) measurement system, PD TTC, is capable of measuring the electric potential throughout a single fatigue crack growth loading cycle, and doing so for many successive cycles. This results in the observation of potential changes which are linked to several crack growth phenomena, such as the timing and magnitude of crack opening and crack closure stresses. The following list summarizes the most important findings of using this PD TTC measurement technique:

1. The known effect of mechanical stress on the electrical resistance is observed in fatigue cycles, affecting the measured potential through Pouillet's law and Ohm's law under assumption of constant current. Two main effects are observed, which have opposite effects on the potential:

   - The Poisson effect: the change of specimen geometry under load. $S \uparrow \propto \phi \uparrow$.
   - Piezoresistivity: the strain dependency of the resistivity. $S \uparrow \propto \phi \downarrow$.

2. During crack growth, two other effects are observed which are subsets of the aforementioned main effects:

   - Crack tip plasticity: changes in strain give a combined effect of the Poisson effect and piezoresistivity.
   - Crack growth: the opening and closing of the crack influences the Poisson effect.

3. Crack tip plasticity and crack growth are readily apparent from a clear deviation of the potential curve around S_{max}. A plateau-like behavior is present at a certain critical cyclic energy level, above which excess energy is dissipated by growth of the crack tip plastic zone and crack growth.

4. The effect of crack extension is several orders of magnitude smaller than plasticity effects, and is therefore not directly observed in PD TTC data given the current measurement resolution. Nevertheless, the observable changes due to plasticity can be correlated with start and end of the crack growth phase.

5. The start and end times $t_{S,\mathrm{op}}$, $t_{S,\mathrm{cl}}$ of the plateau together with the loading spectrum can be used to derive true opening and closure stresses $S_{\mathrm{op,phys}}$ and $S_{\mathrm{cl,phys}}$, with significantly larger accuracy and precision than existing methods such as COD.

The PD TTC method is novel way of measuring the opening and closing stress with greater insight and potentially improved precision and accuracy over existing methods such as COD. The insights and improvements obtained with PD TTC can be useful in reducing opening and closure stress related uncertainties in ΔK_{eff} similitude parameter models and other crack closure models.

Acknowledgments

References

[1] J. J. A. van Kuijk, R. C. Alderliesten, and R. Benedictus, *Measuring crack growth and related opening and closing stresses using continuous potential drop recording,* Engineering Fracture Mechanics **252**, 107841 (2021).

[2] J. Schijve, *Fatigue of Structures and Materials*, 2nd ed. (Springer Science+Business Media B.V., 2009).

[3] J. Bär and D. Tiedemann, *Experimental investigation of short crack growth at notches in 7475-T761,* Procedia Structural Integrity **5**, 793 (2017), 2nd International Conference on Structural Integrity, ICSI 2017, 4-7 September 2017, Funchal, Madeira, Portugal.

[4] A. Gajji and G. Sasikala, *Potential drop method for online crack length measurement during fracture testing: Development of a correction procedure,* Engineering Fracture Mechanics **180**, 148 (2017).

[5] L. Gandossi, S. A. Summers, N. G. Taylor, R. C. Hurst, B. J. Hulm, and J. D. Parker, *The potential drop method for monitoring crack growth in real components subjected to combined fatigue and creep conditions: application of FE techniques for deriving calibration curves,* International Journal of Pressure Vessels and Piping **78**, 881 (2001).

[6] K. Krompholz and G. Ullrich, *Investigations into the fatigue crack initiation and propagation behaviour in austenitic stainless steel X5 CrNi 18 9 (1.4301),* Materialwissenschaft und Werkstofftechnik **16**, 270 (1985).

[7] J. Liu and P. Bowen, *DC potential drop calibration in matrix-cladded Ti MMC specimens with a corner notch,* International Journal of Fatigue **25**, 671 (2003).

[8] R. B. Scarlin, *Fatigue crack growth in a cast Ni-base alloy,* Materials Science and Engineering **21**, 139 (1975).

[9] A. V. Tumanov, V. N. Shlyannikov, and J. M. Chandra Kishen, *An automatic algorithm for mixed mode crack growth rate based on drop potential method,* International Journal of Fatigue **81**, 227 (2015).

[10] Y. Si, J. P. Rouse, and C. J. Hyde, *Potential difference methods for measuring crack growth: A review,* International Journal of Fatigue **136**, 105624 (2020).

[11] ASTM International, *ASTM E647-15e1, standard test method for measurement of fatigue crack growth rates,* ASTM International, West Conshohocken, PA (2015).

[12] M. Andersson, C. Persson, and S. Melin, *Experimental and numerical investigation of crack closure measurements with electrical potential drop technique,* International Journal of Fatigue **28**, 1059 (2006).

[13] W. Elber, *The significance of fatigue crack closure,* ASTM STP 486 (1971), pp. 230–242.

[14] A. U. De Koning, *Crack growth prediction methods, Part 1: A survey*, Tech. Rep. NLR TR 84121 L Part I (Nederlands Lucht- en Ruimtevaartcentrum, 1984).

[15] J. C. Newman Jr., *A crack opening stress equation for fatigue crack growth,* International Journal of Fatigue **24**, 131 (1984).

[16] T. Iwasaki, A. Katoh, and M. Kawahara, *Fatigue crack growth under random loading,* Naval architecture and ocean engineering **20**, 194 (1982).

[17] M. Kurihara, A. Katoh, and M. Kawahara, *Effects of stress ratio and step loading on fatigue crack propagation ratio,* in *Current research on fatigue cracks (Current Japanese Materials Research)* (Elsevier Applied Science, London, 1987).

[18] J. L. Overbeeke and J. de Back, *The influence of stress relieving and R-ratio on the fatigue of welding joints,* in *Fatigue of welded constructions: international conference, Brighton, England, 7-9 April 1987*, edited by S. Maddox (Welding Institute, United Kingdom, 1988) pp. 11–22.

[19] A. K. Vasudevan, K. Sadananda, and N. Louat, *A review of crack closure, fatigue crack threshold and related phenomena,* Materials Science and Engineering **A188**, 1 (1994).

[20] R. S. Vecchio, J. S. Crompton, and R. W. Hertzberg, *Anomalous aspects of crack closure,* International Journal of Fracture **31**, R29 (1986).

[21] R. E. Garz and M. N. James, *Observations on evaluating fatigue crack closure from compliance traces,* International Journal of Fatigue **11**, 437 (1989).

[22] R. I. Murakami, Y. H. Kim, and W. G. Ferguson, *The effects of microstructure and fracture surface roughness on near threshold fatigue crack propagation characteristics of a two-phase cast stainless steel,* Fatigue & Fracture of Engineering Materials & Structures **14**, 741 (1991).

[23] M. Okazaki, A. J. McEvily, and T. Tanaka, *The wedge mechanism of fatigue crack growth in silicon nitride,* Materials Science and Engineering: A **143**, 135 (1991).

[24] B. K. Parida and T. Nicholas, *Effect of stress ratio on fatigue crack growth in a titanium aluminide alloy,* International Journal of Fracture **52**, R51 (1991).

[25] S. A. Seetharam and P. K. Dash, *Load-CMOD data analysis for crack closure,* International Journal of Fracture **53**, R53 (1992).

[26] M. P. Gómez, H. Ernst, and J. Vázquez, *On the validity of Elber's results on fatigue crack closure for 2024-T3 aluminum,* International Journal of Fracture **12**, 178 (1976).

[27] M. N. James and J. F. Knott, *Critical aspects of the characterization of crack tip closure by compliance techniques,* Materials Science and Engineering **72**, L1 (1985).

[28] R. Pippan, G. Haas, and H. P. Stüüwe, *Comparison of two methods to measure crack closure in ultra-high vacuum,* Engineering Fracture Mechanics **34**, 1075 (1989).

[29] J. Schijve, *Fatigue crack closure, observations and technical significance*, Tech. Rep. LR-485 (Delft University of Technology, Department of Aerospace Engineering, 1986).

[30] J. J. A. van Kuijk, R. C. Alderliesten, and R. Benedictus, *Unraveling the myth of closure corrections: Sharpening the definition of opening and closure stresses with an energy approach,* International Journal of Fatigue **143**, 106016 (2021).

[31] R. C. Alderliesten, *The explanation of stress ratio effect and crack opening corrections for fatigue crack growth in metallic materials,* in *11th International Fatigue Congress*, Advanced Materials Research, Vol. 891 (Trans Tech Publications Ltd, 2014) pp. 289–294.

[32] FAA US, *Metallic materials properties development and standardization (MM-PDS),* Federal Aviation Administration, Washington, DC, Paper No. MMPDS-05 (2010).

[33] F. Bloch, *Über die Quantenmechanik der Elektronen in Kristallgittern,* Zeitschrift für Physik **52**, 555 (1929).

[34] S. C. Hunter and F. R. N. Nabarro, *The propagation of electrons in a strained metallic lattice,* in *Proceedings of the Royal Society of London*, Series A, Math. and Phys. Sciences, Vol. 52 (1953) pp. 542–561.

[35] G. C. Kuczynski, *Effect of elastic strain on the electrical resistance of metals,* Phys. Rev. **94**, 61 (1954).

[36] M. J. Druyvesteyn, *The variation of the resistivity of some metals with elastic deformation,* Physica **17**, 748 (1951).

[37] J. K. Mackenzie and E. H. Sondheimer, *The theory of the change in the conductivity of metals produced by cold work,* Phys. Rev. **77**, 264 (1950).

[38] J. S. Koehler, *A calculation of the changes in the conductivity of metals produced by cold-work,* Phys. Rev. **75**, 106 (1949).

[39] P. W. Bridgman, *The effect of homogeneous mechanical stress on the electrical resistance of crystals,* Phys. Rev. **42**, 858 (1932).

[40] M. Morozov, G. Y. Tian, and P. J. Withers, *Elastic and plastic strain effects on eddy current response of aluminium alloys,* Nondestructive Testing and Evaluation **28**, 300 (2013).

[41] National Instruments, *NI cRIO-9072/9073/9074. User manual and specifications,* National Instruments (2019), accessed on 2019-12-05.

[42] J. J. A. van Kuijk, R. C. Alderliesten, and R. Benedictus, *Data underlying the research on: Al 2024-T3 center crack tension constant amplitude fatigue tests with potential drop through the cycle measurements,* 4TU.ResearchData publication (2021).

[43] J. A. Harter, *AFGROW users guide and technical manual*, Tech. Rep. AFRL-VA-WP-TR-1999-3016 (Wright-Patterson Air Force Base, 1999).

3

4

Experimental observations on the plastic zone development

This chapter discusses in more detail the relation between the crack tip plastic zone development with the observed signal of potential drop through the cycle (PD TTC) measurements, supplemented with digital image correlation (DIC). The PD TTC technique is explained in Chapter 3, and a short introduction to DIC is given in the current chapter. The correlation between DIC data and PD TTC curve is shown for two load cycles close to the end of life of a CA fatigue test on Al 2024-T3. Finally, a discussion on the merits and challenges of this combined measurement technique is given.

This chapter has not been published separately, but is provided here as an addendum to Chapter 3.

4.1. Digital image correlation (DIC) technique

The essence of digital image correlation is comparing two or more images of a specific area on a fatigue specimen, to measure the deformation or strain in this area. The technique has been widely used for examining the strain field around fatigue cracks, e.g., Refs. [1–4], and to study metal microstructures, e.g., Ref. [5].

Photography of this area of interest is done using one or more digital cameras. For an in-plane, two-dimensional analysis of the specimen surface, a single camera is used. For a three-dimensional analysis, a stereo camera setup is used to obtain extra information about the out-of-plane deformation. The stereo camera setup consists of two cameras at different locations but pointing at the same area on the specimen. The resulting difference in viewing angle gives information about the out of plane deformation component.

DIC software is used to track the movement of points on each image, and calculating the absolute deformation and strain. Because the software needs visual cues to position and track these points, a high contrast speckle pattern is applied to the specimen surface, as shown in Figure 4.1. The software then applies a raster to a reference image, Figure 4.2, on which the points are located. In subsequent images the location of each point is derived from an array of pixels around that point, taking into account several speckles in the immediate vicinity of that point, and compared to the reference image (absolute strain) or to the previous image (incremental strain). Therefore, the size and amount of speckles are of large importance. Too small or too little, and the software algorithm loses accuracy. Too large or too much, and the speckles start to overlap, again resulting in less accuracy or even erroneous correlations of between different speckles. When a crack is present and is open, correlation of points very close to the crack edge is inevitably lost as parts of the pixel arrays of these points is incomplete. This does not affect the plastic zone because it extends away from the crack plane.

4.2. The DIC setup

For the DIC analysis of the PD TTC fatigue specimens the two-dimensional DIC setup was used, because the main deformation was in the load direction, ε_{yy} strain, and the 6 mm specimen thickness gave sufficient stiffness in out of plane direction. The speckle pattern can be created using spray paint and ink pad stamping. The speckle patterns shown in this chapter are made in two steps. First, a white spray paint base layer is applied to the aluminum specimens. Second, a 0.007 inch resolution rubber ink stamp is used three times at 60° angular variations, to create the randomized speckle pattern of, uniform density.

DIC is often used to study the plasticity field around the crack tip in fatigue tests by measuring the plastic deformation strain. Pictures are taken every single cycle or every few cycles, to be able to observe the changes during the fatigue life.

This raises the question if DIC is capable to observe the changes in the strain field during a single fatigue cycle. In theory, it is possible to obtain many measurements per cycle, by lowering the fatigue frequency and by increasing the image
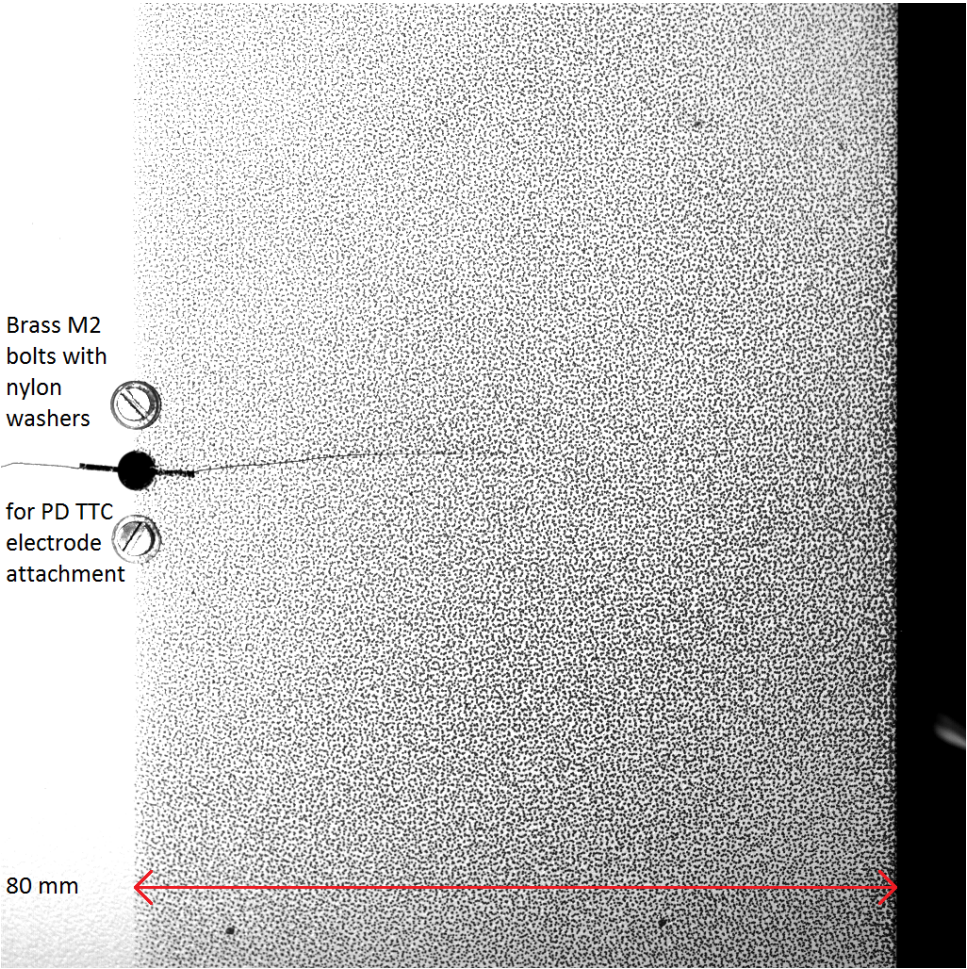
Brass M2
bolts with
nylon
washers

for PD TTC
electrode
attachment

80 mm

Figure 4.1: DIC digital image showing the high contrast speckle pattern on one side of the center crack, at s_{max}, such that the open crack is visible.
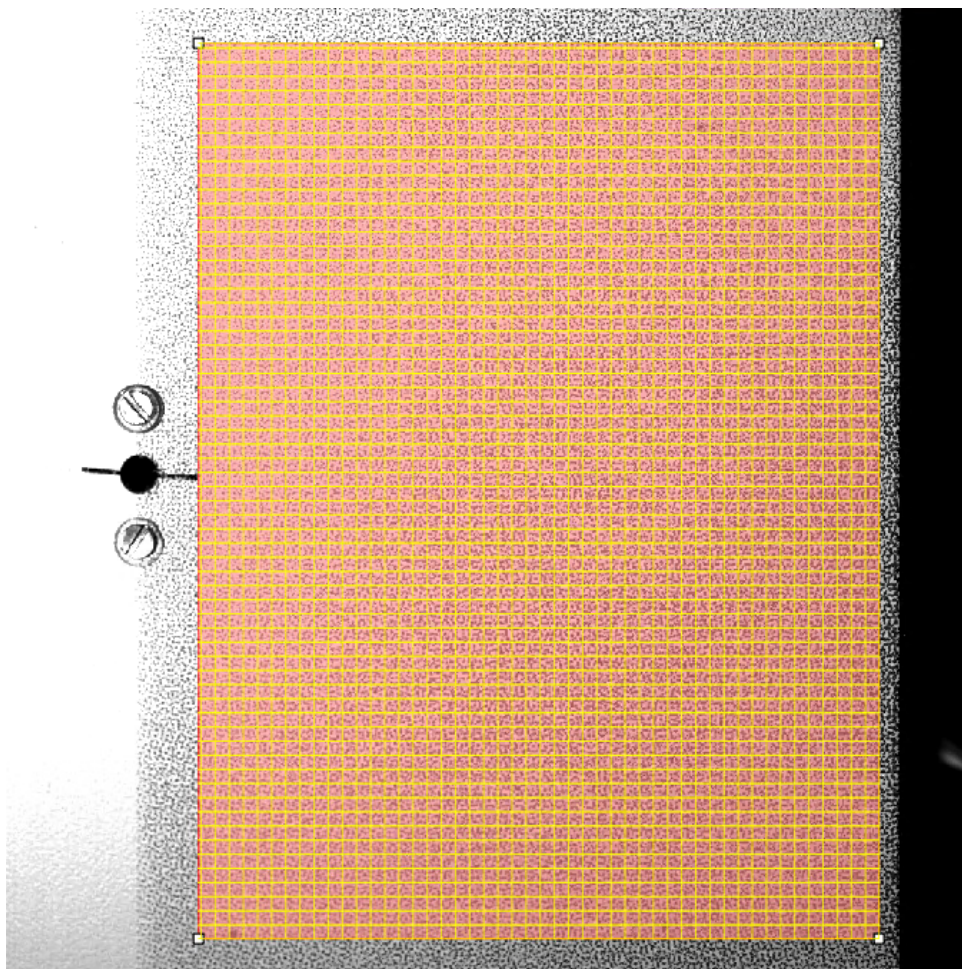
4

Figure 4.2: The rectangular shaded area (red) denotes the DIC analysis field. A raster of points (connected by yellow lines) is applied to the reference image with speckles. Points on subsequent images are referenced against this raster or against each other.

capture frequency. The software strain calculation algorithm and the image resolution should be of sufficient quality to observe the small strain changes. From PD TTC results it is known that the change in plasticity throughout a single cycle can be up to a few orders of magnitude larger than the net change per full cycle, as shown in Chapter 3. However, more images results in smaller relative differences between images. Therefore, the required resolution and software capabilities are still high, and the method is most likely to succeed at larger da/dN during the fatigue life.

Several fatigue tests were done in the DASML lab using the fatigue test setup as described in Chapter 3, with the addition of a high speed DIC setup. A Photron FASTCAM Mini AX high speed black and white digital camera was used, with external LED lighting allowing sufficiently short shutter times. A fatigue specimen was fatigued until a certain crack length, after which one or more load cycles were applied at low frequency, with PD TTC in continuous measurement mode and DIC engaged.

The principal limit of the amount of DIC measurements was given by the 32 GB internal memory of the Photron camera. As several fixed frame rates up to 6400 fps are possible, all images are stored to internal memory during capture, and later transferred to a personal computer via an USB connection. The image resolution of 1024 pixel by 1024 pixel resulted in a maximum capacity of about $21\,800$ images, and a frame rate of 6400 fps resulted in 3.4 s of continuous capture time. Each data set generated close to 32 GB of data, which was post-processed using the VIC-2D 6 software from Correlated Solutions [6] for DIC image processing. A low cycle frequency of 0.5 Hz or 1.0 Hz was chosen in different tests to obtain measurements over at least 1 or 3 consecutive full cycles. The PD TTC measurement frequency of 5 kHz resulted in $10\,000$ and 5000 measurement points per cycle, respectively. The DIC setup then captured $12\,800$ and 6400 images per cycle, respectively.

4.3. Plasticity related correlation of PD TTC and DIC

The link between crack tip plasticity and the PD TTC signal was already explained in Chapter 3. With the DIC technique being capable of measuring the strain field, the elastic and plastic strains can be obtained. This allows investigation of the correlation between the PD TTC and DIC measurements.

A constant amplitude fatigue test was done on an Al 2024-T3 specimen at $S_{\max} = 120$ MPa and $R = 0.05$, to obtain a sufficiently large plastic zone for DIC observation. A 1.0 Hz load cycle with continuous PD TTC and DIC measurements was applied near the very end of the fatigue life, just before final fracture at $a = 44$ mm. The fatigue crack growth rate da/dN was nearing the mm range.

4.3.1. DIC crack tip plasticity translation

The DIC images showed the change in strain during the load cycle. Analysis of the zone around the crack tip was done by evaluating the $\varepsilon_{\mathrm{yy}}$ strain: the strain in loading direction. In order to observe the plasticity at the crack tip stand out from the plastic zone, a lower threshold was applied on the strain color legend. Note that

the engineering yield strain of many metals is defined as $0.2\,\%$, but that the actual onset of plasticity occurs at a lower strain value, i.e. at the proportionality limit. For Al 2024-T3, this proportional strain was assumed to be $0.045\,\%$ based on MMPDS data [7]. All strain values below 4500 microstrain were indicated with a single color, and higher strain value ranges indicating plastic strain and plastic deformation were indicated with different colors according to the ε_{yy} strain magnitude.

Figure 4.3 shows the PD TTC cycle with a manually overlaid corresponding sine loading cycle for reference. The numbered time instants correspond with the DIC ε_{yy} strain fields shown in Figure 4.4. The translation phase from time instant 3 to 6 is shown in more detail in Figure 4.5. The following events can readily be observed:

- The growth of the tip plasticity peak ($\varepsilon \geq 4500$ microstrain) mainly takes place between time instants 0 and 3, thus before the plateau phase.

- This growth happens at a stationary location.

- The peak translates during the plateau phase from time instant 3 to 6 or possibly even to 7.

- The most significant translation occurs between time instants 4 and 6, during the first half of the plateau.

- After the plateau phase, the peak quickly disappears at a new stationary location, from time instant 7 to 9.

4.3.2. Detection of the crack tip plasticity peak location and magnitude using DIC line slice analysis

The peak of the plasticity can be thought of as the position of the crack tip itself, because the deformations are largest around the crack tip. Many crack growth models assume exactly this: the largest strain and stress occur at the crack tip itself, decreasing in magnitude when moving (radially) away from the crack tip. It is therefore interesting to observe and track the development of the peak plasticity, as it appears to be an indirect indicator of the crack length and crack growth itself. This peak and crack tip location are illustrated with a schematic geometry of a strip yield model in Figure 4.6, based on the Dugdale model, [8]. This figure and model also show that the plasticity increases gradually from both sides into the peak.

The translation and the change in magnitude of the peak plasticity can be further examined using DIC software. The ε_{yy} values at specific fixed locations can be gathered from specific DIC images. A line slice consists of a number of such locations spaced equidistant along an imaginary line: 'the line is sliced into points'. For this fatigue test analysis, a line slice was applied to a DIC image every 64 images, resulting in 200 line slices captured during a single cycle. Each line slice was placed at the exact same location for all images, in crack growth direction, just above or below the actual crack. This method allows for the peak location to be accurately determined, and the observed magnitude is close to the true peak
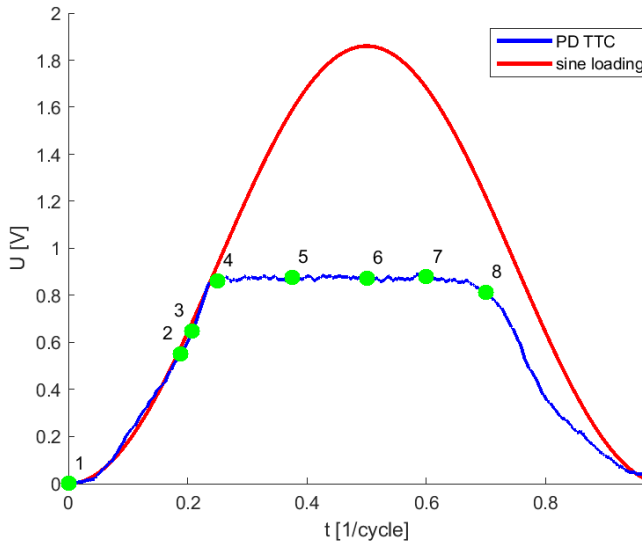
Figure 4.3: PD TTC cycle with an overlaid sine load cycle, near the end of the fatigue life. The plateau is clearly observable. The points mark time instants which correspond to crack tip plasticity DIC results shown in Figures 4.4 and 4.5. The colorbar ranges from 4500 microstrain to 7000 microstrain.

magnitude. Figure 4.7 shows schematically how such a line slice is placed on the image.

The resulting locations and magnitudes are plotted versus time in Figures 4.8 and 4.9, respectively. The plasticity peak magnitude has a very similar shape as the PD TTC curve: the curved start and ending proportional to the loading and the plateau in between are clearly visible. By overlaying these plots onto the loading and PD TTC curves of Figure 4.3, it follows that there are neat correlations between the loading curve and the peak location, and between the PD TTC curve and the peak magnitude.

The location Figure 4.8 at first glance appears to follow the sine loading, indicating that no translation is taking place. Closer inspection of the time interval near and after S_{max} reveals that the location data points are now placed above the sine loading curve. At a given time instant, the location stays at a larger value, i.e. is lagging behind. The amount of lag in vertical direction is proportional to the translation of the plasticity peak. This proves that the plasticity peak indeed undergoes a permanent translation.

The peak magnitude in Figure 4.9 shows an excellent correlation with the PD TTC potential curve, proving that PD TTC is measuring the crack tip plasticity.
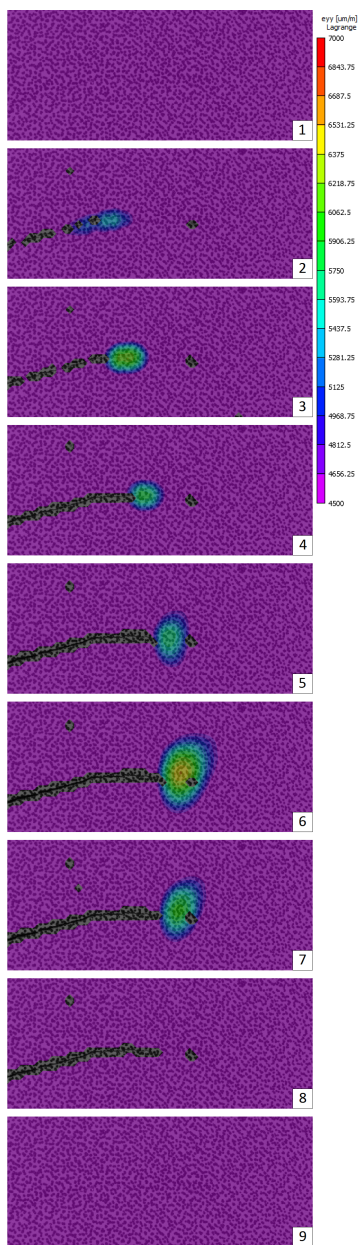
Figure 4.4: DIC results of the crack tip region, corresponding to the time instants shown in Figure 4.3. All images shown are from the same fixed region on the specimen. The peak plastic ε_{yy} strain smoothly and permanently translates between points 3 and 6, corresponding to the first half of the PD TTC plateau. The colorbar ranges from 4500 microstrain to 7000 microstrain.
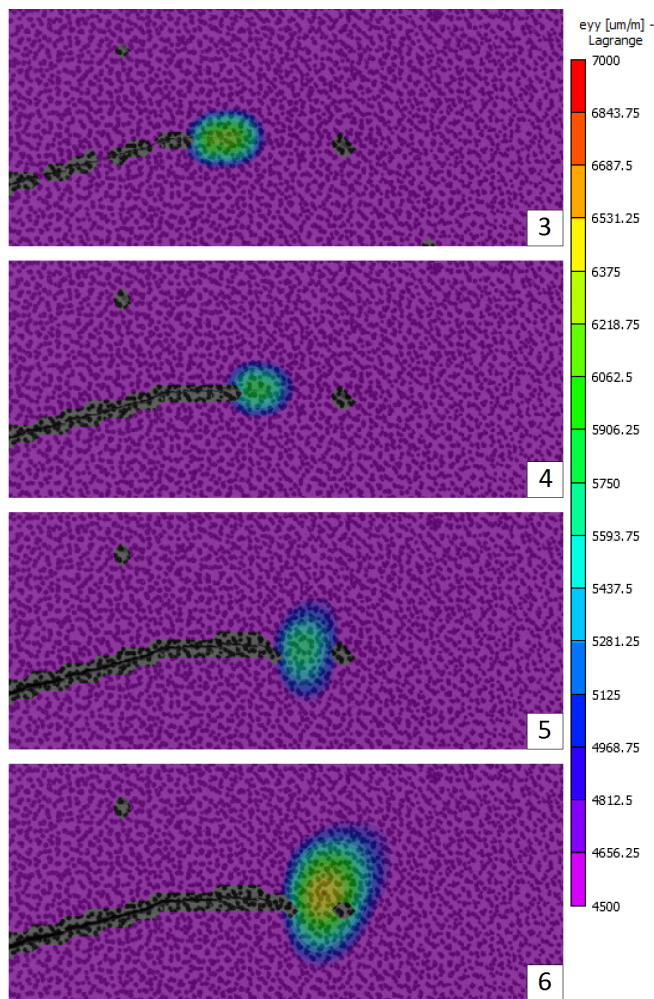
Figure 4.5: DIC results of the crack tip region, corresponding to the time instants shown in Figure 4.3. All images shown are from the same fixed region on the specimen. The peak plastic ε_{yy} strain smoothly and permanently translates between points 3 and 6, corresponding to the first half of the PD TTC plateau. The colorbar ranges from 4500 microstrain to 7000 microstrain.
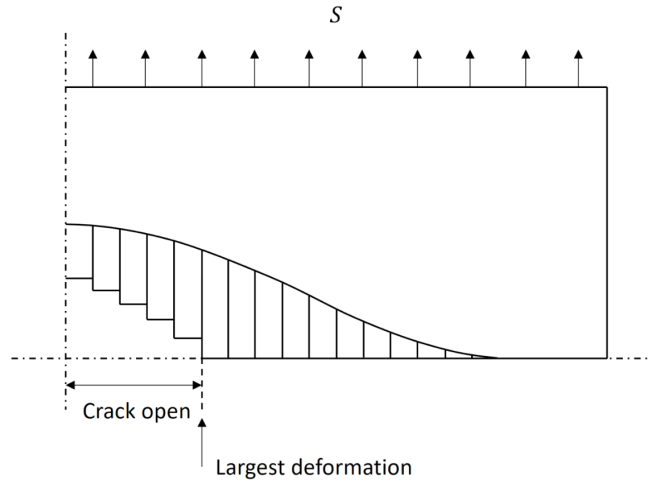
Figure 4.6: Schematic view of a strip yield model showing one quarter of a CCT specimen. The largest deformation and strain can be found at the crack tip, indicating that the peak plasticity is a indirect measure of the crack tip position and crack length.

4.4. Discussion on the combined measurement techniques and their results

The observation of the translation of the peak plastic deformation and the correlation with the PD TTC signal shows how the DIC technique supports the conclusion from Chapter 3 that the PD TTC signal is related to crack tip plasticity. While crack extension is not observed directly, for the correlation of the DIC raster is lost along the crack growth, it is observed indirectly by the movement of the peak plastic deformation.

The measurements shown in this chapter prove that crack growth can indirectly be measured with the DIC technique, but for small crack growth rates often mentioned in literature, the speckle pattern and camera resolution will have to be improved significantly to capture the small strains. The current measurements were taken near the very end of the specimen life at $a = 44$ mm. The crack growth rate da/dN is evidently largest here, in the order of 0.1 mm/cycle to 1 mm/cycle. It remains an estimate (based on similar fatigue tests) since the high speed PD TTC setup at high frequency frame rate could only store a single full cycle, preventing peak to peak measurement of two or more cycles. Nevertheless, the value for a and estimate for da/dN indicate that the crack growth has been significantly and increasingly affected by the finite width effect, also during a single cycle. Consider that the true plastic zone shape is different from the idealized circle shape of the Irwin model [9], as shown in Figure 4.10.

At a sufficiently large crack length, the plastic zone shape might have already been transforming from the true ideal Figure 4.11 condition to the more distorted Figure 4.12 condition. This occurs when the size of the elastic zone around the
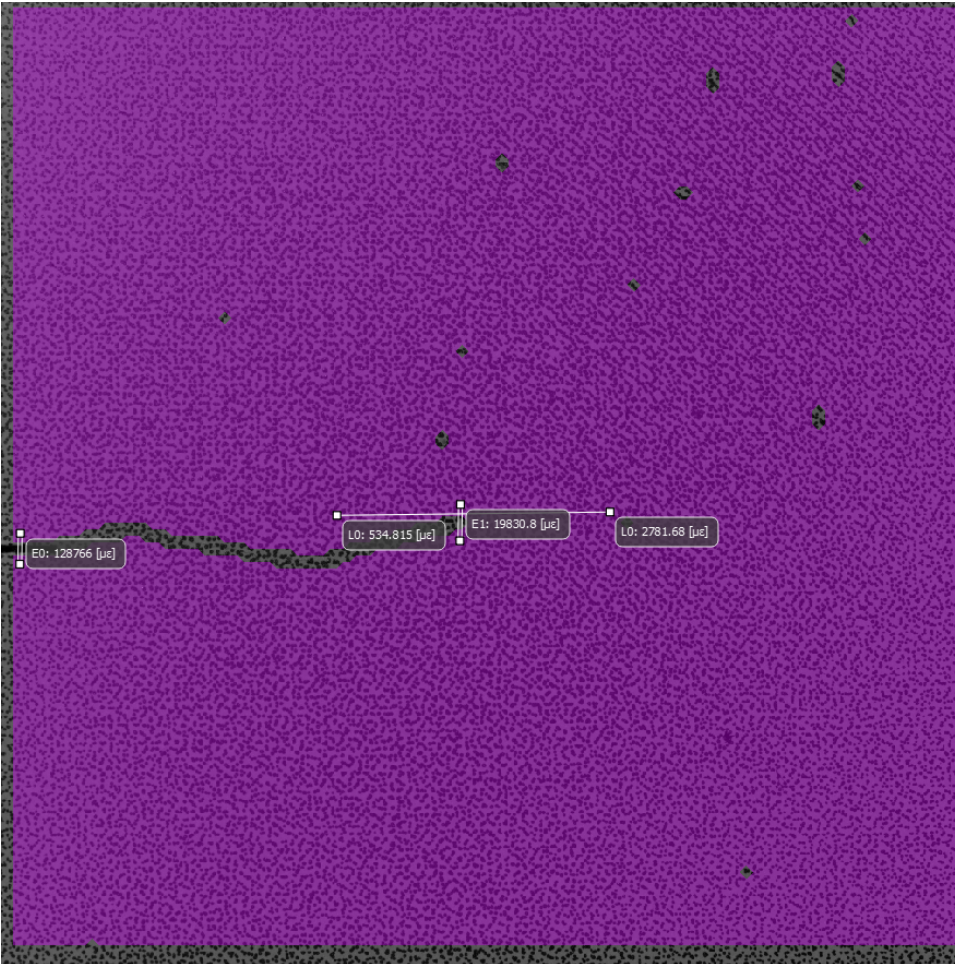
Figure 4.7: The white horizontal line L0 denotes the line slice placed over the crack tip area, parallel to the crack growth direction. Along this line slice, 2000 equidistant measurement points are located which inspect the ε_{yy} values. The vertically placed strain gauges E0 and E1 are not used in this analysis.
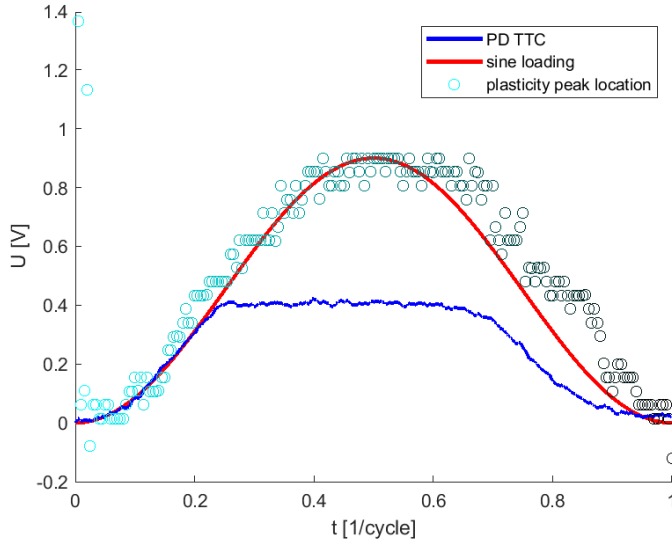
Figure 4.8: DIC line slice results of the peak ε_{yy} strain location superimposed on PD TTC curve by scaling and translating in vertical direction. A sine proportional to the loading is also added. The peak ε_{yy} location clearly follows the sine loading. Between $0.5 < t < 1$ the location value is slightly higher than the loading sine value: this indicates the permanent translation of the crack tip plastic zone and crack growth itself.
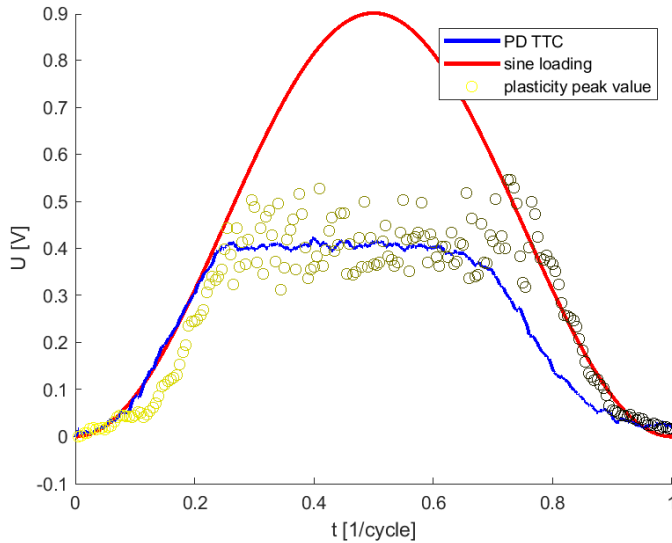

Figure 4.9: DIC line slice results of the peak ε_{yy} strain value superimposed on PD TTC curve by scaling and translating in vertical direction. A sine proportional to the loading is also added. The peak ε_{yy} value clearly follows the PD TTC plateau, and the sine loading before and after the plateau.

plastic zone is sufficiently large, already having reached the specimen edge. The plastic zone will continue growing in this elastically affected region and modifying its shape, until final fracture occurs close to the specimen edge for a sufficiently small $S_{\max}$.

These distortions of the plastic and elastic zones inevitably affect the measurements shown in this chapter, both PD TTC and DIC. The relative changes within a single cycle are still clearly discernible, and therefore the relation between these measurement technique results still holds.

(a)

(b)
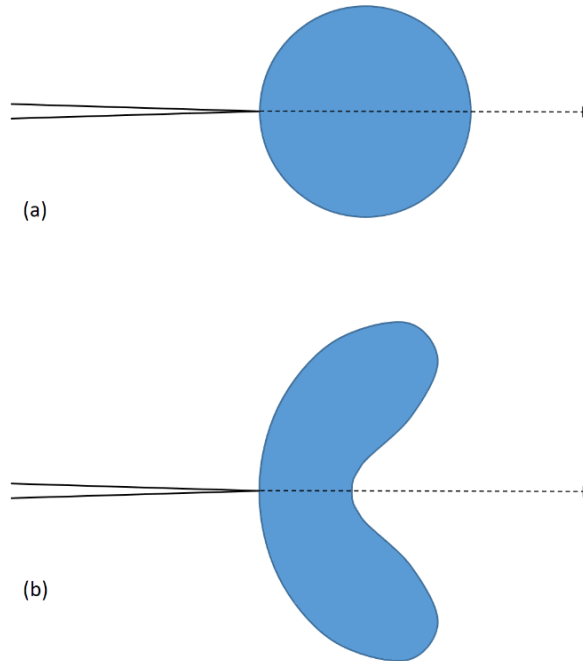
Figure 4.10: Schematic view of a crack tip plastic zone for an ideal, infinite width case. Crack growth direction shown with dashed arrow. (a) shows the idealized circular plastic zone according to Irwin [9]. (b) shows the more realistic but still idealized butterfly shape observed from experiments.

4.5. Conclusions

The results from the DIC measurement technique in combination with the PD TTC results discussed in Chapter 3 strengthen the correlation between the crack tip plasticity magnitude and the PD TTC potential signal. The DIC results show that the crack tip peak plasticity is proportional to the PD TTC curve magnitude, including the plateau phase. Furthermore, the DIC technique can measure the peak plasticity location, which is observed to permanently translate in crack growth direction during a specific time fraction of the cycle. This chapter therefore provides further proof of the scientific analysis results discussed in Chapter 3.
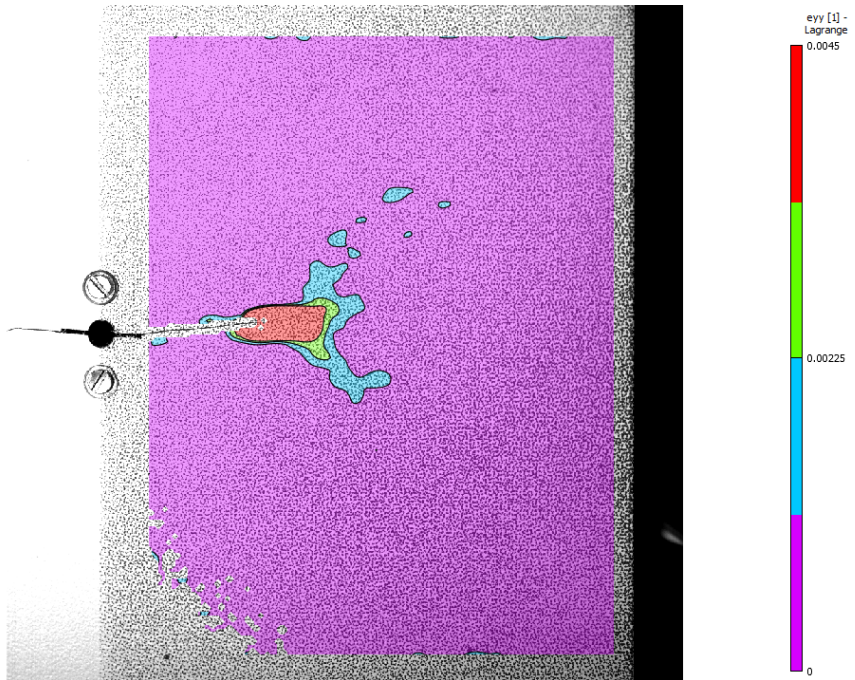
4

Figure 4.11: The true, measured shape of the ε_{yy} zone at a small crack length, with the butterfly shape being somewhat visible. The affected zone is still well surrounded by the plate, the crack tip plastic zone contained within effectively sees a nearly infinite plate. Four strain levels indicated between $0 < \varepsilon_{yy} < 0.0045$, all areas with $\varepsilon_{yy} \geq 0.0045$ fall within the highest strain level indicated.
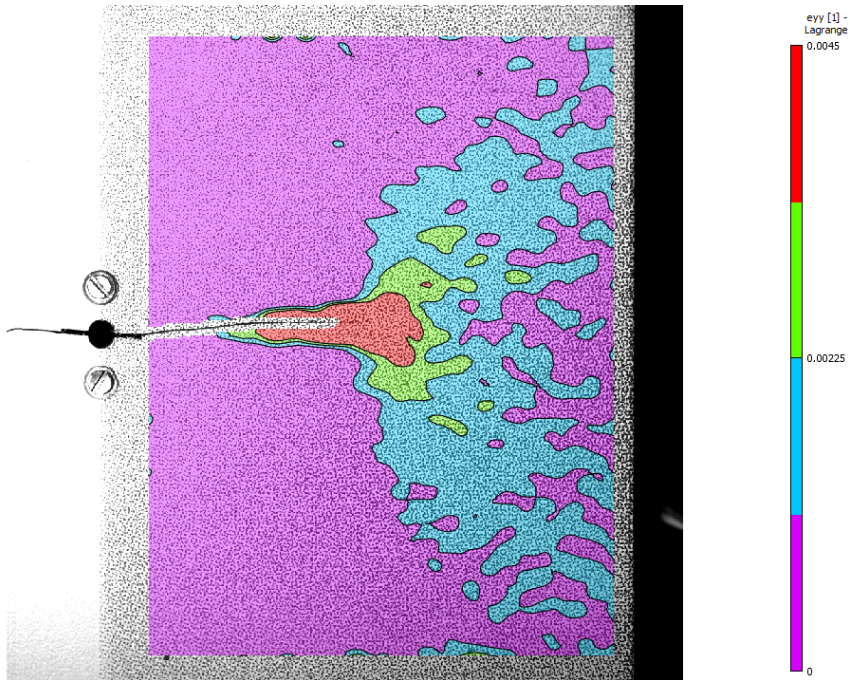
Figure 4.12: The ε_{yy} (butterfly) shape at a large crack length is of sufficient size to be affected by the finite width of the plate: here, the elastic stress zone has just reached the plate edge. Its shape will therefore change, which affects the smaller crack tip plastic zone. Four strain levels indicated between $0 < \varepsilon_{yy} < 0.0045$, all areas with $\varepsilon_{yy} \geq 0.0045$ fall within the highest strain level indicated.

References

[1] S. Hamada, Y. Araki, and H. Noguchi, *Digital-image-correlation observation of cyclic plastic strain field during the damage-accumulation mode of fatigue crack propagation under pure cyclic mode II loading for cold-rolled SUS430 steel,* Materials Science and Engineering: A **845**, 143246 (2022).

[2] S. Vanlanduit, J. Vanherzeele, R. Longo, and P. Guillaume, *A digital image correlation method for fatigue test experiments,* Optics and Lasers in Engineering **47**, 371 (2009), optical Measurements.

[3] M. Sánchez, C. Mallor, M. Canales, S. Calvo, and J. Núñez, *Digital image correlation parameters optimized for the characterization of fatigue crack growth life,* Measurement **174**, 109082 (2021).

[4] M. Koster, C. Kenel, W. J. Lee, and C. Leinenbach, *Digital image correlation for the characterization of fatigue damage evolution in brazed steel joints,* Procedia Materials Science **3**, 1117 (2014), 20th European Conference on Fracture.

[5] J. Carroll, W. Abuzaid, J. Lambros, and H. Sehitoglu, *An experimental methodology to relate local strain to microstructural texture,* Review of Scientific Instruments **81**, 083703 (2010).

[6] Correlated Solutions, Inc., *VIC-2D 6 DIC software,* https://www.correlatedsolutions.com/software-downloads/#vic2d, Online, accessed on 2021 03 15.

[7] FAA US, *Metallic materials properties development and standardization (MM-PDS),* Federal Aviation Administration, Washington, DC, Paper No. MMPDS-05 (2010).

[8] D. Dugdale, *Yielding of steel sheets containing slits,* Journal of the Mechanics and Physics of Solids **8**, 100 (1960).

[9] G. R. Irwin, *Linear fracture mechanics, fracture transition, and fracture control,* Engineering Fracture Mechanics **1**, 241 (1968).

5

Towards a physics based model of fatigue crack growth

Material fatigue is a significant societal and economic problem. To avoid catastrophic failures, most designs require fatigue data to demonstrate reliability. Fatigue research generally adopts the experimentalist approach, in which loading parameters are correlated phenomenologically to observed consequence.

Fatigue damage growth prediction models are predominantly developed by fitting power law relationships through observed correlation. While reasonably accurate, these models always need fatigue data to be predictive.

These models do not provide a deeper understanding of fatigue damage growth physics. Here we demonstrate that fatigue crack growth is well described with physics using an energy balance and a sliding box analogy with friction.

We observed that the energy balance is governed by crack tip plasticity and surface energy. Friction levels correspond to physical crack tip opening. Correlating cyclic loading through cyclic strain energy gives the available energy for dissipation through plasticity and crack advancement.

Our results demonstrate that fatigue crack growth curves can be generated from stress-strain material data, significantly reducing the required amount of fatigue testing.

We expect that this model becomes the starting point for correct physics based approaches towards fatigue damage growth, significantly enhancing our understanding and enabling equal levels of reliability in engineering without costly fatigue testing.

This chapter is a modified version of a manuscript in preparation.

5.1. Introduction

L iterature on fatigue crack growth is largely based on observations and experimental data. In 1839, the word 'fatigue' was used for the first time in writing by Poncelet [1], describing how cast iron axles used in mill wheels became 'tired' after a certain period of usage. The 1842 Versailles rail accident, Ref. [2], at the time the largest in the world, was caused by metal fatigue. Its accident investigation is widely regarded as the start of the fatigue research field, which later expanded to explicitly include the study of the crack growth phenomenon. In the 1950s several important investigations were carried out regarding the stress field and the plastic zone shape, including notably the work of Irwin [3, 4]. This work, combined with the insights from Paris and Erdogan [5] in the 1960s, gave the research field a large impulse. Fatigue crack growth data could be expressed as a simple power law, as a function of a similitude parameter $\Delta K = S_{\mathrm{max}}\beta\sqrt{\pi a}$ based on the crack tip stress intensity, resulting in the 'Paris law':

$$\frac{da}{dN} = C\Delta K^m + b \tag{5.1}$$

Using the similitude parameter $\Delta K_{\mathrm{eff}} = (S_{\mathrm{max}} - S_{\mathrm{op}})\beta\sqrt{\pi a}$ instead of ΔK removed virtually all stress ratio R effects by including opening and closure effects, resulting in a nearly generic crack growth curve for a given material and alloy:

$$\frac{da}{dN} = C\Delta K_{\mathrm{eff}}{}^m + b \tag{5.2}$$

From here on did the field stay largely empirical and phenomenological, with various improved models developed from an engineering perspective to more accurately predict constant amplitude (CA) and variable amplitude (VA) fatigue for industry.

While these models have become rather accurate, none of them are physically correct. The ubiquitous 'Paris law', Equation (5.1), and subsequent models based on Equation (5.2) are dimensionally incorrect, a fact not widely recognized given the many power law models available, such as Refs. [6–10]. Equations (5.1) and (5.2) are only correct when C has the dimension $\mathrm{MPa}^m \mathrm{m}^{(1-m/2)}$, making the constant C a function of the exponent m. This imperfection to some extent has also been noted in literature, even though with some debate, such as Refs. [11–13].

A larger issue can be found with the similitude parameters. The similitude concept in particular is seen as the driving force behind crack growth, with the result being the fatigue crack growth rate through the 'Paris law'. However, this is not quite correct from a physics point of view. Intuitively, one would expect a driving force, being slowed down by resistance, resulting in a net fatigue crack growth rate, whose development might be captured by a similitude parameter. The similitude concept itself relates primarily to the scaling of physical parameters, and cannot equate to a driving force.

On top of that, the widely used similitude parameter ΔK_{eff} uses an opening stress S_{op}. This opening stress is a challenge to measure accurately since the exact crack

tip is hard to reach. It is shown in Ref. [14] that there actually are two distinct opening stresses, which are related. The measured, phenomenological opening stress $S_{\text{op,phen}}$ is different from the true, physical opening stress $S_{\text{op,phys}}$ at the crack tip. It shows that the understanding of crack closure is incomplete, and that the physical understanding of the phenomenon is not yet correct or complete.

The popularity of the power law model with similitude parameters must be sought in its simplicity and ease of use as an engineering approximation, as it appears conveniently as a straight line on a double logarithmic plot. Nevertheless, there are other ways to look at the phenomenon of fatigue crack growth.

The theoretical thermodynamic approach appears appropriate at first glance for it describes the complete system with all the required physical mechanisms, Ref. [15]. However, it does not have a practical approach as it essentially requires a high resolution discretization of the theoretical continuum, effectively resulting in a finite element analysis with all known associated restrictions and limits. For example: mesh distortion in the crack tip plastic zone, and required computation time.

Another physics approach is to consider the energy balance of the fatigue specimen, equating the driving force to the sum of resistance terms. Alderliesten [16, 17] describes the concept and gives a first idea energy balance of the fatigue crack growth phenomenon. It equates the applied work of a single cycle to the energy dissipated by crack growth during that cycle. This energy balance approach appears to be a practical description of the fatigue crack growth phenomenon, but with a physical basis. It is this approach that is further extended in this paper.

5.2. The concept of the energy balance approach to fatigue

Equating energy dissipation to the change in applied work is a method to describe fatigue crack growth based on physical parameters. The resulting equation is a balance of energy terms, hence the name: energy balance (of fatigue crack growth). It is built up using existing models and physical parameters from literature, serving as known building blocks to build a physical model.

The basic form of the energy balance states that the change in applied work equals the dissipation of energy due to crack growth and plastic deformation, plus the elastic energy lost due to the increased plastic zone:

$$\dot{J} = \dot{U}_{\text{a}} + \dot{U}_{\text{p}} + \dot{U}_{\text{ep}} \tag{5.3}$$

Consider a single load cycle of a load-controlled fatigue specimen. Figure 5.1 shows the development of the energy balance terms schematically.

During loading, the applied work is first stored as elastic energy. When plasticity increases and crack growth happens, the specimen compliance increases, which requires extra work. During unloading, the decreased effective stiffness relieves a certain amount of energy as elastic energy, but not all energy. The difference is the sum of energy dissipated by crack extension, plasticity generation, and change
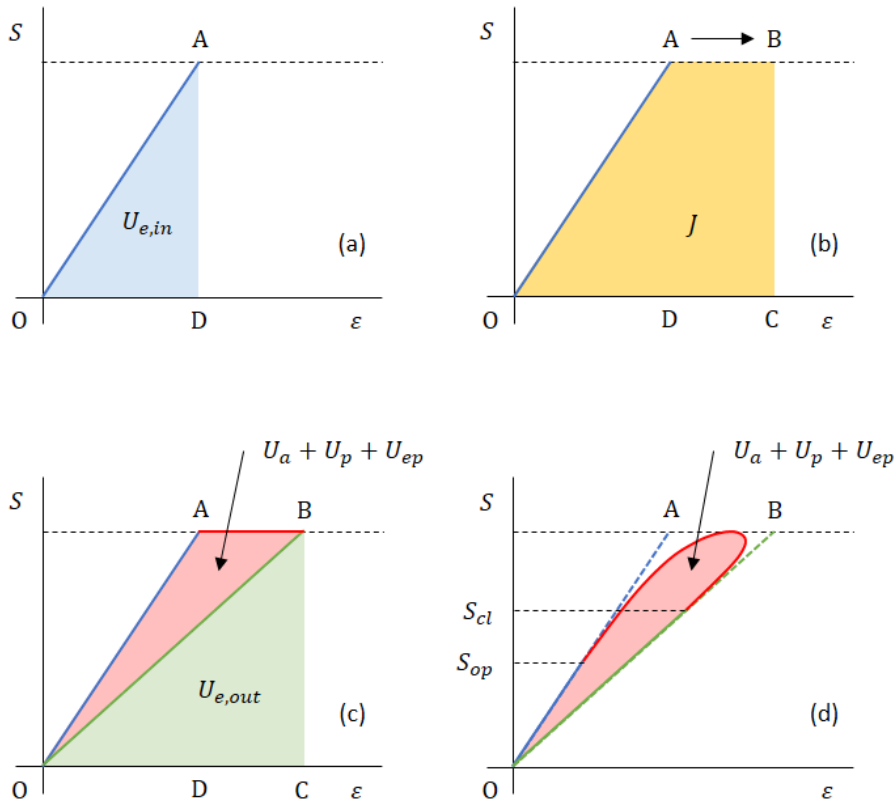
5

Figure 5.1: Applied work and dissipation in a single cycle of a load-controlled fatigue specimen, schematically explained. (a) During loading, applied work is stored as elastic energy. (b) The total applied work increases when the specimen compliance increases from A to B. (c) During unloading, an increased amount of elastic energy is released. The amount of energy not recovered, equals the energy dissipation related to fatigue crack growth, which caused the compliance increase. (d) A more realistic interpretation of a single fatigue cycle. The dissipated work starts and stops at crack opening and crack closure, respectively.

in elastic energy due to the plasticity increase. This total dissipation is equal to the effective or net applied work. In other words, the change in work also equals the change in elastic energy:

$$\dot{J} = \dot{U}_{e,\text{out}} - \dot{U}_{e,\text{in}} \tag{5.4}$$

The energy balance also holds for any arbitrary increase in crack length or amount of cycles, where integrating on both sides gives the respective energy quantities. This basic form is a starting point for a physics based approach to fatigue crack growth.

A surprising result of the mathematical derivation is that fatigue cycles do not need to enter the energy balance equation. Fatigue cycles can be modeled however, by using another physical model, the sliding box analogy. This analogy describes a sliding box over a flat surface as a physical analogy to the crack extension per cycle. It models the growth of da/dN throughout the fatigue life, in accordance with the energy balance.

The energy balance and sliding box analogy are explained in detail below.

5.3. The energy balance

All terms of the energy balance are described in more detail below, thereby constructing a physical model of the applied work and energy dissipation.

5.3.1. Applied work

Loading the uncracked specimen takes a finite amount of energy, based on the stiffness of the material and the volume. The specimen can be modeled as a simple spring with stiffness E, applied stress S, and volume WTL using Hooke's law, Ref. [18]:

$$U_{\text{spring}} = \frac{1}{2}S\varepsilon WTL = \frac{1}{2}\frac{S^2}{E}WTL \tag{5.5}$$

The change in energy per cycle between $S_{\min}$ and $S_{\max}$ equals the difference in spring energy between these loads:

$$\left(\frac{dU}{dN}\right)_{\text{uncracked}} = \frac{1}{2}\frac{\left(S_{\max}^2 - S_{\min}^2\right)}{E}WTL \tag{5.6}$$

As the crack grows, the effective stiffness E^* of the specimen decreases as more deformation is possible in loading direction resulting in more compliance. This finite width effect, β, is well known. Ref. [19] mentions how the applied work and thereby effective stiffness are related to the finite width effect. Several models exist, here the Feddersen model is used, Ref. [20], Equation (5.7), because it is an accurate representation over a large range of $2a/W$ crack life.

$$\beta = \sqrt{\sec\left(\frac{\pi a}{W}\right)} \tag{5.7}$$

This results in the effective stiffness E^* being expressed as:

$$E^* = \frac{E}{\beta} = \frac{E}{\sqrt{\sec\left(\frac{\pi a}{W}\right)}} \tag{5.8}$$

The maximum stored energy at any crack length can be described as the stored energy of the uncracked plate at $a = 0$ with stiffness E, times a finite width correction as function of the crack length:

$$U_{\text{max}} = \frac{1}{2}\frac{S_{\text{max}}^2}{E^*}WTL$$

$$U_{\text{max}} = \frac{1}{2}\frac{S_{\text{max}}^2}{E}WTL\,\beta \tag{5.9}$$

$$U_{\text{max}} = \frac{1}{2}\frac{S_{\text{max}}^2}{E}WTL\sqrt{\sec\left(\frac{\pi a}{W}\right)}$$

The applied work per cycle, Equation (5.6), can be updated with the finite width correction in a similar way to incorporate the fatigue crack:

$$\frac{dU}{dN} = \frac{1}{2}\frac{\left(S_{\text{max}}^2 - S_{\text{min}}^2\right)}{E}WTL\sqrt{\sec\left(\frac{\pi a}{W}\right)} \tag{5.10}$$

5.3.2. Crack surface energy dissipation

The most apparent dissipation term concerns the creation of the crack, and is relatively straightforward. It is explained in more detail below.

$$U_{\text{a}} = \frac{dU_{\text{a}}}{dA}T\gamma\lambda a \tag{5.11}$$

Free surface energy

The free surface energy dU_{a}/dA is the required energy to create a free surface: it is the difference of internal energy in the atom lattice between the center of a unit cell and its surface. It can be taken as a constant for a given material, and a typical value for aluminum is in the order of $1\,\text{J}\,\text{m}^{-2}$, Ref. [21]. As the crack generates two surfaces, the effective energy dissipation becomes $2\,\text{J}\,\text{m}^{-2}$.

Surface roughness

In literature, the crack surface is often implicitly taken to be the projected crack area. For an ideal through crack, this projected area simply equals the crack length a multiplied by the specimen thickness T. In reality, the crack surface is quite rough. The actual grown crack surface is therefore larger than the projected crack surface, and thereby more energy is dissipated per crack length. Figure 5.2 shows schematically how due to surface roughness the actual area is larger compared to the projected area.

3D surface area > 2D surface area

2D crack surface   3D crack surface
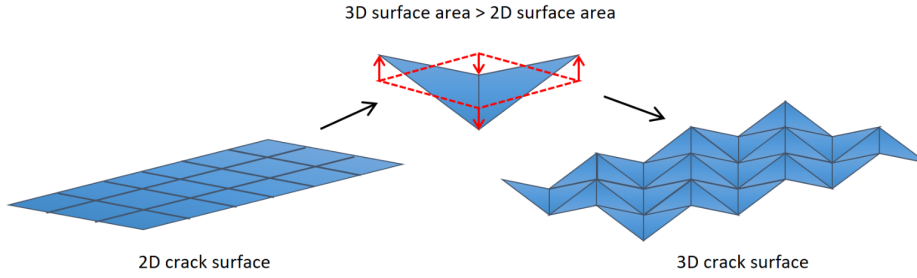
Figure 5.2: Schematic explanation of how crack surface roughness increases the actual surface area over the projected surface area.

The effect of S_{max}, R, and environment on the roughness was experimentally investigated by Hogeveen [22], who showed that the development and magnitude of roughness differ for air and vacuum, and that a larger R or a larger S_{max} causes more roughness. From post-mortem inspection of the crack surface it was observed that the roughness increased during crack growth, and along the crack length.

The scale factor γ allows corrections of the crack surface $\lambda a T$ for the change in roughness, both during the fatigue life and for different test parameters.

There is no full consensus in literature on which of the many definitions of roughness to use, as the geometric concept of roughness has similarities with the mathematical concept of fractals. In this initial study of the energy balance, a constant $\gamma = 1$ was assumed for simplification. A constant value is also valid when examining a sufficiently small part of the specimen life and subsequent crack length range where the roughness does not change significantly.

Shear lip effective area

When a shear lip forms, the effective surface area increases as the crack plane rotates away from the original cross-section plane which is perpendicular to the load direction. This is shown schematically in Figure 5.3. The effective surface area can be modeled as the projected surface area times a scaling factor λ. During the shear lip formation, this scaling factor linearly increases from a value of unity to $\sqrt{2}$ for a shear lip with an angle of $45°$.

5.3.3. Crack tip plasticity dissipation

This term of the energy balance contains the dissipation due to plastic deformation of the material around the crack tip:

$$U_p = \frac{dU_p}{dV_p} V_p \tag{5.12}$$

Where dU_p/dV_p relates to the change in mean plastic energy density in the plastic zone. This zone translates along with the crack tip movement, and also
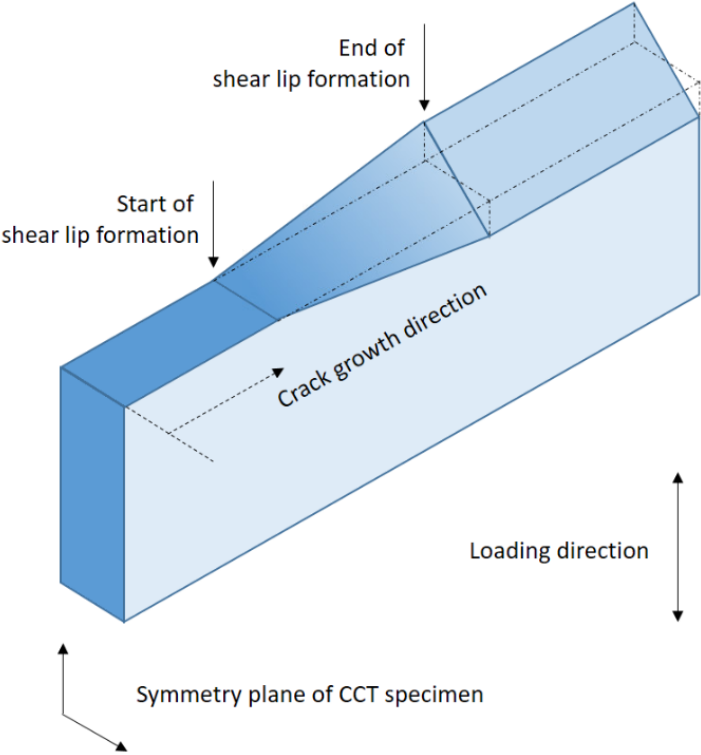
5

Figure 5.3: One quarter of a CCT fatigue specimen, showing the crack plane with shear lip formation. The crack surface area increases as it rotates.

grows in size. The volume increase as function of crack length a is captured in the V_p term. These terms are explained in more detail below.

Change in mean plastic energy density

$$\frac{dU_p}{dV_p} \tag{5.13}$$

The change in mean plastic energy density was modeled using fatigue test data in combination with the energy balance. Fatigue test parameters of four tests on two aluminum alloys and one steel alloy are shown in Table 5.1.

Table 5.1: Fatigue test and modeling parameters of several CCT fatigue tests, indicating different CA fatigue spectra and material/alloy choices. Tests 1 and 2 were performed by the first author.

Test [-]	R [-]	S_{max} [MPa]	S_{yield} [MPa]	S_{op}/S_{max} [-]	Material [-]	a_0 [mm]	W [mm]	Ref. [-]
1	0	60	324	0.74	Al 2024-T3	13.18	160	-
2	0.3	80	324	0.55	Al 2024-T3	11.25	160	-
3	0.1	48.8	503	0.68	Al 7075-T6	6.35	160	[23]
4	0.5	113	460	0.63	Fe 510 Nb	10.00	100	[24]

Solving the energy balance equation with dU_p/dV_p as unknown resulted in curves with similar trend: decreasing values for increasing crack length, shown in Figure 5.4.
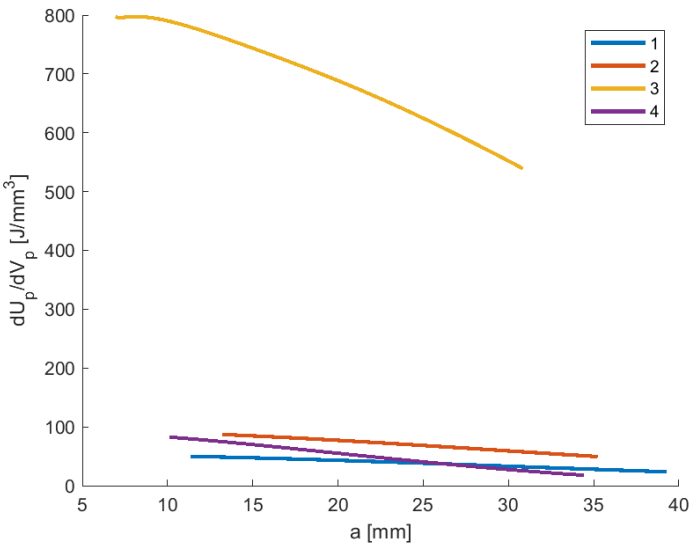
Figure 5.4: dU_p/dV_p curves of several fatigue tests (Table 5.1) versus the crack length a.

However, each loading and geometry combination produces a unique dU_p/dV_p curve. Scaling these curves by $(S_{max}/S_{yield})^2$ and using the normalized crack length $2a/W$ makes the curves collapse onto each other. This allows the use of a generic curve $Q = f(a)$, which can be fitted with a power law with an exceptional exponent: the golden ratio $\phi = (1 + \sqrt{5})/2$, which is related to the Fibonacci sequence, which can be found in many ways in nature. Generic curve Q becomes:

$$Q = \pi \left[1 - 2\left(\frac{2a}{W}\right)^{\phi} \right] \tag{5.14}$$

The scaled curves and Q are shown in Figure 5.5. The one exception is test 2, which is only qualitatively correct, which must be sought in a different value for U_{max}. Nevertheless, with generic curve Q the resulting equation for dU_p/dV_p becomes:

$$\frac{dU_p}{dV_p} = Q\left(\frac{S_{yield}}{S_{max}}\right)^2 = \pi \left[1 - 2\left(\frac{2a}{W}\right)^{\phi} \right]\left(\frac{S_{yield}}{S_{max}}\right)^2 \tag{5.15}$$

Of particular interest is the value of $2a/W$ for $Q = 0$, by extrapolation of the curve fit: the value is not reached at the plate edge $2a/W = 1$, but before at $2a/W \approx 0.65$. This suggests that the required energy density goes to zero at a certain normalized crack length, where the plastic volume becomes infinite. As the plastic zone approaches and eventually reaches the plate edge, long before the crack tip arrives, the stress distribution and plastic zone shape will change. The basic assumptions of linear elastic fracture theory, such as the Irwin plastic zone model and small scale yielding, are no longer applicable. This interaction and change of the plastic zone make it possible for the crack tip to reach beyond $2a/W \approx 0.65$ for high cycle fatigue. Regardless, the plastic energy density tends to grow towards infinity at some point during crack growth which is physically impossible, and instead final fracture happens: a runaway crack growth during the last cycle.

Plastic volume

The plastic zone volume V_p can be expressed as function of the crack length. A well known model for the plastic zone is the Irwin plasticity model, Ref. [4], where the plastic zone is modeled as a cylinder with a height equal to the specimen thickness T, and a radius r_p. The total volume equals $V_p \propto r_p^2 T$, schematically shown in Figure 5.6. The radius is a function of the applied stress and crack length.

$$r_p = \frac{1}{\pi}\left(\frac{K}{S_{yield}}\right)^2 = \frac{1}{\pi}\left(\frac{S_{max}\beta\sqrt{\pi a}}{S_{yield}}\right)^2 = a\beta^2 \left(\frac{S_{max}}{S_{yield}}\right)^2 \tag{5.16}$$

The finite width correction β is again given here by the Feddersen correction, Equation (5.7). The total plastic zone volume is expressed as:

$$V_p = a^2\beta^4 \left(\frac{S_{max}}{S_{yield}}\right)^4 T = a^2 \sec^2\left(\frac{\pi a}{W}\right)\left(\frac{S_{max}}{S_{yield}}\right)^4 T \tag{5.17}$$
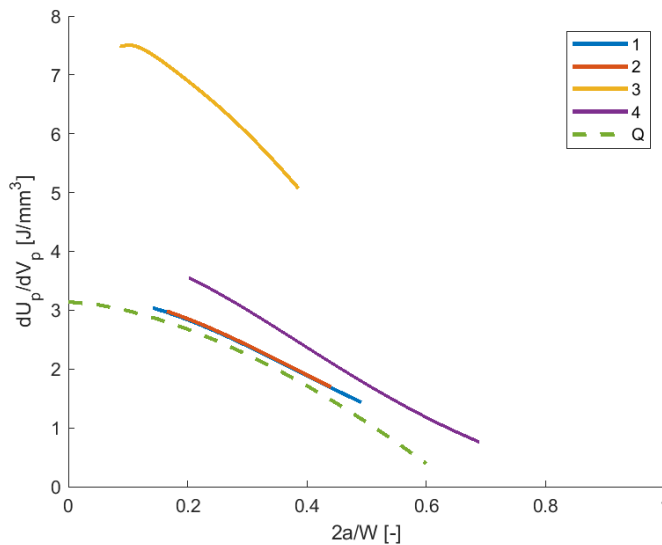
Figure 5.5: The dU_p/dV_p curves of several fatigue tests (Table 5.1) scaled using Equation (5.15). Also shown is generic curve Q from Equation (5.14), which is extrapolated reaching $dU_p/dV_p = 0$ before the edge of the plate, suggesting a $2a/W < 1$ value where fatigue specimens will fail.
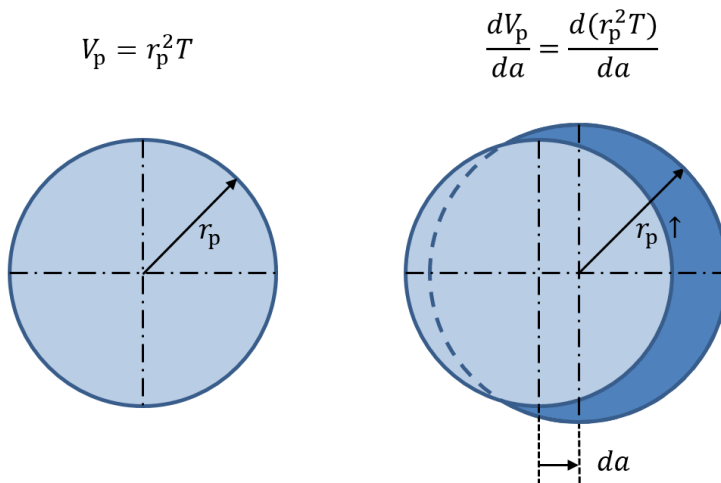
$$V_p = r_p^2 T \qquad\qquad \frac{dV_p}{da} = \frac{d(r_p^2 T)}{da}$$

Figure 5.6: Schematic view of the cylindrical plastic zone of Irwin [4], and the growth as function of the crack length. The crescent volume increase results from the combination of a translation da and an increased radius r_p.

The actual shape of the plastic zone is not circular, as is widely known and reported in literature. Furthermore, Ref. [25] notes that in the Irwin model, r_p actually relates to the diameter of the cylindrical plastic volume rather than the

radius. This likely results from the increased local stress being capped by S_{yield}, effectively redistributing the increased local stress and resulting deformations over a larger volume. Nevertheless, the plastic volume shape remains rather constant throughout the fatigue life, and the applicability of the Irwin plasticity model is considered sufficiently valid, for the relative growth of the modeled cylinder versus the plastic zone is proportional.

5.3.4. Elastic energy dissipation

$$U_{\text{e}} \tag{5.18}$$

The elastically stored energy during loading in the first half of the load cycle is released during unloading in the second half of the load cycle, and therefore does not contribute to dissipation. However, the plastically deformed volumes do not return to their original state and impose a certain elastic energy loss. As the plastic volume grows, this loss grows proportionally. Given that the plastic strain is significantly larger than the elastic strain, the loss of elastic energy is expected to be significantly smaller than the plastic energy dissipation.

For CA fatigue it is assumed that the elastic energy dissipation is proportional to the plastic energy dissipation, Equation (5.19). Therefore the former term can be neglected as it can be included in the latter term, as a small, implicit constant scale factor.

$$\frac{dU_{\text{e}}}{dN} \propto \frac{dU_{\text{p}}}{dN}. \tag{5.19}$$

For VA fatigue this might not hold, and a cycle-by-cycle approach is necessary to properly assess the change in elastic energy dissipation.

The applied work and the three energy dissipation mechanisms of the energy balance are now defined. For CA fatigue, this reduces to the applied work and two energy dissipation mechanisms. The energy balance equation in the current state cannot be solved for fatigue crack growth: it is a continuous equation without a dependency on the cycles N. Furthermore, a cycle does not have a dimension. The energy balance can be rewritten by taking the derivative with respect to a to include a suitable physical parameter and by multiplying by the fatigue crack growth rate da/dN to include the cycles N.

$$\frac{dU}{dN} = \frac{dU}{da}\frac{da}{dN} = \left[\frac{dU_{\text{a}}}{da} + \frac{dU_{\text{p}}}{da}\right]\frac{da}{dN} \tag{5.20}$$

The fatigue crack growth rate da/dN appears on both sides and therefore cancels out. The result is again a continuous energy balance that holds for any given crack length, but without a dependence on N:

$$\frac{dU}{da} = \frac{dU_{\text{a}}}{da} + \frac{dU_{\text{p}}}{da} \tag{5.21}$$

From Equation (5.17) it is already clear that a derivative dV_{p}/dN is not possible, as there is no term containing N. Equation (5.21) uses a derivation with respect

to a, which is possible. The plasticity term in the energy balance can be written as $dU_p/da = (dU_p/dV_p)(dV_p/da)$. The derivative of the plastic volume with respect to the crack length, dV_p/da, follows from derivation of Equation (5.17) resulting in Equation (5.22).

$$\frac{dV_p}{da} = \frac{d}{da}\left[a^2 \sec^2\left(\frac{\pi a}{W}\right)\left(\frac{S_{\max}}{S_{\text{yield}}}\right)^4 T\right]$$

$$\frac{dV_p}{da} = 2\left(\frac{S_{\max}}{S_{\text{yield}}}\right)^4 T \sec^2\left(\frac{\pi a}{W}\right)\left[a + a^2\frac{\pi}{W}\tan\left(\frac{\pi a}{W}\right)\right] \tag{5.22}$$

5.3.5. Analogy for the absence of cycles in the energy balance

Consider a marble falling straight down. As the altitude decreases, the potential energy increases. The altitude and potential energy are linked through a continuous energy balance, valid at any position along the vertical trajectory of the marble.

Now consider a staircase, with the marble placed near the top. When dropped, the marble will fall from step to step, in a discrete way. Either it is stationary on a step, or falling in between two steps. The spacing of the steps does not have to be constant. Neither velocity nor step spacing is of importance to the continuous energy balance, because only the vertical position is taken into account: the energy balance still holds at all positions.

In this analogy the staircase equals the fatigue spectrum, with each step representing a single fatigue cycle. The vertical fall direction is the crack length, with the marble indicating the crack tip location. The start of each new fatigue cycle can be seen as the instant removal of the step where the marble is currently residing on. The marble is then free to continue its journey downward during that particular cycle, and advance to the next position: the crack extends during one cycle.

Human beings tend to count fatigue life in load cycles, as it is a very tangible parameter to measure. Therefore, intuitively dN needs to be present, since a finite amount of work is applied and dissipated during each single loading cycle, which can therefore be quantified with respect to that cycle. ΔN is an alternative to dN when averaging the applied work and dissipation over a range of cycles. However, note that cycles are dimensionless: they are invisible to the energy balance. While the energy can be quantified per cycle, it is not necessary, and the energy balance itself does not provide this step size. Therefore, the dN terms do not have a place in the physical description of energy during fatigue crack growth, a fact often overlooked given the abundance of measurements and models in literature incorporating the da/dN fatigue crack growth rate.

5.3.6. A discrete version of the energy balance

The absence of cycles in the energy balance means that the fatigue crack growth rate da/dN cannot be predicted with the energy balance only. The required step size $\Delta a/\Delta N$ requires a discrete form of the energy balance. Equation (5.15) already introduced a discrete step size originating from fatigue data sets in one of the

energy terms. Previously, the change in cycles dN was used as step size, but it was necessarily removed to allow the energy terms to be expressed by physical parameters only. As a solution, Equation (5.21) can be discretized with finite steps over the crack length, Δa, as shown in Equation (5.23):

$$\frac{dU}{da}\Delta a = \left[\frac{dU_a}{da} + \frac{dU_p}{da}\right]\Delta a$$

$$U(a + \Delta a) - U(a) \approx \left[\frac{dU_a}{da} + \frac{dU_p}{da}\right]\Delta a \tag{5.23}$$

It can be understood as a linearization of the crack growth at a given crack length, over a finite crack extension Δa, as shown in Figure 5.7. The applied work over the range Δa can be calculated as the difference between the total energy over this range as shown in Equation (5.23), which is a close approximation becoming exact for the limit $\Delta a \to 0$. Modeling a fatigue crack using measurement data of a, N, and U, is therefore possible by implicitly assuming that $\Delta a = \Delta a / \Delta N$, which is mathematically correct as cycles are dimensionless.
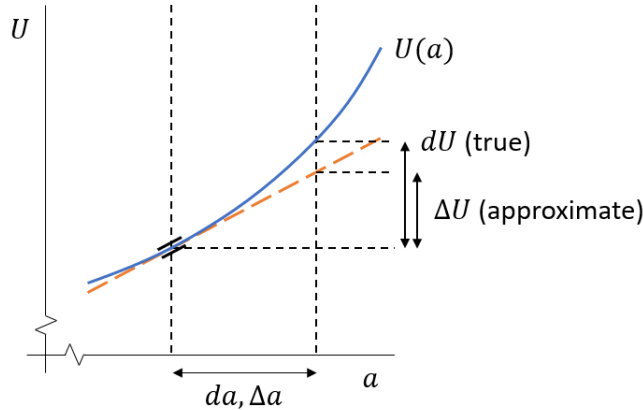
Figure 5.7: Schematic difference between two methods of calculating ΔU at a given crack length a from the energy balance. The linearization over a distance Δa results in ΔU, while the true difference results in a larger ΔU.

Substituting Equations (5.15) and (5.22) into Equation (5.23) results in the discretized energy balance for constant amplitude fatigue crack growth:

$$U\left(a + \Delta a\right) - U\left(a\right) \approx \left[\frac{dU_a}{dA} T\gamma\lambda + \pi\left[1 - 2\left(\frac{2a}{W}\right)^\phi\right]\right.$$

$$\left(\frac{S_{\text{yield}}}{S_{\text{max}}}\right)^2 2\left(\frac{S_{\text{max}}}{S_{\text{yield}}}\right)^4 T\sec^2\left(\frac{\pi a}{W}\right)$$

$$\left. \left[a + a^2\frac{\pi}{W}\tan\left(\frac{\pi a}{W}\right)\right]\right]\Delta a \tag{5.24}$$

While the energy balance by itself cannot predict Δa, ΔN, or da/dN directly, a method towards prediction of fatigue crack growth based on another physical model is given in the next section.

5.4. Sliding box analogy for the fatigue crack growth rate

Presented here is a separate physical model which iteratively calculates the fatigue crack growth rate da/dN based on material parameters and specimen geometry. It is shown that it can be coupled to the energy balance of Section 5.3, proving that it is possible to predict the fatigue crack growth rate using the energy balance.

5.4.1. The sliding box analogy

The energy balance Equation (5.23) is continuous, and does not provide information on step sizes Δa and/or ΔN. The discrete version, Equation (5.24), requires original fatigue data as input to model the crack growth rate with any required step size Δa: even with a constant ΔN, it needs to know the increasing step size Δa over the continuous a versus N curve. The acceleration of the fatigue crack growth rate da/dN can be modeled using a physical analogy: the sliding box or stiction-friction analogy. Figure 5.8 shows this model schematically. A box with mass M is resting on a horizontal surface. It is pulled forward by a force $F(t)$. The box experiences an opposite reaction force F_{fric} when it is moving and when it comes to rest after moving, due to friction. At the threshold from rest to moving, a higher stiction force F_{stic} first needs to be overcome instantaneously, after which the moving box experiences F_{fric}. While the box is moving, it experiences a net force $F_{\text{net}}(t) = F(t) - F_{\text{fric}}$. If the pulling force is decreased or disappears, the box will only experience friction, slowing down until rest.

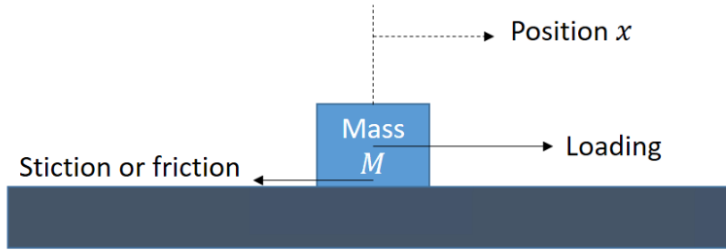The acceleration $z(t)$ of the box follows from Newtonian mechanics:

Figure 5.8: Schematic understanding of the sliding box mechanism.

$$z(t) = \frac{F_{\text{net}}(t)}{M} \qquad (5.25)$$

Integrating $z(t)$ once with respect to time gives the velocity $v(t)$, and integrating once more results in the distance traveled $x(t)$. The development of these parameters is shown qualitatively in Figure 5.9. In this example, the stiction force is overcome at $t = 0.25$. Because the friction is lower than the stiction, the resulting net force produces a nonzero initial acceleration. When the box comes to standstill at $t = 0.84$, stiction takes over, and the box remains still for the remainder of the cycle.
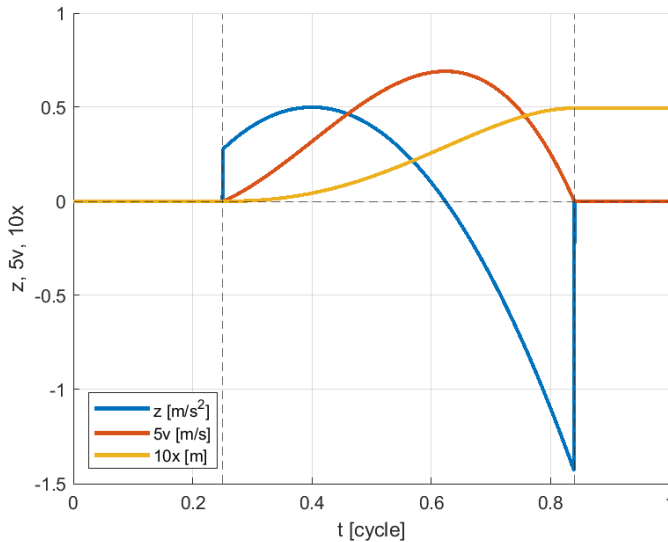
Figure 5.9: Schematic results of the acceleration $z(t)$, velocity $v(t)$, and distance $x(t)$ of the moving box during a single fatigue cycle.

In this analogy, the maximum applied force F_{max} is proportional to the applied

work during a single cycle. A sine fatigue load is applied. With strain being proportional to applied stress, the applied work or force follows as $F(t) \propto \sin^2$. It is scaled to reach $F_{\max} = U_{\max}(a)$ for each cycle. The stiction threshold can be seen as the smallest starting value. The amount of friction can be seen as energy lost due to generation of new crack surface, plastic energy dissipation, and change in elastic energy. The traveled distance per cycle is assumed to be the crack length increment:

$$x = \frac{da}{dN} = \frac{\Delta a}{\Delta N} = \Delta a \tag{5.26}$$

5.4.2. The iterative numerical implementation of the sliding box analogy

A flow chart is shown in Figure 5.10. This iterative model needs specimen geometry and material parameters as input. It stops at a predetermined $(2a/W)_{\text{stop}} < 1$ value, for the crack growth rate would approach infinity near $2a/W = 1$, and in reality the plastic zone shape gets affected by the plate edge, contrasting the Irwin model. The input for the total applied work $U_{\max}$ at each cycle has two options:

- Directly from $U_{\max}$ in Equation (5.9).

- Indirectly from the summation of ΔU from the energy balance, Equation (5.24). Note that $\Delta N/\Delta a$ and $\Delta a/\Delta N$ cancel out as all Δa per cycle are now equal.

Two constants are needed as input: C_{stic} and C_{fric}. C_{stic} should be below unity to allow the model to start. It is set to 0.9999 for all tests, such that $F_{\text{stic}} = C_{\text{stic}} U_{\max}(a = 0)$ is just below the maximum force. This allows the box to start moving even at small da/dN. In a similar way, C_{fric} influences $F_{\text{fric}} = C_{\text{fric}} U_{\max}(a = 0)$. It is assumed equal to the closure correction parameter $S_{\text{op,phys}}/S_{\max}$, hereby including $S_{\max}$ and R effects into the model. The resulting da/dN is used to calculate the ranges of a, N, and ΔK_{eff} to complement the ranges of dU/dN and $U_{\max}$.

5.4.3. Results of the sliding box analogy

The sliding box analogy with energy balance option was used to recreate the fatigue data shown in Table 5.1. Figure 5.11 shows the modeled da/dN versus ΔK_{eff} crack growth curves overlaid with test data. Note how both data types have linear trends on double logarithmic scales, which can be fitted well with a power law. Many fatigue crack growth models indeed use a power law as basis, with various experimentally derived constants and scale factors. The sliding box with energy balance results give nearly the same result, but with a physical basis.

The sliding box analogy simulates every single fatigue cycle. The obtained da values are per definition equal to da/dN. Integrating over the fatigue life results in the total crack length and the a versus N curve. Figure 5.12 shows these curves for the same tests as Figure 5.11.
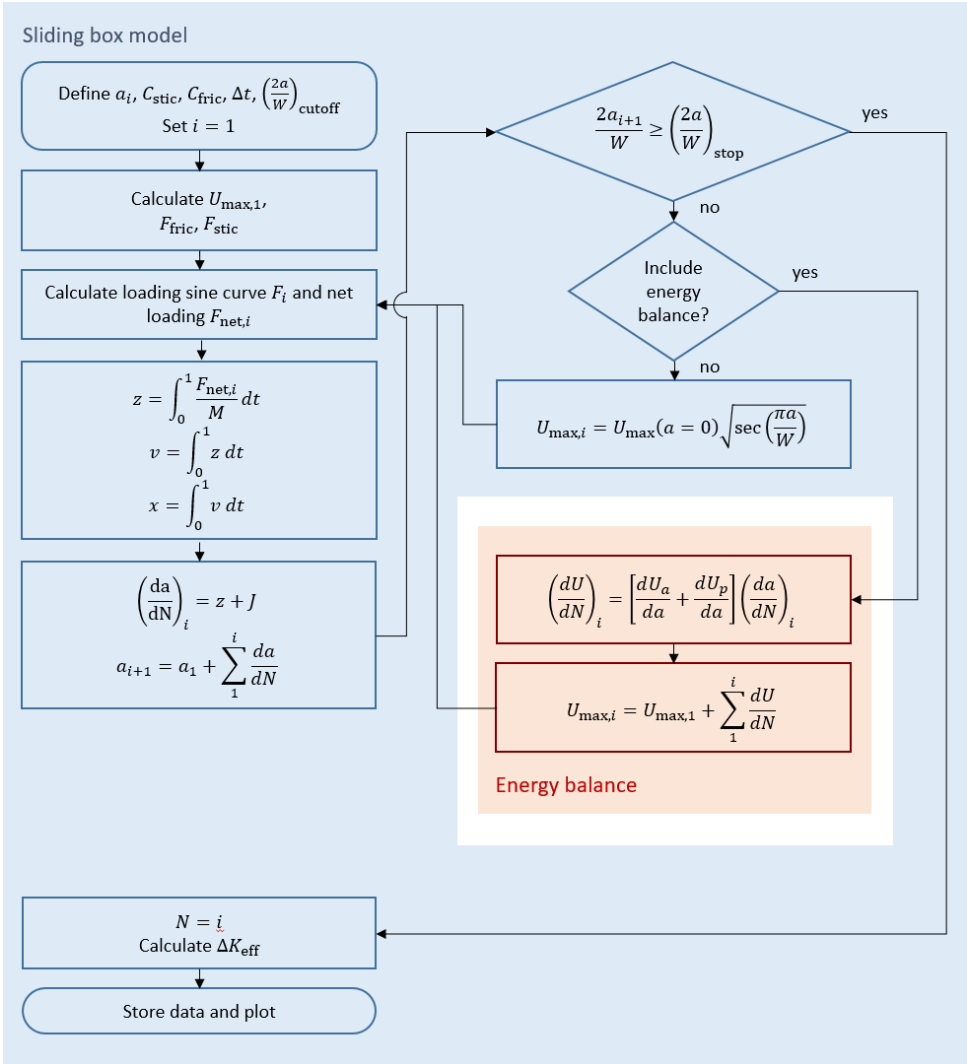
5

Figure 5.10: Flowchart of sliding box analogy for da/dN modeling, with and without the energy balance in the loop for calculating ΔU.
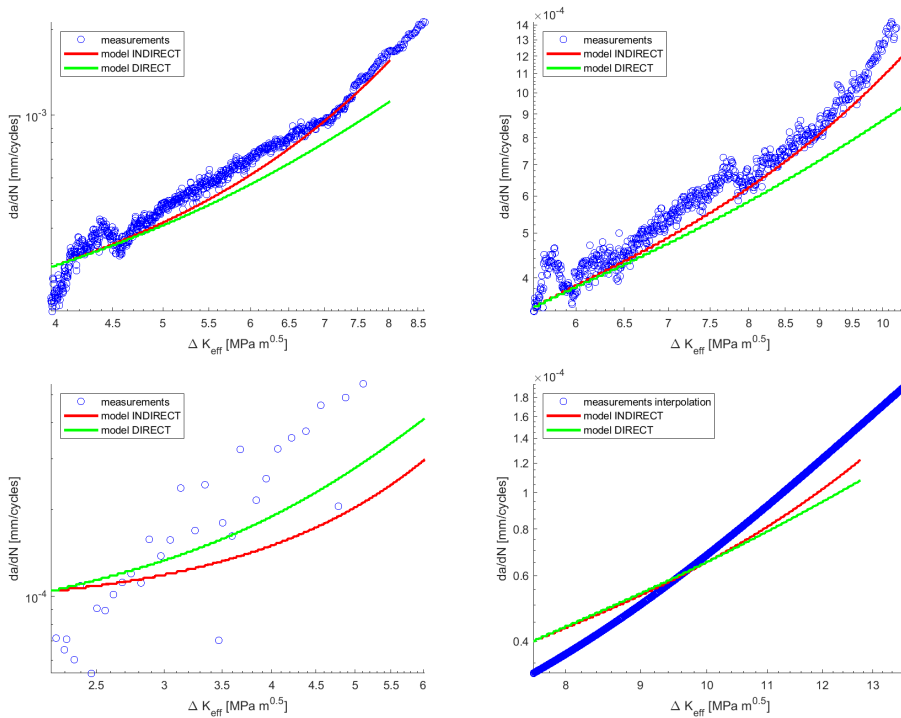
Figure 5.11: Fatigue curves of the tests in Table 5.1. Data from measurements, and data modeled with the sliding box analogy with energy balance.
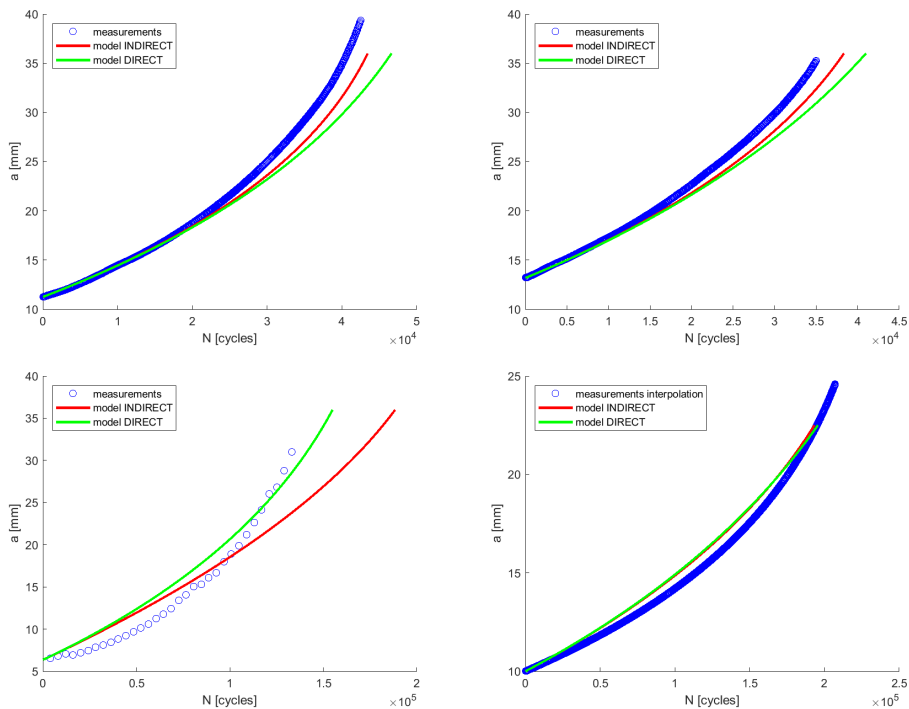
Figure 5.12: Crack length versus amount of cycles for the tests in Table 5.1. Data from measurements, and data modeled with the sliding box analogy with energy balance.

The results are in good agreement with test data from different alloys. They show that the combined model is at least qualitatively correct for isotropic materials and metals in general. The direct model, without the energy equation, proves that sliding box analogy is definitely qualitatively correct, with fatigue test data showing that it is quantitatively correct too. The underlying physical model must therefore be a close analogy to the actual process causing fatigue crack growth, increasing our understanding of the phenomenon.

5.5. Discussion

Four important aspects related to the energy balance are further discussed here. First, the possibility of using FEA to investigate the change in mean plastic energy density. Second, what the energy balance can teach us, even if it is not predicting da/dN. Third, how the sliding box analogy points to a physical model of fatigue crack growth. Fourth, the implication of this physics based approach to fatigue.

5.5.1. FEA to investigate the change in mean plastic energy density term

The decrease of $dU_{\mathrm{p}}/dV_{\mathrm{p}}$ with increasing crack length is intuitive, as the plastic volume grows faster than the applied work. The generic curve Q, Equation (5.14), is an acceptable (manual) curve fit from test data, but the exact reason for this shape is not yet known.

Although Q is a power law like the 'Paris law' and similar power law based fatigue crack growth rate models, the criticism on the 'Paris law' as outlined in Section 5.1 does not hold for Q. Consider that the exponent ϕ in the generic curve is constant for all tested alloys and metals. Also, Q is dimensionally correct. The applied scaling factor $(S_{\mathrm{yield}}/S_{\mathrm{max}})^2$ is dimensionless too. And lastly, the combination of the energy balance with the sliding box analogy does not apply a customized power law to directly predict da/dN for a specific alloy, as does the 'Paris law'.

Finite element analysis (FEA) can provide more insight into the origin of this generic curve, and also if fatigue crack growth is governed by the golden ratio which shows up in various ways in nature. Ideally, a good FEA will be able to find the plastic volume and plastic energy at any given crack length. From this data the derivative $dU_{\mathrm{p}}/dV_{\mathrm{p}}$ and Q can be calculated. During the fatigue life, the crack is also affected by the following factors, which can be studied with FEA.

- The transition from plane strain to plane stress

- Shear lip formation

- The finite width effect

Another feature of FEA is that both the finite width effect on $dU_{\mathrm{p}}/dV_{\mathrm{p}}$ and the (near) infinite width case can be observed. This provides insight to remove the finite width effect from $dU_{\mathrm{p}}/dV_{\mathrm{p}}$ curves. Since most theoretical crack growth models are based on the infinite width case, a better understanding of the physics

of crack growth is possible by using FEA. It can be used to generate dU_p/dV_p data for infinite width specimens, and a more accurate generic curve Q.

There is, however, a reason why FEA was not considered here to study the physics of fatigue crack growth. Modeling crack growth in FEA has its own set of challenges, primarily related to the numerical approach of the crack tip region. The finite mesh size and mesh element behavior upon deformation pose challenges in accurate modeling of the crack tip region. While FEA most definitely has merit, the authors wanted to prevent having to choose a suitable FEA model out of many variants to construct or validate the model outlined in this paper. Nevertheless, FEA most definitely can have a large supporting role to further understand the factors listed above.

5.5.2. Predictive use of the energy balance

The energy balance cannot provide predictions as it is a continuous equation without dependence on the fatigue cycles N. Nevertheless, it can provide information on the respective energy and dissipation terms at any crack length. Therefore it is capable of predicting the absolute amounts and relative sizes of the dissipated energy terms.

The discrete form of the energy balance can be used to remap existing fatigue data using any arbitrary choice of Δa range. Numerical integration then results in the corresponding ΔN and da/dN values. Together with the sliding box analogy it can be used to model and predict da/dN.

As stated earlier, this energy balance works for CA fatigue, but needs extra input for VA fatigue to incorporate the varying fatigue spectrum. A partial solution might be possible for CA fatigue with an overload. Before and after the overload there is CA fatigue, while the overload itself is a single large increment in dU_p/dN, and a step function in dU_p/dV_p. During the crack growth retardation period following the overload, the dU_p/dV_p will slowly revert back to the original curve description. This method is similar to the crack opening and closure behavior described in Ref. [26], and refers to the explanation of the cyclic energy development given by Ref. [14], and the link between plasticity and crack opening and closure as given by Ref. [27].

5.5.3. The sliding box analogy

The physics based sliding box analogy stands out through its simplicity, while still generating realistic da/dN results. The results are qualitatively robust for several data sets of different alloys, and are generated using mainly physical input parameters. The authors therefore claim that the structure of this model makes it an excellent starting point for a deeper understanding of the physics of fatigue crack growth. Improvements to incorporate VA fatigue will likely be possible in the energy balance as discussed before, and by making $C_\text{fric} = f(S_\text{max}, R, S_\text{op,phys})$ variable and following the varying $S_\text{op,phys}/S_\text{max}$.

5.5.4. The implications of physics based fatigue modeling

The physical models presented here make it possible to predict Paris curves based almost solely on material and loading parameters such as the material stress-strain curve. A power law is present in the generic curve for the mean plastic energy density term, but it is decoupled from any particular fatigue test, such that it has a different role compared to the Paris power law. A better understanding of the physics could mean that instead of doing numerous fatigue tests to gather crack growth data, this data could be generated by modeling in the future. The time and cost reduction would be of great value to the engineering industry, who need lower bound Paris curves for designing against fatigue.

5.6. Conclusions and recommendations

The development of the energy balance in combination with the sliding box analogy, in order to have a better physical model of fatigue crack growth, results in the following conclusions:

1. A physics approach to fatigue crack growth modeling is feasible; an energy balance equation is presented for constant amplitude fatigue which correlates the change in work done per cycle to the dissipated energy due to crack growth and crack tip plasticity.

2. Fatigue cycles are dimensionless, and therefore they are inherently absent from the fatigue crack growth energy balance. This also implies that the fatigue crack growth rate da/dN and the fatigue life N cannot be predicted from the energy balance.

3. The energy balance is a continuous function $f(a)$. It can be written in a discrete form, allowing remodeling of existing $\Delta a/\Delta N$ fatigue data to any arbitrary choice of Δa step sizes.

4. The energy balance with the sliding box analogy as presented here can be applied to different alloys and for different isotropic materials (metals).

5. The energy balance with the sliding box analogy as presented here can be applied to CA fatigue. For VA fatigue it is necessary to include load history effects on the plastic zone, as the value and trend of $dU_\mathrm{p}/dV_\mathrm{p}$ are affected by the load history.

6. The change in mean plastic energy density $dU_\mathrm{p}/dV_\mathrm{p}$ can be modeled using a generic curve Q which includes the golden ratio.

The approach outlined in this paper provides a method to predict Paris curves based almost solely on material and loading parameters. It can reduce the need for time consuming and expensive fatigue testing. Furthermore, the approach does not rely on similitude parameters with a questionable physical basis.

The energy balance put forward in this paper provides a first link between the local phenomenon of crack growth and the global physical parameters. The 'marble on the staircase' analogy explains intuitively why cycles have no role in the energy balance. FEA can give insight in the origins of the generic change in mean plastic energy density curve and the link with the golden ratio.

The sliding box analogy presented in this paper uses a physical model to generate da/dN data, complementing the energy balance for the lack of fatigue cycle dependency. It is remarkable that this initial and somewhat basic model generates such realistic fatigue results for CA fatigue. Improvements to incorporate VA fatigue must be sought in the energy balance plastic dissipation term, and in the friction coefficient of the sliding box analogy.

The use of the energy balance and sliding box analogy makes modeling of fatigue crack growth possible, and offers insights into prediction of fatigue crack growth, with a proper physical basis.

Acknowledgments

References

[1] J. V. Poncelet, *Cours de mécanique appliquée aux machines* (Gauthier-Villars, Paris, 1874).

[2] C. F. Adams, *Notes on railroad accidents* (G. P. Putnam's Sons, New York, 1879) pp. 58–61.

[3] G. R. Irwin, *Analysis of stresses and strains near the end of a crack traversing a plate,* Journal of Applied Mechanics **24**, 361 (1957).

[4] G. R. Irwin, *Linear fracture mechanics, fracture transition, and fracture control,* Engineering Fracture Mechanics **1**, 241 (1968).

[5] P. Paris and F. Erdogan, *A Critical Analysis of Crack Propagation Laws,* Journal of Basic Engineering **85**, 528 (1963).

[6] W. Elber, *Fatigue crack closure under cyclic tension,* Engineering Fracture Mechanics **2**, 37 (1970).

[7] N. E. Dowling and J. A. Begley, *Fatigue crack growth during gross plasticity and the J-integral,* in *Mechanics of crack growth* (ASTM International, 1976) pp. 82–103.

[8] J. A. Harter, *AFGROW users guide and technical manual*, Tech. Rep. AFRL-VA-WP-TR-1999-3016 (Wright-Patterson Air Force Base, 1999).

[9] R. C. McClung, *NASGRO Fracture Mechanics & Fatigue Crack Growth Analysis Software*, Tech. Rep. (Southwest Research Institute, 2002).

[10] J. C. Newman Jr. *et al.*, *FASTRAN. A fatigue crack growth life-prediction code based on the crack-closure concept. User guide version 5.4*, Tech. Rep. (Fatigue & Fracture Associates, LLC, 2013).

[11] E. H. Niccolls, *A correlation for fatigue crack growth rate,* Scripta Metallurgica **10**, 295 (1976).

[12] L. N. McCartney and P. E. Irving, *Comments on: "A correlation for fatigue crack growth rate",* Scripta Metallurgica **11**, 181 (1977).

[13] M. B. Cortie, *The irrepressible relationship between the Paris law parameters,* Engineering Fracture Mechanics **40**, 681 (1991).

[14] J. J. A. van Kuijk, R. C. Alderliesten, and R. Benedictus, *Unraveling the myth of closure corrections: Sharpening the definition of opening and closure stresses with an energy approach,* International Journal of Fatigue **143**, 106016 (2021).

[15] J. A. Bhangale, *Fatigue analysis of wind turbine blade materials using a continuum damage mechanics framework (Ph. D. thesis),* (2021).

[16] R. C. Alderliesten, *How proper similitude principles could have improved our understanding about fatigue damage growth,* in *34th ICAF Conference and 28th ICAF Symposium (ICAF 2015)*, Vol. 1, edited by A. Siljander, 28th International Committee on Aeronautical Fatigue and Structural Integrity (ICAF) Symposium (VTT Technical Research Centre of Finland, 2015) pp. 47–57.

[17] R. C. Alderliesten, *How proper similitude can improve our understanding of crack closure and plasticity in fatigue,* International Journal of Fatigue **82**, 263 (2016), 10th Fatigue Damage of Structural Materials Conference.

[18] R. Hooke, *Lectiones cutlerianae, or, a collection of lectures,* (1679).

[19] Y. Zhao, R. C. Alderliesten, Z. Wu, Z. Zhou, G. Fang, J. Zhang, and R. Benedictus, *Determining finite-width-correction factors for fatigue crack growth prediction in GLARE using the equivalent compliance method,* International Journal of Fatigue **127**, 74 (2019).

[20] C. E. Feddersen, *Discussion,* ASTM STP 410 , 77 (1966).

[21] A. J. Kinloch, *Adhesion and Adhesives: Science and Technology* (Springer Science & Business Media, London, 1987).

[22] J. Hogeveen, *Towards a proper understanding of fatigue crack growth and crack closure (M.Sc. thesis),* (2016).

5

[23] H. Quan and R. C. Alderliesten, *The relation between fatigue crack growth rate and plastic energy dissipation in 7075-t6,* Engineering Fracture Mechanics **252**, 107765 (2021).

[24] P. A. Houdijk, *Het effect van de proefstukdikte en proefstukgeometrie op de vermoeiingsscheurgroei in Fe510Nb,* (1993).

[25] R. A. Tomlinson, Y. Du, and E. A. Patterson, *Applied Mechanics and Materials*, Vol. 70 (2011) pp. 153–158.

[26] J. Schijve, *Fatigue of Structures and Materials*, 2nd ed. (Springer Science+Business Media B.V., 2009).

[27] J. J. van Kuijk, R. C. Alderliesten, and R. Benedictus, *Measuring crack growth and related opening and closing stresses using continuous potential drop recording,* Engineering Fracture Mechanics **252**, 107841 (2021).

5

6

Crack area as similitude parameter

This paper discusses the appropriateness of crack length as a reference dimension for fatigue damage. Current discussion on short crack versus long crack data is still divided between various approaches to model small crack growth. A proper physical explanation of the probable cause of the apparent differences between short crack and long crack data is not yet provided. Long crack data often comprises crack growth in constant thickness specimens, with a through crack of near constant crack front geometry. This is not true for corner cracks or elliptical surface crack geometries in the small crack regime where the crack front geometry is not symmetric or through-thickness. This affects similitude parameters that are based on the crack length. The hypothesis in this paper is that a comparison between long crack data and short crack data should be made using similar increments in crack surface area. The work applied to the specimen is dissipated in generation of fracture surface, whereas fracture length is a result. The crack surface area approach includes the two-dimensional effect of crack growth geometry in the small crack regime. A corner crack and a through crack are shown to follow the same power law relationship when using the crack area as base parameter. The crack front length is not constant, and its power law behavior for a corner crack is shown.

6.1. Introduction

Most fatigue crack growth data is published as da/dN versus ΔK[1]. The data often appears as one or more straight lines in a graph with log-log scales, and is known as the 'Paris law'. In industry, this Paris relation is widely used for its simplicity. However, small crack data is not so well-defined and a mismatch with Paris relations is often seen in this region.

Alderliesten [2, 3] questions the general idea that the Paris relation in all its forms should be taken as a 'law', as there is no physical basis for the power law. He suggests that a better understanding of fatigue crack growth could be obtained by looking at the energy balance throughout fatigue cycles. Amsterdam et al. [4] agree with the notion that the power law approach is flawed from a physical point of view, as the equation is not dimensionally correct.

The relationship of da/dN versus ΔK_a on the 'base parameter' crack length a seems to work fine for through cracks, where the crack front is ideally straight, and perpendicular to side of the specimen. For any other crack front shape, this does not necessarily hold. The mean a along the crack front is different from the observed a at the specimen edge, and different local da/dN values are present along the crack front. Another choice of base parameter might improve the understanding of fatigue crack growth, and could help in understanding the energy balance cycle during crack growth. Murakami et al. [5], and Murakami [6] noted that for surface cracks of arbitrary shape, the use of the square root of the crack area as the effective crack length improved their K_max equations. The use of crack area rather than crack length as base parameter is further investigated here.

6.2. Hypothesis

Given the large spread in small crack da/dN data, and the dependency on a which is questionable for several crack front geometries, further search for a more suitable base parameter seems warranted.

It is hypothesized that the crack area A is a better choice than the crack length a, because the area can be related to the energy in the cross-section, providing a path to relate the energy input to the crack growth. A schematic view of a specimen cross-section with cracked surface and geometric parameters is shown in Figure 6.1.

During crack growth the cross-sectional area decreases, whereas the crack length is a result of this area decrease along one dimension. Only for an ideal through crack with straight crack front are a and A directly related by the specimen thickness. With literature mostly dealing with through cracks and a being readily measurable from the specimen surface, it is understandable why a is such a popular parameter to describe crack growth (rate).

Note that potential drop measurements are essentially crack area measurements, as the area is related to the electrical resistance of the current. When the

---

[1]As the stress intensity factor is a function of the crack length, the notation ΔK_a will be used to distinguish it from another stress intensity factor introduced in this paper being a function of the crack area: ΔK_A.
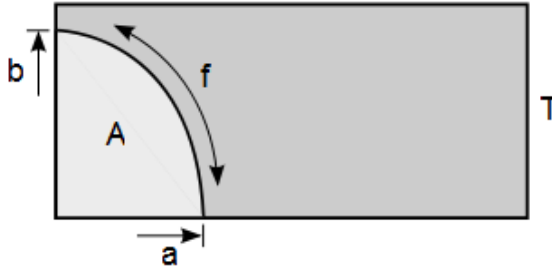
Figure 6.1: Schematic view of a specimen cross-section with cracked surface A and thickness T. Crack lengths a and b are indicated, as well as crack front length f.

area measurement is normalized by the specimen thickness T it directly transforms into a mean a measurement.

With A as base parameter, it is straightforward that dA/dN becomes the crack growth parameter. Related to this choice is the suitability of similitude parameter ΔK_a. To comply with the choice of A as base parameter, an equivalent similitude parameter $\Delta K_A = \Delta S \sqrt{\pi A}$ is used. Again, this change would hardly affect through-cracks, or the through-crack phase of other crack types.

A corner crack grows along two dimensions (a and b) instead of one (a), and as such the crack front length f, measured from free surface to free surface along a crack front, is also growing per cycle. It is hypothesized that this lengthening of f can be correlated to da/dN or dA/dN as well, as the available energy for crack growth per cycle is divided over da and f.

6.3. Examples from literature

Two examples from literature are shown. The first contains data from fatigue tests, while the second presents a common analytical corner crack model.

6.3.1. Corner cracks in PMMA

There is ample literature on fatigue crack growth rate da/dN versus ΔK_a data. Very few include crack front geometry data. Grandt et al. [7] discuss various corner crack and surface crack tests by Snow [8] where the crack front geometry was recorded during the test. An example is given in Figure 6.2. From this data both a and A can be obtained. The number of analyzed crack fronts and data points per front are rather limited, but it provides insight into the change of a and A during the growth of a corner crack.

The corresponding da/dN versus ΔK_a plot is given in Figure 6.3. The scatter in the corner phase is evident, and when the crack becomes a through crack, the curve becomes a smooth power law. From textbook crack growth curves, one would expect a through crack to have a steeper curve during small crack growth, starting
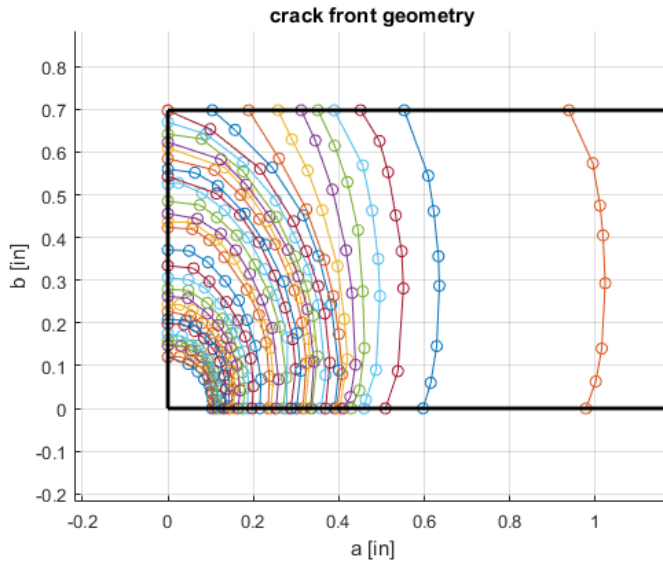
Figure 6.2: Corner crack geometry of several crack fronts of Test 6 by Snow [8] Measurement points belonging to identical crack fronts have been joined by lines for clarity.

at a ΔK_{th} (e.g. Schijve [9], Fig. 8.6). For the corner crack shown in Figure 6.3, the opposite is seen.
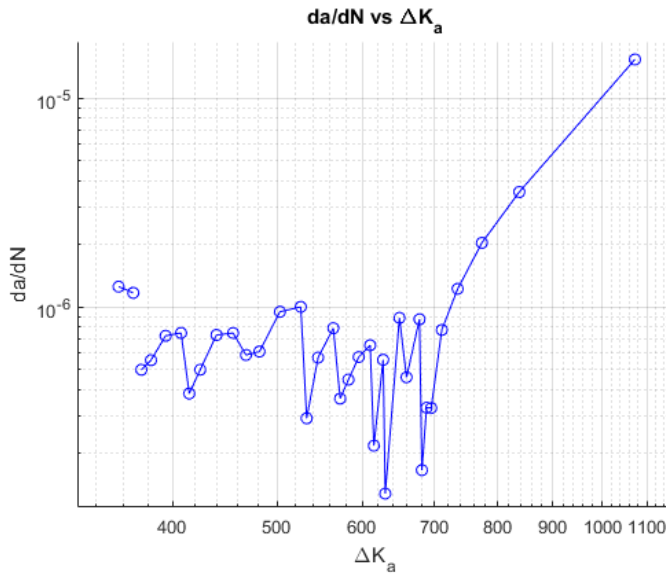

Figure 6.3: da/dN versus ΔK_a belonging to Test 6 by Snow [8].

6.3.2. Corner crack model of Newman and Raju

A simple model of a corner crack is presented by Newman and Raju [10]. A quarter ellipse corner crack is modeled, after which it becomes instantly a through crack. There is no transition phase between the corner- and through crack phases, and the model is based on the crack length throughout all phases; which gives the false impression that the da/dN curve is smooth. Figure 6.4 shows this transition at $a/T = 0.675$. This model is of interest, however, because a good comparison example is given with experimental data of Hsu et al. [11].
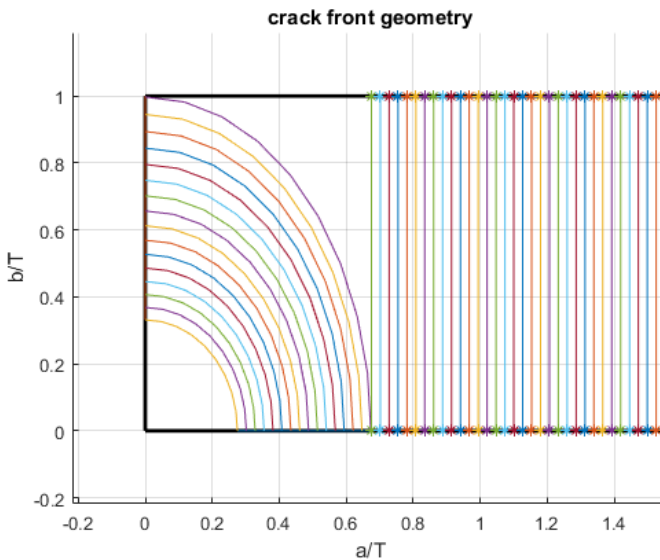
Figure 6.4: Model of a corner crack. Redrawn from Newman and Raju [10]. With a as base parameter, da/dN appears smooth while there is a large, unrealistic step in A at $a/T = 0.675$.

6.4. Numerical Modeling

Two numerical models are presented here that are used to predict crack front geometries during crack growth. The first is an extension of an existing model. The second one is a radically different approach, yielding similar results.

6.4.1. Corner crack and through crack comparison model

The premise here is that dA/dN versus ΔK_A is a power law. A could be a more suitable parameter for comparison of several crack types, and it would still compare with da/dN versus ΔK_a for the through crack. A model was created which simulates a corner crack, together with an equivalent through crack. Although the appearance of the corner crack might be similar to the previously discussed Newman-Raju model, it is partially more detailed as the three phases are modeled separately. By

modeling the transition region with a smooth dA/dN, the unrealistic behavior of the Newman-Raju model (a significant dA between two cycles, both at identical a) is largely mitigated. Furthermore the crack length a or crack growth ratio da/dN is not used as base parameter, but dA/dN is.

The corner crack is modeled as a quarter ellipse crack front, whose aspect ratio (minor axis over major axis) γ is varied exponentially by a factor β during growth to mimic crack behavior seen in literature and in reality. Per iteration N, γ is multiplied by β^N. The area of a quarter ellipse area is $A = \pi ab/4$. With $b = a\gamma$, reworking gives $a = \sqrt{(4A)/(\pi\gamma)}$, and a and b are obtained. Then b is calculated using a and γ. Input consists of specimen width, thickness, and the stress range ΔS. The values of dA/dN and β are given, and the model grows a corner crack until it becomes through-thickness; at $b \geq T$.

For the transition phase, a given number of cycles is chosen such to represent real crack front development when transforming a corner crack into a through crack. The dA/dN power law to drive the area growth is still used, while graphically the crack is deformed from a quarter ellipse to a straight line, by flattening the elliptical curve gradually into a straight line, i.e. it takes account of the growth of dA and A but does only approximate the crack front development graphically.

The model then also simulates a true through crack for a given number of cycles, matching up with the through crack phase from the corner crack model. For two cases, each containing a corner and a through crack, the da/dN versus ΔK_a and dA/dN versus ΔK_A are obtained, and discussed below. An example of the crack geometry of the first case is given in Figure 6.5.
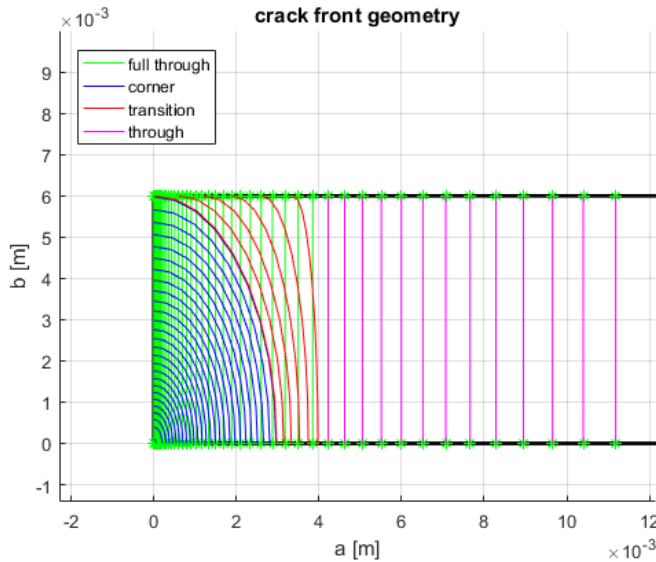

Figure 6.5: A corner crack in three phases, with an overlaid true through crack, both following the same dA/dN power law.

The da/dN data from this model is presented in Figure 6.6. It is not unreasonable as it correlates to real results, e.g., Figure 6.2. When looking at the dA/dN data in Figure 6.7, the values are found to be continuous and increasing all the time. There is some slight deviation from the linear power law behavior in this log-log plot, in the very beginning of the crack growth. This is because the power law[2] $f(x) = ax^b + c$, has $c \neq 0$ because of a finite starting crack area present. Nevertheless it is evident that various crack geometries can be compared much better when based on A instead of a.
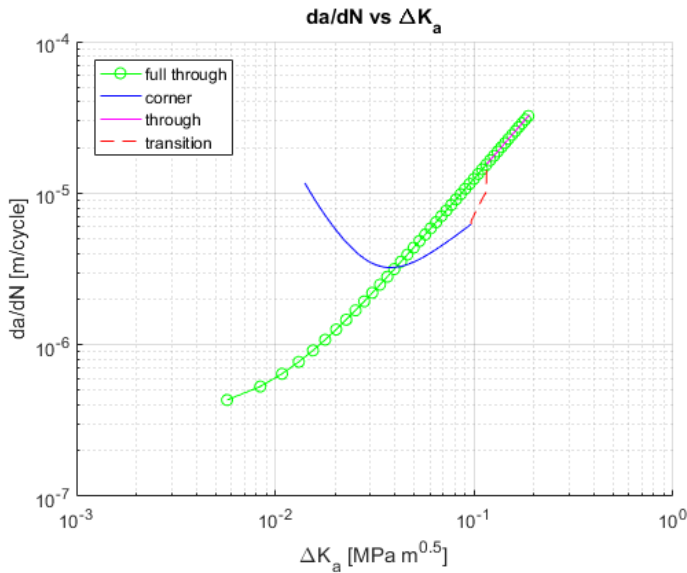
Figure 6.6: The standard da/dN versus ΔK_a curve of this model. Note how irregular the corner and transition phases behave, while the true through crack is faithful to the power law.

Slight changes in starting parameters (mainly constant β, which acts as an exponential function on γ), can alter the ellipse aspect ratio γ during crack growth such that the da/dN actually decreases during the corner crack phase. It increases again through the transition and through crack phases. This is the second case. An example of that is given in Figure 6.9, together with the crack front geometry in Figure 6.8. The dA/dN data of this case is equal to the data shown in Figure 6.7.

6.4.2. Cellular Automaton

A cellular automaton procedure was programmed to predict crack front growth, based on unpublished work by Conen [12]. The specimen cross-section is modeled as a matrix. Every iteration N, all indices of a probability matrix are updated based on certain surrounding indices, and a binary version of this matrix is stored, indicating which part of the cross-sectional area is still solid and which part has

---

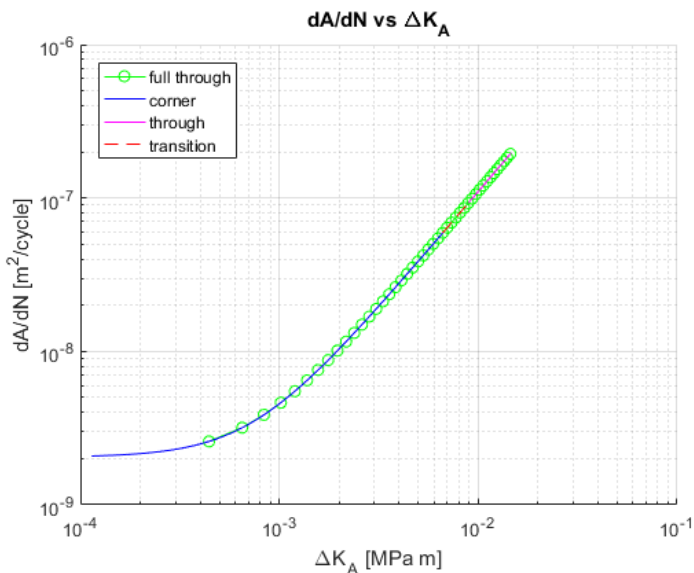[2]In this example equation, a, b, and c are generic constants, with x a generic variable.

Figure 6.7: When presenting the crack growth data as dA/dN versus ΔK_A, both crack types predictably collapse onto the same power law (since it was programmed to follow this relation), even though they are geometrically different.
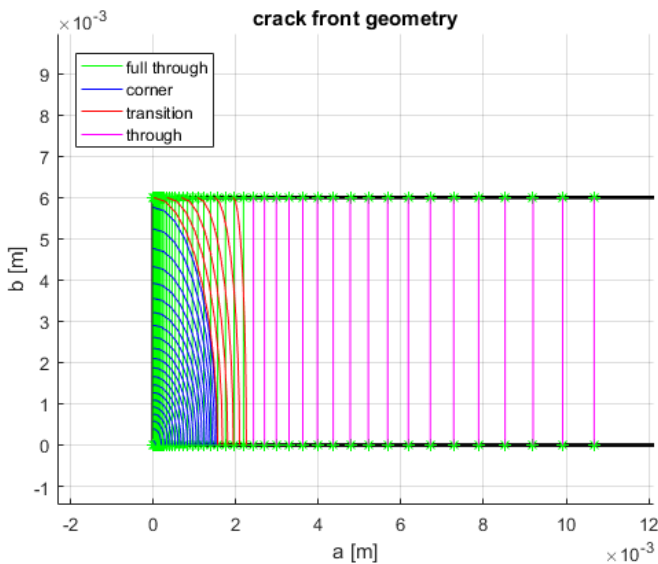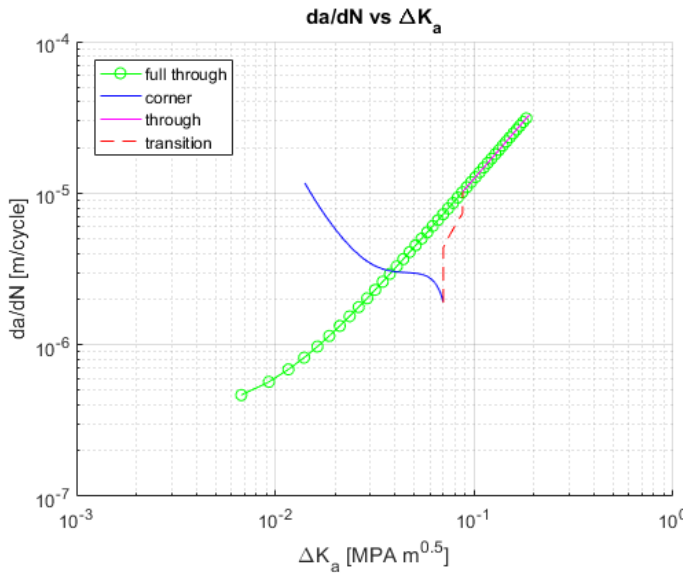
6

Figure 6.8: A corner crack in three phases, with an overlaid true through crack, both following the same dA/dN power law.

Figure 6.9: The standard da/dN versus ΔK_a curve of this model. Note how irregular the corner and transition phases behave, while the true through crack is faithful to the power law.

disappeared (cracked). The crack fronts are generated every N, and as such do not follow any growth law. A crack growth relation is introduced separately to read out the correct crack fronts. A power law relation on dA is chosen to obtain the growth intervals. From the data also the crack length a is determined, to calculate ΔK_a. Figure 6.10 shows an example of a grown corner crack. (Note the similarity with Figure 6.8). Figure 6.11 gives the corresponding da/dN versus ΔK_a.

Given the nature of the simulation, da/dN here appears also realistic, but given the model resolution, less smooth.

And again, when plotting the growth with A as base parameter, a smooth power law shows up: Figure 6.12.

To show the power of the cellular automaton, consider the example crack growth in Figure 6.13. A corner crack is present, as well as a single slit radiating perpendicular from the center hole. The zebra-striped pattern shows clearly how the cracks start to grow independently, and then link up to form one crack front.

6.5. Crack front length

Another parameter often overlooked in (small) crack literature is the crack front length f. There is a marked increase and decrease of f in respectively the corner and transition phase. Energy is used to increase the crack surface area along two dimensions here, which also modifies f. For an ideal through-crack, only the surface area is increased, and f is constant.

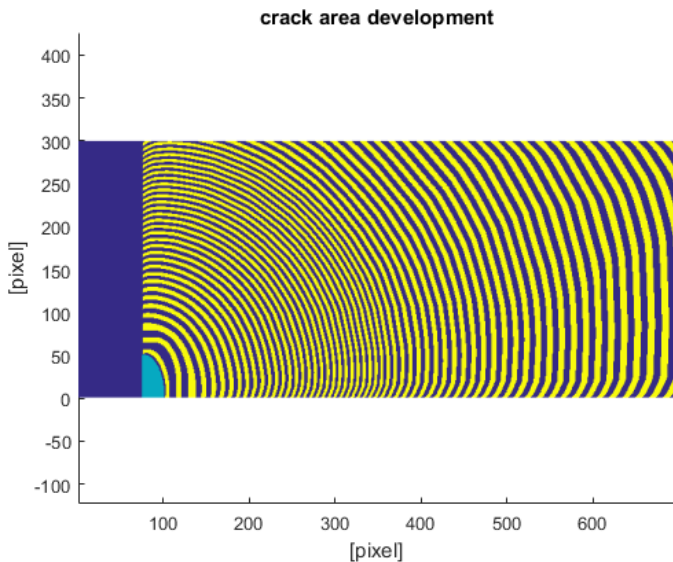When plotting the crack front length development for the literature case of

Figure 6.10: Cellular Automaton has grown a corner crack, from left to right. Half of the centre hole is visible as the dark rectangle on the left, and the initial crack in turquoise. Dimensions in pixels.
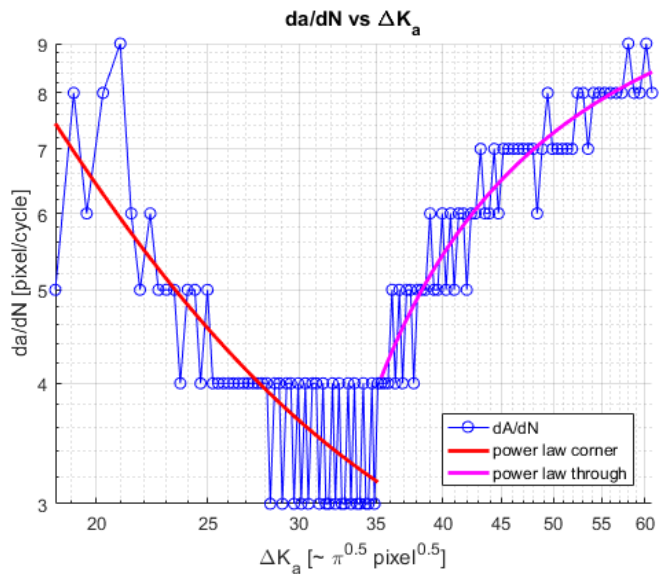

Figure 6.11: The standard da/dN versus ΔK_a curve of this model. The corner phase clearly has a decreasing growth rate, an only after becoming through-thickness it assumes a normal growth behavior.
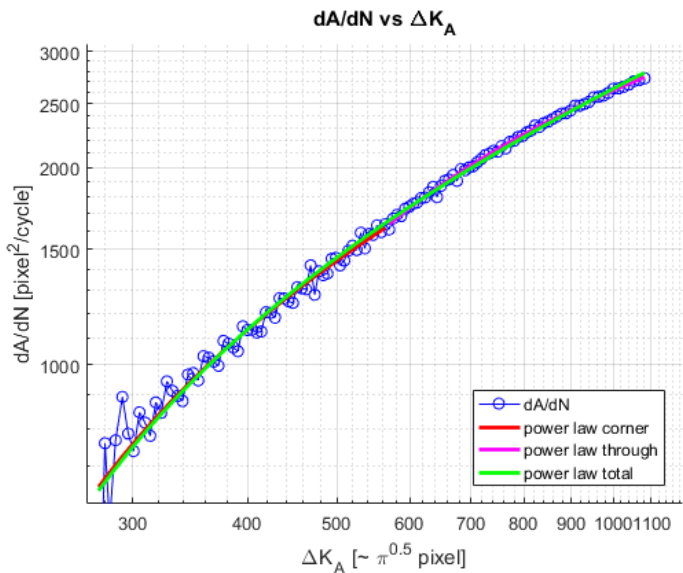
Figure 6.12: When showing the crack growth data as dA/dN versus ΔK_A, both crack phases connect with nearly equal slopes The complete crack follows a power law relationship neatly.
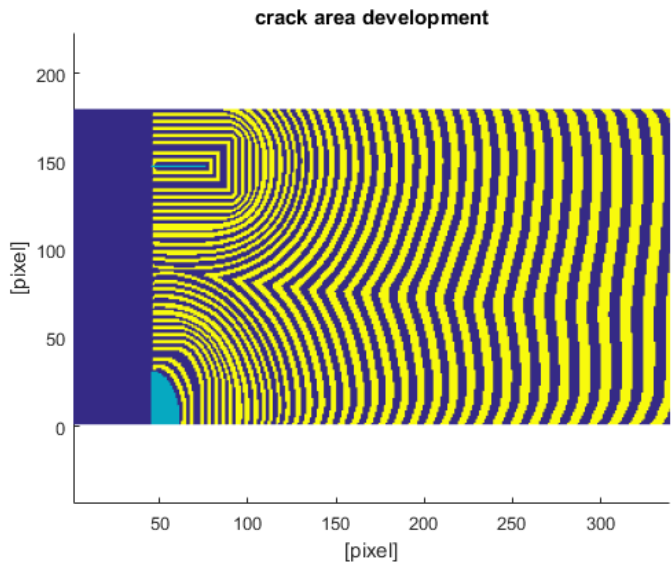

Figure 6.13: A corner crack and a slit crack (both in turquoise) are grown. Note how the crack fronts join and become one through crack.

Grandt et al. [7] in Figure 6.14 again a power law relationship is found for the corner phase. The decrease in the transition phase is small, and not enough data points are available to make reliable curve fit estimations. The power law is not a surprise, as it follows from the power law dependency of dA/dN.
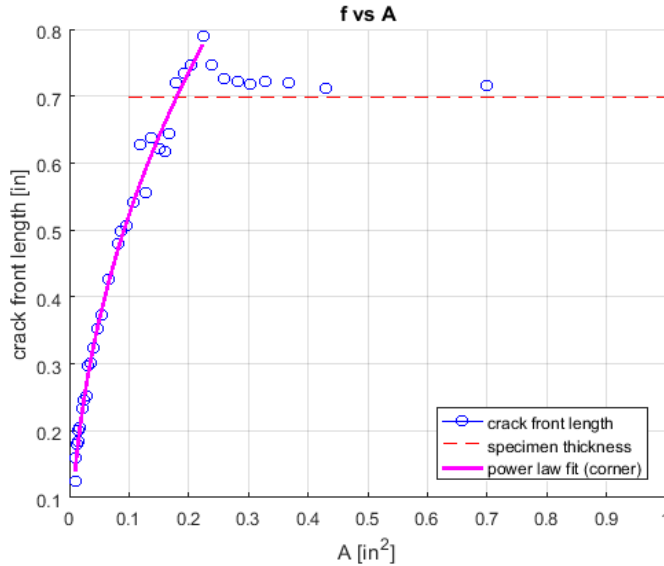

Figure 6.14: Snow Test 6 [8]. Crack front length f increases until the crack becomes a through crack, after which it decreases to a constant value. This end value is slightly larger than the specimen thickness since the crack front is slightly curved. Some data scatter is present.

Evaluating the crack front lengths of the cases presented in Section 4.1, very good power law fits are found for both the corner and transition phases, as shown in Figure 6.15 and Figure 6.16.

This power law relation for f versus A also holds in the cellular automaton simulation, see Figure 6.17. Only here a small step in absolute value is seen when the crack goes 'around the corner'. The crack is not exactly a quarter-ellipse, so some crack length is lost in the very corner at $b = T$. This is visible from the yellow markings in the top left corner in Figure 6.10. Beyond the corner phase, the transition phase asymptotically nears a real through crack phase, but again with a good power law fit.

6.6. Discussion

The figures from Grandt et al. [7] are very illustrative. However, these cracks were grown in PMMA material, a polymer. Most fatigue crack growth data in literature is gathered from metals (aluminium/steel/titanium), which tend to be more isotropic than a polymer. Nevertheless these results are very similar to the results found in metals. The crack growth mechanism for cracks at this scale might
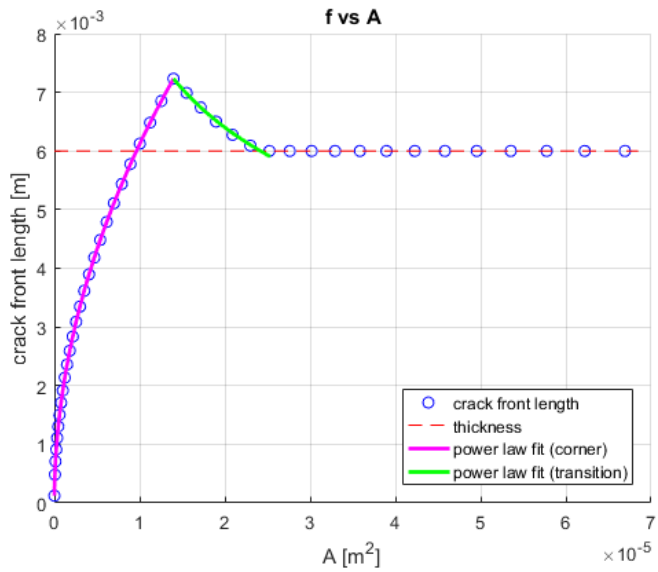
Figure 6.15: Crack front length plot belonging to Figure 6.5. Crack front length f increases with a near perfect power law fit until becoming a through crack. Beyond that, f decreases to the specimen thickness (straight through crack), again following a power law.
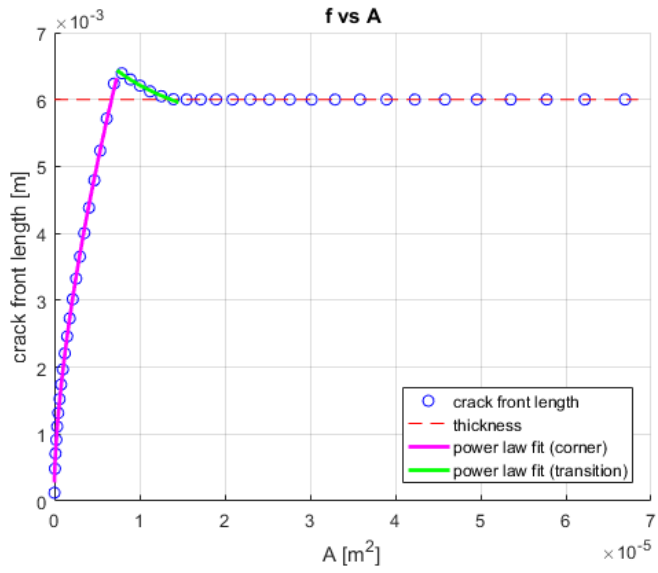
6

Figure 6.16: Crack front length plot belonging to Figure 6.8. Crack front length f increases with a near perfect power law fit until becoming a through crack. Beyond that, f decreases to the specimen thickness (straight through crack), again following a power law.
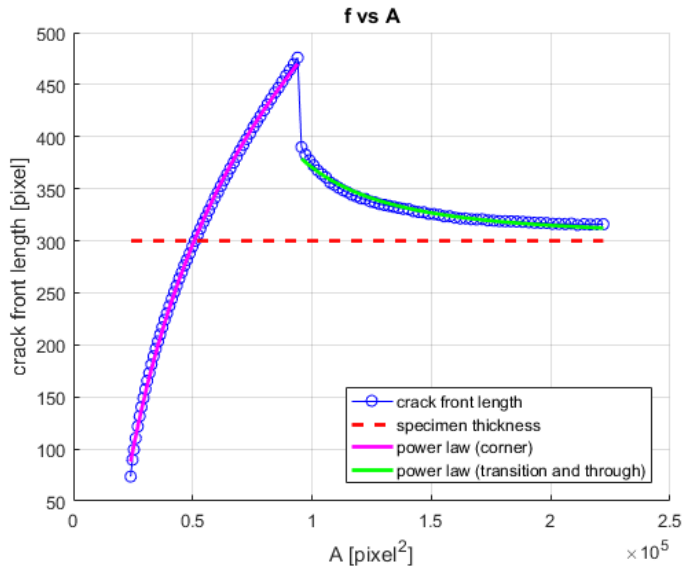
Figure 6.17: Cellular automaton: f increases with a near perfect power law fit until becoming a through crack. Beyond that, f decreases asymptotically to a value slightly larger than the specimen thickness (curved through crack), again following a power law. See also Figure 6.10.

not be very sensitive to anisotropic material structures.

Given the behavior of da/dN versus ΔK_a as seen in Figure 6.6 and Figure 6.9, the use of a Paris relationship for a corner crack is incorrect. The model of the author (Section 4.1) does not show such a change in slope when using dA/dN versus ΔK_A, see Figure 6.7. However, introducing a different crack growth rate power law for the small crack regime in this model does not make it exactly match up with corner crack growth rate curves either, although close. The geometry effect can significantly affect the crack growth rate in the small crack growth regime.

Furthermore, consider a surface crack inside a hole in a plate. Such a crack also grows through the three phases. In the first phase, by definition, a is constant as the crack first has to grow to a through-thickness crack. In the standard da/dN versus ΔK_a plot, $da/dN = 0$ here, such that these points cannot be shown on the log-log plot. The ΔK_a parameter is constant during this phase, while the crack is growing. This shows up as a ΔK_{th}, while the second dimension is not present in this similitude parameter.

The cellular automaton is an interesting method, in the sense that it has absolutely no physical connection with fatigue crack growth, yet it produces eerily similar crack growth geometries. Two major arguments can be made against using this method:

- The growth dA/dN is artificially and a priori introduced using a power law. The automaton grows crack fronts, but lacks a coupling with the number of cycles. The relevant crack fronts are found using an area-related relationship.

- The growth rate along a single crack front is not constant, but the variation in local stress intensity factors, linked to local growth rate, seems to be smaller than observed in reality.

Regarding the latter argument, the Newman-Raju model and the author's model correct slightly for this by changing γ of the ellipse during growth, but do limit the shape to the ellipse. The cellular automaton tends to make crack fronts slightly too curved or too much alike a circular arc compared to reality, but captures the transition region wonderfully realistically. While these arguments are valid concerns, the results do appear similar to geometries observed in practice and reported in literature.

6.7. Conclusions and recommendations

The choice of crack length a as base parameter for fatigue crack growth measurements is questionable for crack types other than through cracks. It is shown that corner cracks behave differently in the small crack growth region. The crack surface area A is shown to be a more suitable parameter, as the results for both through cracks and corner cracks are now similar in magnitude and slope on a graph with log-log scales, making comparisons easier. This change in base parameter affects the similitude parameter too. The common da/dN versus ΔK_{a} plot can then be transformed into an equivalent dA/dN versus ΔK_{A}.

It is shown that in a quarter-elliptical corner crack, the crack front length during the corner phase grows along a similar power law behavior as introduced for dA. The energy used for crack growth is basically split into crack area increase and crack front length extension.

It is shown that a corner crack has three distinct phases; corner, transition, and through crack. The crack length growth rate behaves markedly different from a power law during the corner phase, and the transition phase links the corner and through phases together.

The cellular automaton approach can create great insight in the behavior of the crack growth, especially when unique and/or multiple initial cracks are present. Although the automaton routine has no physical link to fatigue crack growth, it can be used as a prediction tool for fatigue crack growth geometry, especially when multiple starter cracks are present.

As there is scarcely crack growth data available which also includes the crack front geometry development, more fatigue tests are needed with high accuracy measurements of the crack front geometry. This has proven to be difficult but not impossible, and warrants further study to create data sets to compare the models with.

Another recommendation is to include more fatigue crack types into the models, to see if the results for the corner crack versus through crack also hold for these types.

6

Acknowledgments

References

[1] J. J. A. van Kuijk, R. C. Alderliesten, and R. Benedictus, *Fatigue crack surface area and crack front length: New ways to look at fatigue crack growth,* in *Proceedings of the 12th International Fatigue Congress (FATIGUE 2018)*, Vol. 165, edited by G. Hénaff, 12th International Fatigue Congress (FATIGUE 2018) (MATEC Web of Conferences, 2018) p. 13009.

[2] R. Alderliesten, *How proper similitude can improve our understanding of crack closure and plasticity in fatigue,* International Journal of Fatigue **82**, 263 (2016), 10th Fatigue Damage of Structural Materials Conference.

[3] R. C. Alderliesten, *How proper similitude principles could have improved our understanding about fatigue damage growth,* in *34th ICAF Conference and 28th ICAF Symposium (ICAF 2015)*, Vol. 1, edited by A. Siljander, 28th International Committee on Aeronautical Fatigue and Structural Integrity (ICAF) Symposium (VTT Technical Research Centre of Finland, 2015) pp. 47–57.

[4] E. Amsterdam and F. Grooteman, *The influence of stress state on the exponent in the power law equation of fatigue crack growth,* International Journal of Fatigue **82**, 572 (2016).

[5] Y. Murakami and S. Nemat-Nasser, *Growth and stability of interacting surface flaws of arbitrary shape,* Engineering Fracture Mechanics **17**, 193 (1983).

[6] Y. Murakami, *Analysis of stress intensity factors of modes i, ii and iii for inclined surface cracks of arbitrary shape,* Engineering Fracture Mechanics **22**, 101 (1985).

[7] A. F. Grandt Jr., J. Harter, and D. Tritsch, *Semielliptical cracks along holes in plates and lugs,* Technical Report AFWAL-TR - Air Force Wright Aeronautical Laboratories (United States) , 132 (1983).

[8] J. R. Snow, *A Stress Intensity Factor Calibration for Corner Flaws at an Open Hole*, Tech. Rep. AFML-TR-74-282 (Technical Report AFML-TR - Air Force Institute of Technology, 1975).

[9] J. Schijve, *Fatigue of Structures and Materials*, 2nd ed. (Springer Science+Business Media B.V., 2009).

6

[10] J. Newman and I. Raju, *Prediction of fatigue crack-growth patterns and lives in three-dimensional cracked bodies,* in *Fracture 84*, edited by S. R. Valluri, D. M. R. Taplin, P. Rama Rao, J. F. Knott, and R. Dubey (Pergamon, 1984) pp. 1597–1608.

[11] T. M. Hsu, W. M. McGee, and J. A. Aberson, *A Stress Intensity Factor Calibration for Corner Flaws at an Open Hole*, Tech. Rep. AFFDL-TR-77-83 (Technical Report AFFDL/FBE - Air Force Flight Dynamics Laboratory, 1978).

[12] M. Conen, *Appendix B: Cellular Automator*, Tech. Rep. (unpublished work) (Faculty of Aerospace Engineering, Delft University of Technology, 2008).

6

7

Conclusions and recommendations

In this chapter, the conclusions of the previous chapters are presented together, to give an overview the research results. It becomes clear that the opening and closure conclusions can be linked to the potential drop through the cycle research. The energy balance includes the surface energy for crack area extension, which links to the idea of using the crack area rather than the crack length as a better similitude parameter to compare different crack geometries. Recommendations are given for further study or improvements on methods and models used.

7.1. Unraveling the myth of closure corrections

Ample fatigue crack growth closure corrections exist which result in opening stress S_{op} values used in the ΔK_{eff} approach. Literature shows that these corrections still do not fully account for closure effects, and that they have a large spread. This led to the hypothesis that there are two distinct S_{op} values: $S_{op,phen}$ used in the ΔK_{eff} approach, and $S_{op,phys}$ which is the true crack opening stress. The subsequent investigation has shown that this is true, and resulted in the following conclusions:

1. Many known closure corrections result in different corrections for the same phenomenon, for unknown reasons. Our research suggests that existing closure corrections do not properly take into account the physical opening stress $S_{op,phys}$.

2. The same known closure corrections contain empirically determined correction factors, and different corrections result in different S_{op}/S_{max} values based on $S_{op,phen}$ for the same load cycle. Our results suggest that these observations may be explained by a failure to correctly account for the effect of S_{max} and a/W on the physical opening stress $S_{op,phys}$. Thus the corresponding $S_{op,phen}$ needs to be corrected to make up for this.

   By applying the equivalent energy approach, a value of $S_{op,phen}$ can be determined based on the correct $S_{op,phys}$, as found via FEA. The $S_{op,phen}$ values found in this way matches the $S_{op,phen}$ found via previously known correction methods, but without relying on empirical correction factors. Thus our new method is more physically realistic, and potentially requires less experimental calibration than existing methods.

3. FEA shows that $S_{op,phys}$ follows four distinct regions over the full R range. From low to high R, these are: tensile-compressive loading with closure, tensile-tensile loading with closure, transition to an always open crack, and an always open crack. In the last case, it can be assumed that $S_{op,phys} = S_{min}$. Using the energy equivalent area analogy to obtain $S_{op,phen}$ values for the full R range, the FEA results show close agreement with known correction curves, especially for $R \geq 0$. This confirms that $S_{op,phen}$ in $S_{op,phen}/S_{max}$ is not the true opening stress.

4. FEA confirmed that it at least holds that $S_{op,phys} = f(R, S_{max})$ and that the derived $S_{op,phen}/S_{max} = f(R, S_{max})$ too.

   During crack growth, the local net-section stress in the crack plane increases due to the finite width effect. This does not affect S_{max}, but it does affect the local phenomenon which is crack closure. During crack growth at constant R and S_{max}, the $S_{op,phen}/S_{max}$ or $S_{op,phys}/S_{max}$ values slowly decrease because of the decreasing cross-section area. This dependency on a/W is not mentioned in literature, but may partly explain the spread of closure corrections.

Furthermore, several closure corrections include a fitting parameter to match measurement data, which tends to be dependent on R. In literature it is noted that $S_{\mathrm{op,phen}}$ also depends on the ratio between $S_{\max}$ and σ_0, where σ_0 is related to S_{yield}.

These observations combined suggest that $S_{\mathrm{op,phen}} = f(R, S_{\max}, S_{\mathrm{yield}}, a/W)$ and $S_{\mathrm{op,phys}} = f(R, S_{\max}, S_{\mathrm{yield}}, a/W)$.

Inclusion of the energy approach into the ΔK_{eff} equation may improve the accuracy over known models. $S_{\mathrm{op,phys}}$ might be found through FEA or strip yield models. For VA fatigue a cycle-by-cycle integration of the loading history might still be necessary to keep track of changes in $S_{\mathrm{op,phys}}$ and subsequent $S_{\mathrm{op,phen}}$.

7.2. Potential drop through the cycle

The extended potential drop (PD) measurement system, PD TTC, is capable of measuring the electric potential throughout a single fatigue crack growth loading cycle, and doing so for many successive cycles. This results in the observation of potential changes which are linked to several crack growth phenomena, such as the timing and magnitude of crack opening and crack closure stresses. The following list summarizes the most important findings of using this PD TTC measurement technique:

1. The known effect of mechanical stress on the electrical resistance is observed in fatigue cycles, affecting the measured potential through Pouillet's law and Ohm's law under assumption of constant current. Two main effects are observed, which have opposite effects on the potential:

   - The Poisson effect: the change of specimen geometry under load. $S \uparrow \propto \phi \uparrow$.
   - Piezoresistivity: the strain dependency of the resistivity. $S \uparrow \propto \phi \downarrow$.

2. During crack growth, two other effects are observed which are subsets of the aforementioned main effects:

   - Crack tip plasticity: changes in strain give a combined effect of the Poisson effect and piezoresistivity.
   - Crack growth: the opening and closing of the crack influences the Poisson effect.

3. Crack tip plasticity and crack growth are readily apparent from a clear deviation of the potential curve around $S_{\max}$. A plateau-like behavior is present at a certain critical cyclic energy level, above which excess energy is dissipated by growth of the crack tip plastic zone and crack growth.

4. The effect of crack extension is several orders of magnitude smaller than plasticity effects, and is therefore not directly observed in PD TTC data given the current measurement resolution. Nevertheless, the observable changes

7

due to plasticity can be correlated with start and end of the crack growth phase.

5. The start and end times $t_{S,op}$, $t_{S,cl}$ of the plateau together with the loading spectrum can be used to derive true opening and closure stresses $S_{op,phys}$ and $S_{cl,phys}$, with significantly larger accuracy and precision than existing methods such as COD.

The PD TTC method is novel way of measuring the opening and closing stress with greater insight and potentially improved precision and accuracy over existing methods such as COD. The insights and improvements obtained with PD TTC can be useful in reducing opening and closure stress related uncertainties in ΔK_{eff} similitude parameter models and other crack closure models.

7.3. Experimental observations on the plastic zone development

The results from the DIC measurement technique in combination with the PD TTC results mentioned in Chapter 3 strengthen the correlation between the crack tip plasticity magnitude and the PD TTC potential signal. The DIC results show that the crack tip peak plasticity is proportional to the PD TTC curve magnitude, including the plateau phase. Furthermore, the DIC technique can measure the peak plasticity location, which is found to permanently translate in crack growth direction during a specific time fraction of the cycle. This chapter therefore provides further proof of the ideas discussed in Chapter 3.

7.4. Towards a physics based model of fatigue crack growth

The development of the energy balance in combination with the sliding box analogy, in order to have a better physical model of fatigue crack growth, results in the following conclusions:

1. A physics approach to fatigue crack growth modeling is feasible; an energy balance equation is presented for constant amplitude fatigue which correlates the change in work done per cycle to the dissipated energy due to crack growth and crack tip plasticity.

2. Fatigue cycles are dimensionless, and therefore they are inherently absent from the fatigue crack growth energy balance. This also implies that the fatigue crack growth rate da/dN and the fatigue life N cannot be predicted from the energy balance.

3. The energy balance is a continuous function $f(a)$. It can be written in a discrete form, allowing remodeling of existing $\Delta a/\Delta N$ fatigue data to any arbitrary choice of Δa step sizes.

4. The energy balance with the sliding box analogy as presented here can be applied to different alloys and for different isotropic materials (metals).

5. The energy balance with the sliding box analogy as presented here can be applied to CA fatigue. For VA fatigue it is necessary to include load history effects on the plastic zone, as the value and trend of $dU_\mathrm{p}/dV_\mathrm{p}$ are affected by the load history.

6. The change in mean plastic energy density $dU_\mathrm{p}/dV_\mathrm{p}$ can be modeled using a generic curve Q which includes the golden ratio.

The approach outlined in this paper provides a method to predict Paris curves based almost solely on material and loading parameters. It can reduce the need for time consuming and expensive fatigue testing. Furthermore, the approach does not rely on similitude parameters with a questionable physical basis.

The energy balance put forward in this paper provides a first link between the local phenomenon of crack growth and the global physical parameters. The 'marble on the staircase' analogy explains intuitively why cycles have no role in the energy balance. FEA can give insight in the origins of the generic change in mean plastic energy density curve and the link with the golden ratio.

The sliding box analogy presented in this paper uses a physical model to generate da/dN data, complementing the energy balance for the lack of fatigue cycle dependency. It is remarkable that this initial and somewhat basic model generates such realistic fatigue results for CA fatigue. Improvements to incorporate VA fatigue must be sought in the energy balance plastic dissipation term, and in the friction coefficient of the sliding box analogy.

The use of the energy balance and sliding box analogy makes modeling of fatigue crack growth possible, and offers insights into prediction of fatigue crack growth, with a proper physical basis.

7.5. Crack area as similitude parameter

The choice of crack length a as base parameter for fatigue crack growth measurements is questionable for crack types other than through cracks. It is shown that corner cracks behave differently in the small crack growth region. The crack surface area A is shown to be a more suitable parameter, as the results for both through cracks and corner cracks are now similar in magnitude and slope on a graph with log-log scales, making comparisons easier. This change in base parameter affects the similitude parameter too. The common da/dN versus ΔK_a plot can then be transformed into an equivalent dA/dN versus ΔK_A.

It is shown that in a quarter-elliptical corner crack, the crack front length during the corner phase grows along a similar power law behavior as introduced for dA. The energy used for crack growth is basically split into crack area increase and crack front length extension.

It is shown that a corner crack has three distinct phases; corner, transition, and through crack. The crack length growth rate behaves markedly different from a

power law during the corner phase, and the transition phase links the corner and through phases together.

The cellular automaton approach can create great insight in the behavior of the crack growth, especially when unique and/or multiple initial cracks are present. Although the automaton routine has no physical link to fatigue crack growth, it can be used as a prediction tool for fatigue crack growth geometry, especially when multiple starter cracks are present.

As there is scarcely crack growth data available which also includes the crack front geometry development, more fatigue tests with high accuracy measurements of the crack front geometry are needed. Obtaining these has proven to be difficult but not impossible, and warrants further study to create data sets to compare the models with.

Another recommendation is to include more fatigue crack types into the models, to see if the results for the corner crack versus through crack also hold for these types.

7

Acknowledgments

A PhD is meant to be a personal research project. And while that is true in theory, in practice it could not have been accomplished without the support and help from many people. I would like to specifically thank the following people for their help.

Promotor, supervisor, and section leader dr. ir. René Alderliesten. Always very correct in your work, with a great focus on both technical details and writing style. Our technical discussions were fun and inspiring. Although exceptionally busy, your door was still open for a quick question. Not infrequently, this led to a half-hour debate at the whiteboard, great fun!

Promotor and department chairperson prof. dr. ir. Rinze Benedictus. Thank you for the interesting discussions and fresh insights on fatigue and other topics. The information and literature on piezoresistivity is much appreciated.

Second supervisor dr. Dimitrios Zarouchas, for your occasional feedback and the interesting and fun summer school on fatigue and composites at our faculty.

Gemma van der Windt, for running the department smoothly, and arranging paperwork and other practical stuff. Your 'Dutch subtlety' is refreshing.

Hongwei Quan, for working together on the physics of fatigue crack growth, often with in-depth theoretical discussions on the whiteboard, and for sharing a data set for my research. Much appreciated! Good memories of our fun visit to the FATIGUE 2018 congress in Poitiers, France.

Bram Jongbloed, for our many lunches and afternoon tea breaks with good conversations and many jokes. It was always nice to hear about your adventures in the lab, at the graduate school, or during travels. Houdoe en bedankt!

Borrdephong Rattanagraikanakorn for our long and deep discussions on various topics, from radio controlled drones to automatic currency trading, life in Thailand versus life in the Netherlands, and many other interesting topics.

Faculty dean prof. dr. Henri Werij, for our talks about human powered aircraft, hang gliding, space flight, and sustainable aviation. Always very busy, but still finding some time to talk about aviation and space. It is much appreciated.

Yasmine Mosleh, for our many tea breaks and funny or philosophical conversations. Your lively character added laughter to an otherwise (too) quiet department.

You never seemed too fond of your pied-à-terre in Delft, so I hope you enjoy the nice weather in your castle on the hill.

Akansha Rathi, for our deep philosophical discussions about life and goals, or sometimes just light conversations over a cup of tea. These were welcome breaks from working in the lab, often when neither of our machines were behaving properly.

And, of course, many other (PhD) coworkers who joined for lunch at the woefully small table near the coffee machine. There were so many of you, and from so many countries, which resulted in fun conversations, often about cultural and linguistic differences. Your native countries in alphabetical order: Belgium, Brazil, Canada, China, France, Germany, Greece, India, Iran, Italy, Kenya, Nepal, the Netherlands, Nigeria, Pakistan, Portugal, Russia, Spain, Thailand, Turkey, and probably some more. Thank you for your company!

None of the experimental work would have been accomplished without excellent technical assistance from the DASML technicians; Berthil, Gertjan, Cees, Frans, Dave, and Alexander. I would like to specifically mention the following two persons for their contributions beyond helping out with the test setups: Berthil Grashof, for creating and developing the PD TTC measurement device with FPGA which made possible the interesting crack opening and closure observations, and Gertjan Mulder, for explaining and supporting the use of the DIC camera system and your perpetual positive and practical attitude.

The specimens and some custom tooling were prepared with great care by the DEMO workshop team. Always busy, but results of excellent quality.

My PhD project was part of the PROF project: 'Prediction of fatigue in engineering alloys', a joint effort between research and industry, organized and chaired by Emiel Amsterdam from NLR (Netherlands Aerospace Centre). Our biannual meetings at NLR with various industry partners were interesting and resulted in fruitful discussions. Over the years there were many different attendees, I hope to have included everyone in the following lines. NLR: Emiel Amsterdam, Frank Grooteman, Marcel Bos. GKN Fokker: Tim Janssen. Airbus: Derk Daverschot, Jyothirmai Buddharaju. Embraer: Giorgia Aleixo, Marcelo Barros. Wärtsilä: Jiajun Wang †, Edgar Snelders, Aarif Zaheer. Lloyd's Register: Li Xu. TU Delft: René Alderliesten.

M2i (Materials innovation institute), for the interesting PhD project connected to industry. There were many interesting biannual cluster meetings, and yearly conferences in Noordwijk. The presentations of other M2i researchers' work gave me a broader view of the materials, science, and fatigue research landscape both in academia and industry. And, of course, the conference dinners were fun.

The user committee ('gebruikerscommissie') of this PhD research project from

Curriculum Vitæ

Jesse Johan Adriaan VAN KUIJK

03-10-1989   Born in Budel, the Netherlands

Education

2001–2008   Pre-university education
Bisschoppelijk College, Weert

2008–2012   BSc, Aerospace Engineering
Delft University of Technology

2012–2015   MSc, Aerospace Engineering
Delft University of Technology

2017–2022   PhD, Aerospace Engineering
Delft University of Technology
Dissertation: Novel insights into the physics
of fatigue crack growth
Promotor: Prof. dr. ir. R. C. Alderliesten

Work

2021–ongoing   Heat and Mass Transfer Architect, Development & Engineering
department, working on direct cooled mirrors
of semiconductor lithography machines
ASML

2015–2017   Mechanical Engineer, project owner of the foldable pusher
propeller for a flying car
PAL-V

Awards

2010   Delft University of Technology, Wall of Fame
         Development of the first successful Dutch human powered
         aircraft (private project, 2006–2010, first flight in 2009)

List of Publications

Journal Papers

3. **J.J.A. van Kuijk, R.C. Alderliesten, R. Benedictus**, *Towards a physics based model of fatigue crack growth*, (in preparation).

2. **J.J.A. van Kuijk, R.C. Alderliesten, R. Benedictus**, *Measuring crack growth and related opening and closing stresses using continuous potential drop recording*, Engineering Fracture Mechanics **252**, 107841 (2021).

1. **J.J.A. van Kuijk, R.C. Alderliesten, R. Benedictus**, *Unraveling the myth of closure corrections: Sharpening the definition of opening and closure stresses with an energy approach*, International Journal of Fatigue **143**, 106016 (2021).

Conference Papers

3. **J.J.A. van Kuijk, R.C. Alderliesten, R. Benedictus**, *Fatigue crack surface area and crack front length: New ways to look at fatigue crack growth*, in Proceedings of the 12th International Fatigue Congress (FATIGUE 2018), Vol. 165, edited by G. Hénaff, 12th International Fatigue Congress (FATIGUE 2018) (MATEC Web of Conferences, 2018) p. 13009.

2. **T. Sinnige, J.J.A. van Kuijk, K.P. Lynch, D. Ragni, G. Eitelberg, L.L.M. Veldhuis**, *The Effects of Swirl Recovery Vanes on Single-Rotation Propeller Aerodynamics and Aeroacoustics*, in Proceedings of the 21st AIAA/CEAS aeroacoustics conference, 21st AIAA/CEAS Aeroacoustics Conference (2015), p. 2015-2358

1. **J.J.A. van Kuijk**, *How a high-school student built the first Dutch human powered aircraft*, in 28th Congress of the International Council of the Aeronautical Sciences, Vol. 28, edited by I. Grant, International Council of the Aeronautical Sciences (ICAS 2012), p. 2012-1.6.3

Data Publications

1. **J.J.A. van Kuijk, R.C. Alderliesten, R. Benedictus**, *Data underlying the research on: Al 2024-T3 center crack tension constant amplitude fatigue tests with potential drop through the cycle measurements*, in 4TU.ResearchData.

TUDelft Delft University of Technology

NWO
Nederlandse Organisatie voor Wetenschappelijk Onderzoek

M2i materials innovation institute